SEMICONVECTION IN HALO STARS

AND THE PRIMORDIAL HELIUM ABUNDANCE

Thesis by

Theodore Dean Tarbell

In Partial Fulfillment of the Requirements

For the Degree of

Doctor of Philosophy

California Institute of Technology

Pasadena, California

1976

(Submitted February 24, 1976)

To Flash

ACKNOWLEDGMENTS

rewarding escapes from Caltech.

My parents have patiently encouraged and supported me during more than twenty years of school, and much of the credit for my successful completion belongs to them. Finally, I thank my wife, Flash, for moving to Pasadena and tolerating my eccentricities, especially during the final preparation of this thesis.

ABSTRACT

Convective overshooting and semiconvection in core-helium burning stars are studied with emphasis on laboratory experiments and terrestrial observations. A necessary condition for the onset of semiconvection is derived, and the Schwarzschild neutrality criterion for the semiconvective zone is justified. Six evolutionary sequences for horizontal branch stars in the globular cluster M3 are computed. They illustrate the effects of different treatments of overshooting and semiconvection, helium-burning nuclear reaction rates, and the primordial helium abundance Y_0. By comparing horizontal branch and red giant lifetimes with observations of the relative numbers of stars, the result $Y_0 = 0.20 \pm 0.04$ is derived for M3. This agrees well with results of standard Big Bang nucleosynthesis, but it is definitely smaller than the "normal" Population I helium abundance.

Evolutionary models for subdwarf B stars are computed which show excellent agreement with observed gravities and effective temperatures; subsequent evolution will probably match observations of subdwarf O stars. These models are burning helium at their centers with thin, inert hydrogen envelopes. The hypothesis of mass loss at the helium flash can explain the small envelope masses and the observed gaps in the color distribution of blue halo stars. An upper limit to the initial helium abundance of sdB stars is

derived from their light-to-mass ratios. The limit is

$Y_0 \leq 0.25 - 0.05 (\log Z + 2)$, and this limit is uncertain

by at least $\pm$ 0.10 because of the small sample size and

the possibility of systematic observational errors.

TABLE OF CONTENTS

1. INTRODUCTION

The metal-deficient stars of the galactic halo are generally thought to be the oldest stars in our galaxy. According to the conventional picture of galaxy formation (Eggen et al. 1962), the halo globular clusters formed just before the proto-galaxy collapsed into its present disk configuration. Thus, an important goal of observational and theoretical work is the deduction of globular cluster ages, for comparison with the Hubble time and the age of r-process elements. Cluster ages can be found only if the primordial helium abundance (by mass-fraction), Y_0, is known, because the lifetime of a hydrogen-burning main sequence star is very sensitive to Y_0. Y_0 is an interesting quantity in its own right because calculations of Big Bang nucleosynthesis predict helium production in the range $Y_0 = 0.2 - 0.3$. Table 1 summarizes recent measurements of Y_0.

The horizontal branch stars of globular clusters have been studied exhaustively by observers and theoreticians in order to determine Y_0. Since the pioneering work of Hoyle and Schwarzschild (1955), these have been identified as stars burning helium in their cores and hydrogen in thin shells at the base of hydrogen-rich envelopes. In prior evolution, a star moves off the main sequence as hydrogen is exhausted at its center, up the red giant branch, when hydrogen burns in a shell surrounding a degenerate helium core, and to the horizontal branch, after helium

ignites explosively in the core (the helium flash). When
helium is exhausted at the center, the star leaves the hori-
zontal branch and evolves along the asymptotic branch,
burning hydrogen and helium in two shells around an inert
core of carbon and oxygen. Detailed evolutionary computa-
tions by many workers have succeeded in reproducing most
observed characteristics of horizontal branch stars (see
Rood 1973 and Iben 1974). However, Y_0 (and therefore the
age of the galaxy) has remained uncertain by more than 30%.

Schwarzschild (1970) pointed out a serious error
in previously published models for horizontal branch stars.
Specifically, he showed that the central convective zone
must increase in size by overshooting; eventually, a "semi-
convective" zone of varying composition must appear between
the convective core and the exterior radiative zone of un-
burned helium. The nature of the mixing mechanisms and the
resulting structure of the semiconvective zone have remained
mysterious, and a controversy among different workers has
arisen over the proper treatment of these phenomena in model
calculations. These questions are resolved in Chapter 2.
In Chapter 3, six evolutionary sequences of theoretical mod-
els for horizontal branch stars are discussed. The major
effect of semiconvection is a large increase in the life-
time of a star in its horizontal branch phase. Using our
computed lifetimes, we derive an accurate measurement of
Y_0 : $Y_0 = 0.20 \pm 0.04$.

As a second application of our study of semiconvection, we present evolutionary models for subdwarf B stars in the last chapter. Recently, detailed observations of these faint, blue halo stars have been published, and previous workers have failed to match the observations with theoretical models because they neglected evolutionary effects and semiconvection. A subdwarf B star is a horizontal branch star which has lost most of its hydrogen envelope (probably during the helium flash), so that hydrogen burning makes a negligible contribution to the total luminosity. An upper limit to Y_0 is derived from the observations:

$$Y_0 \leq 0.25 - 0.05 \ (\log Z + 2) \pm 0.10.$$

It is consistent with our result for globular cluster stars but is very uncertain because of the difficulty of the observations.

2. CONVECTIVE OVERSHOOTING AND SEMICONVECTION

2.1. INTRODUCTION

One of the major unsolved problems of stellar evo-
lution theory is the redistribution of chemical elements
caused by moving boundaries of convective zones. Since a
reliable theory of turbulent convective motion is lacking,
a number of prescriptions have been used by different
workers, with varying degrees of justification on physical
grounds. After a brief description of these various ap-
proaches, this chapter will describe in detail the problems
of convective mass transport encountered in core helium
burning stars and will solve them subject to the limita-
tions imposed by our admittedly imperfect knowledge of the
hydrodynamics involved.

The classical treatment of interior convective
zones has been succinctly described by Schwarzschild
(1958). From the mixing-length theory, we know that the
lifetime of a convective eddy, τ_c, is many orders of mag-
nitude shorter than the timescale for nuclear burning, τ_N,
at least for the hydrostatic burning stages which we are
considering (see Despain 1975 for an example where this is
not the case.) Therefore, uniform composition within the
interior of a convective zone is an accurate approximation.
Schwarzschild recommended that the boundary of a convec-
tive core be located at a point where matter with the

interior composition satisfies the neutrality condition,

$\nabla_{rad} = \nabla_{ad}$, where $\nabla \equiv d \ln T/d \ln P$ and the subscripts in-
dicate radiative and adiabatic heat transfer. The pres-
sure and temperature vary smoothly across the boundary,
but the chemical composition, density and opacity may be
discontinuous. One of several problems may arise with this
prescription, simple and appealing as it is. First, ther-
mal buoyancy accelerates convective eddies all the way up
to the core boundary, and it is reasonable to assume that
they will overshoot by a finite amount, mixing with fluid
of the exterior composition. This overshooting leads to
observable differences in the evolutionary tracks of main
sequence stars (Prather and Demarque 1974; Maeder 1974)
and of horizontal branch stars. Second, in upper main se-
quence stars, a situation arises where fluid near the ex-
pected boundary may be stable with the interior composition
but unstable if given the exterior (unburned) composition.
Incomplete mixing gives rise to a sizable zone of varying
composition and uncertain stability; the lower opacity of
helium-rich interior fluid is the cause of this "semicon-
vection," which was discovered by Schwarzschild and Härm
(1958). A third problem is encountered if the neutrality
criterion applied with the interior composition leads to
an apparently unbounded increase in the size of the convec-
tion zone; that is, material adjacent to the convective
zone always becomes unstable if mixed with interior fluid.

Convective cores in horizontal branch stars and flash-
driven convective zones in helium-shell burning stars dis-
play this behavior (Christy-Sackmann 1975).

Clearly, a more careful treatment of mass transfer
at convective zone boundaries is needed. A diffusion ap-
proach has been suggested by Uchida et al. (1967) and by
Eggleton (1972). For each nuclear species, the mass frac-
tion X_i is required to satisfy

$$\frac{\partial}{\partial M} \left(\sigma \frac{\partial X_i}{\partial M} \right) = \frac{\partial X_i}{dt} + \left(\frac{\partial X_i}{\partial t} \right)_N, \qquad (2.1)$$

where M is the Lagrangian mass variable, t is time, and the
last term is the net production rate from nuclear burning.
The diffusion constant σ is a function of the superadia-
batic temperature gradient $\nabla_r - \nabla_a$ and is taken to be zero
in radiative zones. In a convective zone ($\nabla_r > \nabla_a$), it may
be estimated very crudely using flow speeds derived from
the local mixing-length theory. Eggleton has calculated
the evolution of a massive main sequence star and a hori-
zontal branch star, using the expression

$$\sigma = 10^4 \frac{M_*}{\tau_N} (\nabla_r - \nabla_a)^2. \qquad (2.2)$$

M_* is the star's total mass and τ_N the nuclear lifetime, as
before; they are introduced merely to give a "reasonable"
order-of-magnitude to the diffusion term. Semiconvection
appears naturally and his horizontal branch star shows
qualitative behavior similar to our evolutionary sequences

discussed in Chapter 3.

Two major objections may be raised to the diffusion approach. First, there is no quantitative physical basis for the value of σ shown. The Japanese workers have derived a more complex expression based on a transport theory of turbulent eddies traveling one mixing-length. However, numerical solution of the resulting equations appears to be very difficult (they report no results), and in any case the mixing-length theory is invalid near a zone boundary, where diffusion is most important. The second objection is that several additional difference equations corresponding to (2.1) must be solved simultaneously with the four stellar structure equations. In the Henyey method of solution (see Clayton 1968), the computer time necessary is roughly proportional to the cube of the number of equations multiplied by the number of mass zones in the star. Thus, the diffusion approach is exceedingly expensive, unless a solution of low accuracy is acceptable.

The treatment of convective mixing adopted in this work attempts to remedy the two shortcomings of the diffusion approach. Although it is neither simple nor elegant, it is built on physical models for mass transport and it is compatible with the Henyey method. Suppose that we are given a stellar model containing a convective core and perhaps a semiconvective zone with composition profiles computed according to any prescription; the model must

satisfy the four stellar structure equations. The next
step is to estimate the flow patterns which must occur in
the model, using whatever means are available -- the mixing
length theory, dimensional analysis, analogy with terres-
trial experiments and observations, etc. Thus the regions
of the model where compositions are changing can be identi-
fied, and timescales τ_c for the turbulent motions perform-
ing the mixing can be estimated. As noted above, the fluid
motions proceed much more rapidly than nuclear burning.
Therefore, the model is self-consistent only if its flow
patterns, when averaged over an intermediate timescale τ_{av},
distribute the elements present according to the composi-
tion profiles used in calculating those flow patterns.
Physically, τ_{av} represents the amount of time necessary for
the mixing to attain a stationary abundance distribution
$X_i(M)$, which evolves on a nuclear timescale τ_N.

Self-consistent models, in the sense defined above,
can be computed with a Henyey-type stellar evolution pro-
gram by an iteration method. An initial model for a given
time-step is extrapolated from the preceding time-step; it
is converted to a solution of the four structure equations
by the usual Henyey method, with no changes in the abun-
dances $X_i(M)$. Next, the consistency of the model is tested;
abundances are varied by a mixing algorithm to improve con-
sistency. A new model is calculated with the varied $X_i(M)$,
and the procedure is repeated until a prescribed level of

consistency is achieved. This consistent model is used to compute abundance changes from burning and to extrapolate to the next time step.

In the iteration procedure, the time dependences of $X_i(M)$ due to burning and mixing have been computed separately and independently. If this is to be an accurate technique, then the following inequalities must be satisfied:

$$\tau_c \ll \tau_{av} \ll \tau_N. \qquad (2.3)$$

The first says that details of the fluid motions may be ignored; collectively, they lead to a consistent model. The second says that burning does not change the integrated abundances over a time τ_{av}. Finally, we must require that the time step Δt be long enough for a consistent model to be established:

$$\tau_{av} \leq \Delta t. \qquad (2.4)$$

These inequalities must be checked throughout the calculation of an evolutionary sequence.

In this chapter, we will discuss in detail the types of mixing which occur in the cores of horizontal branch stars. In Section 2.2, the early, overshooting phase of evolution is discussed. The onset of semiconvection and the resulting zone of varying composition is described in Section 2.3. Our aim is to infer the general nature of the flow patterns present, to estimate τ_{av}, and

to derive the structure of the resulting consistent model.

2.2 THE OVERSHOOTING PHASE OF HORIZONTAL BRANCH EVOLUTION

Helium burning in the core of a horizontal branch star produces carbon and oxygen at temperatures and densities of approximately $10^{8\,\circ}K$ and 10^4 gm/cm^3. In unmixed regions outside of the convective core, the composition is nearly pure helium with a small fraction of ^{12}C (3% in our models) produced during the helium flash. For these values of temperature and density, the Rosseland mean opacity κ is dominated by free election scattering, which is independent of composition for He - C - O mixtures, and by free-free absorption (inverse bremsstrahlung by an electron in the Coulomb field of a nucleus). The free-free contribution to the opacity for the ion $^A Z$ is proportional to Z^2/A, and therefore the material of the convective core becomes increasingly more opaque than unburned matter outside the core.

Instability to convection occurs when the radiative temperature gradient ∇_{rad} exceeds the adiabatic ∇_{ad}, which is insensitive to the composition and very nearly equal to the ideal gas value, 0.4. The radiative gradient is given by

$$\nabla_{rad} = \frac{3}{16\pi acG} \cdot \frac{\kappa PL}{MT^4} \qquad (2.5)$$

where the independent variable M is the mass interior to

the point under consideration, a is the radiation pressure
constant, and all other symbols have their usual meanings.
Material which is stable initially with the unburned com-
position may become unstable if mixing with core material
increases its opacity enough. Furthermore, if hydrostatic
equilibrium is maintained during mixing, compression occurs
simultaneously because the mean molecular weight μ in-
creases; this also tends to increase the opacity. In early
computations of horizontal branch evolution (Faulkner and
Iben 1966; Iben and Rood 1970b), no mixing above the con-
vective core boundary was allowed, and consequently the
size of the convective core remained nearly constant during
evolution. To make consistent models, however, we must es-
timate the rate and extent of mixing by convective over-
shooting; if mixing is efficient, layers outside the core
will continually become unstable, and the core will march
outwards until mixing no longer causes a large enough opac-
ity change. This enlargement of the core significantly in-
creases the amount of fuel to be burned and lengthens the
horizontal branch lifetime of the star. These effects of
overshooting were first discussed by Schwarzschild and
Härm (1969; Schwarzschild 1970) and by Paczynski (1970).

Convective overshooting in a stellar core has been
studied in a laminar flow approximation by Saslaw and
Schwarzschild (1965) and in terms of the mixing-length
theory by Roxburgh (1965). Both of these treatments

ignored composition differences between core and exterior matter and are therefore irrelevant as we shall see below. Castellani et al. (1971a) repeated Roxburgh's analysis with composition effects included and derived an expression for the growth rate of the core essentially identical to ours below. The following argument justifies this result by comparison with terrestrial observations.

Laboratory experiments on highly turbulent convection in air and water (Townsend 1959, 1964; Turner 1973) have shown that most heat transport takes place via thermals, parcels of fluid with organized flow patterns which rise intermittently from a heated surface and travel to the top of the convecting layer; slow, disorganized descending currents are present to satisfy the continuity equation. Equations of motion for a single thermal have been derived and solved with successful interpretations of transport properties in the earth's and sun's atmospheres (Priestly 1959; Ulrich 1970; Nordlund 1974). The mixing length theory is a crude approximation to these treatments which predicts velocities in order of magnitude agreement. Our problem is to determine what happens when a thermal of known vertical velocity reaches the convective core boundary and encounters an environment of varying composition.

First, we assume that the composition change is discontinuous; this will be justified later. The buoyant force density on the thermal fluid is

$$F_b = -g(\rho_t - \rho_e) \equiv -g\delta\rho \qquad (2.6)$$

where ρ_t, ρ_e and g are the densities in the thermal and the environment, respectively, and the acceleration of gravity. Assuming subsonic velocities, P_e and P_t are equal; also, in convective cores (not atmospheres), both the thermal and the environment have nearly adiabatic temperature gradients, which implies T_e and T_t are approximately equal. Using the ideal gas law, we have

$$\frac{\rho_t}{\mu_t} = \frac{\rho_e}{\mu_e} \qquad (2.7)$$

and, therefore,

$$\frac{\delta\rho}{\rho_t} = \frac{\delta\mu}{\mu_t}. \qquad (2.8)$$

If a thermal penetrates into unburned matter (nearly pure helium), it feels an effective gravitational acceleration of $g\delta\mu/\mu_t$, which we call the "μ-barrier."

The vertical velocity of a thermal attempting to penetrate the μ-barrier is easily found from the mixing-length theory (as in Clayton 1968) to be, typically,

$$v = \left[\frac{\delta}{10} \cdot \frac{L}{4\pi r^2 \rho_t} \cdot \left(1 - \frac{\nabla_{ad}}{\nabla_{rad}}\right) \right]^{1/3} \qquad (2.9)$$

where δ is the ratio of mixing-length to pressure scale height. As with all results of the mixing length theory, this expression is uncertain by a factor probably not

exceeding ten; it should be evaluated at the point half a mixing-length from the core boundary. Inserting reasonable values for a horizontal branch core ($g = 10^7 cm/s^2$, $\delta\mu/\mu_t = 0.05$, $v = 2000$ cm/s), we find by equating kinetic and potential energies that a thermal could penetrate the μ-barrier by only 4 cm!

The μ-barrier is very hard, indeed, and this fact has been demonstrated experimentally. Saunders (1962) has studied the motion of thermals of dyed salt water dropped into a tank of fresh water on top and salt water below, separated by a sharp interface. They accelerate through the first layer and strike the barrier of dense lower fluid (denser than the thermal). When the penetration distance expected from the above reasoning is a small fraction of the thermal's size, no measurable penetration is seen; instead, the thermal flattens against the barrier, and its vertical flow is deflected into a shear flow parallel to the barrier. We may expect a similar shear flow boundary layer to occur in the stellar case, where the barrier is much stiffer than that of Saunder's experiment because of the large value of g. This shear layer is also present in laboratory convection with a solid upper boundary, as discussed by Kraichnan (1962) and Spiegel (1971).

Shear flow in a stratified fluid with a μ-barrier becomes turbulent when the Richardson number R_i is less than or equal to a critical value of order one (Richardson

1920; Turner 1973):

$$R_i \equiv -g\frac{\partial \ln\rho}{\partial r}\left(\frac{\partial v}{\partial r}\right)^{-2} \leq 1; \qquad (2.10)$$

here, v is the velocity parallel to the barrier, which is presumably of the same order as the vertical velocity of the thermal before reaching the barrier. This criterion leads to a rough estimate of the thickness h of the turbulent layer, namely,

$$h \simeq \frac{v^2}{g}\left(\frac{\delta\mu}{\mu_t}\right)^{-1}, \qquad (2.11)$$

which is the same very small distance (4 cm) obtained above. Surely, this represents an extreme lower limit to the extent of the mixing region; for example, gravity-wave oscillations of the barrier, excited by the thermal, may become unstable and generate more turbulence. Furthermore, the μ-barrier will not be perfectly spherically symmetric, and composition gradients transverse to r may lead to more mixing and widening of the partially mixed region. We can find the rate of expansion of the convective core v_{pen} by assuming (conservatively, again) that a distance h is added in one "turnover time," the travel time of a thermal from the center to the core boundary:

$$v_{pen} = \frac{hv}{r} = \frac{v^3}{rg}\left(\frac{\delta\mu}{\mu}\right)^{-1}. \qquad (2.12)$$

More useful is the rate of increase of core mass,

$$\dot{M}_{pen} = \frac{4\pi r\rho v^3}{g}\left(\frac{\delta\mu}{\mu}\right)^{-1}. \qquad (2.13)$$

This has been computed for several models of Chapter 3 and is shown in Table 3; the quantity $\dot{M}_{req}$ tabulated is the minimum rate of overshooting required to ensure convective stability on the inner side of the μ-barrier. We see that, at least for central helium abundance $Y_c > 0.6$, $\dot{M}_{pen}$ exceeds $\dot{M}_{req}$ by a large factor, and so this stability condition must be satisfied in a consistent model.

So far, the assumption has been made that the μ-barrier is a discontinuity, not a smooth transition zone. Can a situation like this evolve from an initial model with homogeneous core composition? In the initial model, buoyancy is caused by temperature differences only, and the above analysis is invalid. Shaviv and Salpeter (1973) have studied overshooting in this case using an ensemble of thermals to generalize the local mixing length theory; they find that overshooting will thoroughly mix a deceleration zone of thickness approximately 0.07 l (l = mixing length) above the point where $\nabla_{rad} = \nabla_{ad}$. This is confirmed by meteorological observations (Priestly 1959; Saunders 1962) and experiments in water (Abraham and Eysink 1969) where even larger penetrations are seen. Partial mixing will occur beyond the deceleration zone caused by the relatively rare thermals which penetrate further than average.

As nuclear evolution decreases Y_c, a μ-barrier develops in the partially mixed zone so that thermal buoyancy becomes negligible there. Also, the lower part of the

deceleration zone becomes unstable as κ rises, causing the partially mixed zone to move outwards. We can calculate a self-consistent composition profile by assuming that the penetration distance, Z, of a thermal is given by energy conservation:

$$\frac{1}{2}\rho_t v^2 = \int_0^Z g \, \delta\rho(Z') \, dZ' \qquad (2.14)$$

or

$$v^2(Z) = \int_0^Z \frac{2g\delta\mu(Z')}{\mu_c} \, dZ' \qquad (2.15)$$

where $\delta\mu(0) = 0$ and μ_c refers to core composition. If the velocity distribution $f(v)$ is given, then the probability of a thermal penetrating to height Z is

$$P(Z) = P[v(Z)] = \int_{v(Z)}^{\infty} f(v') dv' \qquad (2.16)$$

Thermals continuously exchange mass with their surroundings (Turner 1963), and this mixing may be crudely modeled by

$$Y(Z) = Y[v(Z)] = Y_c \, P(Z) + Y_e[1 - P(Z)], \qquad (2.17)$$

with similar equations for carbon and oxygen; $\delta\mu$ follows from (2.17). To impose self-consistency, rewrite (2.15) as

$$v^2(Z) = \frac{2}{\mu_c} \int_0^{v(Z)} g\delta\mu(v') \, \frac{dZ}{dv'} \, dv' \qquad (2.18)$$

and differentiate to obtain

$$\frac{dv}{dZ} = \frac{g\delta\mu(v)}{\mu_c v} \, . \qquad (2.19)$$

Given $f(v)$ and the core and exterior compositions, (2.19)

may be solved numerically to find $v(Z)$ and, using (2.17), $Y(Z)$.

Numerical solutions of (2.19) have been computed for all compositions of interest using the convenient velocity distributions

$$f_n(v) = \frac{(n+1)^{n+1}}{n!} v^n e^{-(n+1)v} \qquad (2.20)$$

for $n = 0$, 1, 3, and 8. The mean and variance are given by

$$\bar{v} = 1$$
$$\sigma_n^2(v) = (n+1)^{-1}. \qquad (2.21)$$

A fourth order predictor-corrector algorithm from Ralston (1965) was used. The integration must be started at a point where $Y = Y_c + \delta$ ($\delta \simeq 10^{-4}$), or else the exact solution $v = 0$, $Y = Y_c$ would be found. $Y(Z)$ is plotted in Figure 1 for the case $Y_c = 0.9$, $Y_e = 0.969$. Most of the transition occurs in a very narrow shell for every case studied; if ΔZ is the interval between $P(Z) = 0.10$ and $P(Z) = 0.90$, then a general result is

$$\Delta Z = \frac{C_n \bar{v}^2}{g} \left(\frac{\mu_c - \mu_e}{\mu_c} \right)^{-1} \qquad (2.22)$$

where C_n lies between one and three. This is essentially equal to the thickness of the shear flow layer given by (2.11). The region of initial rise, from $Y = Y_c + \delta$ to $Y_c + 0.1(Y_e - Y_c)$, is of comparable thickness; thermal buoyancy may compete with the μ-barrier here, but the

general result would be unchanged.

We have shown that the homogeneous initial model will evolve into a model with a very narrow μ-barrier above the deceleration zone. Therefore, the dimensional analysis leading to equation (2.11) for $\dot{M}_{pen}$ is correct as a lower limit, with one modification: v should be the speed at the top of the deceleration zone, which may be considerably less than the mixing length result (2.9). However, if $\dot{M}_{pen}$ should fall below $\dot{M}_{req}$, then the deceleration zone itself would become unstable, v would increase, and the enhanced overshooting would return the model to self-consistency. Each consistent model during the overshooting phase must have an adiabatic core of uniform composition extending a small fraction of a mixing-length beyond the point where $\nabla_{rad} = \nabla_{ad}$; the models of Chapter 3 show that the precise thickness of the deceleration zone is unimportant.

2.3 THE SEMICONVECTIVE PHASE OF HORIZONTAL BRANCH

EVOLUTION

From the discussion of the last section, it would appear that overshooting would cause the convective core to grow without limit. However, the structure of the core changes significantly when it exceeds a critical value, corresponding roughly to $Y_c = 0.6$. The radiative gradient ∇_{rad} passes through a minimum point and increases with M, implying greater instability at the top of the core; this

situation is sketched in Figure 2. Continued overshooting adds fresh helium to the core, reducing the opacity and eventually causing the vicinity of the minimum point of ∇_{rad} to become neutral. Subsequent behavior of the two convective zones will be discussed below, but clearly the evolution is qualitatively different from that during the overshooting phase. This termination of the overshooting phase was also discovered by Schwarzschild and Härm (1969; Schwarzschild 1970) and by Paczynski (1970). First, we shall derive a general criterion for the existence of a minimum in ∇_{rad} in a convective core. We assume the core is an ideal gas: partial electron degeneracy increases the pressure by about 10% over the ideal value, and radiation pressure is completely negligible in a horizontal branch core. Then the state variables obey the adiabatic relations

$$P = k\rho^{5/3} = k'T^{5/2}, \qquad (2.23)$$

where k and k' are constants. Furthermore, the opacity is fairly well approximated by the classical formula, electron scattering plus Kramers' law,

$$\kappa = \kappa_{es} + \kappa_0 \rho T^{-3.5}. \qquad (2.24)$$

Define a dimensionless temperature variable

$$t \equiv T/T_0, \qquad (2.25)$$

where T_0 will be chosen later, and let α be the ratio of Kramers to electron scattering opacity at the reference

point where $T = T_0$. Using (2.5), the radiative gradient may now be written, apart from a constant factor, as

$$\nabla_{rad} = LM^{-1}t^{-1.5}(1 + \alpha t^{-2}); \qquad (2.26)$$

L is constant away from the center and will be ignored. It is simple to show that a minimum will occur if the equation

$$\frac{\partial \ln t}{\partial \ln M} = -\frac{1 + \alpha t^{-2}}{1.5 + 2\alpha + 1.5\alpha t^{-2}} \qquad (2.27)$$

is satisfied within the convective core.

To clarify this result, rewrite the temperature derivative as

$$\frac{\partial \ln t}{\partial \ln M} = -\frac{2}{5} \cdot \frac{GM^2}{4\pi r^4 P} = -\frac{2}{5}\frac{V}{U}, \qquad (2.28)$$

where the "homology invariants" U and V are defined by (Schwarzschild 1958)

$$U = \frac{4\pi r^3 \rho}{M}$$
$$\qquad (2.29)$$
$$V = \frac{\rho}{p} \cdot \frac{GM}{r} \cdot$$

Choosing T_0 to be the temperature at the minimum point, the criterion (2.27) becomes

$$\frac{3V}{5U} = \frac{1 + \alpha}{1 + 7/3\alpha}. \qquad (2.30)$$

For any star made of adiabatic ideal gas, V/U increases monotonically from 0 at the center to ∞ at the surface, and α increases monotonically throughout the core. Therefore, any sufficiently large convective core (large in

dimensionless variables, i.e., homology invariants) will
have one minimum point of ∇_{rad}, and no local maximum be-
yond it; the dilemma of an ever-increasing convective core
is a general phenomenon, not caused by, say, peculiarities
of a given opacity table. To understand this result phys-
ically, observe that radiative energy flux is determined by
the gradient of radiation pressure. In an adiabatic core
dominated by gas pressure, P_{rad}/P decreases rapidly away
from the center; if the core extends far enough, the energy
flux decreases relatively slowly, and an ever-larger loga-
rithmic gradient of P_{rad} is required to carry the flux.
Note that this can occur even for a constant opacity:
P_{rad}/P is the determining factor.

   This minimum is never reached in hydrogen-burning
convective cores because they are not large enough in di-
mensionless extent. Table 4 illustrates this, using models
from Kushwaha (1957), which were computed using the input
physics assumed above; more recent models would show the
same general behavior. The accuracy of criterion (2.30)
for helium-burning cores is shown in Table 5, using our
models of Chapter 3. We can also understand why the loca-
tion of the minimum, M_{min}, changes so little during evolu-
tion. The value of α is nearly constant because the
effects of higher temperature and higher ionic charges tend
to cancel in the Kramers opacity; thus, M_{min} corresponds
to the same value of $3V/5U$ throughout evolution. From

Chandrasekhar (1939), we know that the mass at a given value of dimensionless extent (U or V) is proportional to $\rho_c^{-2} P_c^{3/2}$. This is nearly constant, as shown in the table, and so M_{min} is constant. Another statement of this result is that the structural evolution of the core is well approximated by uniform expansions and contractions, for which $\rho(M)^{-2} P(M)^{3/2}$ and M(U) are precisely constant.

We return now to the problem of the structure of the second unstable zone when overshooting has extended the core boundary beyond M_{min}. Castellani et al. (1971b) argue that overshooting at the top of the second zone will continually increase its helium abundance, causing its lower boundary to move outwards as the opacity drops. The overall result is a convective core extending slightly beyond M_{min} (because of the deceleration zone), an intermediate zone of varying abundances which is approximately neutrally stable, and a small convective zone at the top, too feeble to overshoot appreciably into the large μ-barrier. By some unspecified mixing mechanism, helium is transported through the intermediate semiconvective zone to the core on a nuclear timescale, causing the point M_{min} to remain neutrally stable and the intermediate zone to grow. This is a consistent model only if the mysterious mixing process proceeds at a precise rate determined by the nuclear evolution of the core, an assumption which has led to some skepticism (e.g., Rood 1973). We should also mention that

semiconvection in massive main sequence stars (mentioned in Section 2.1) is caused by an entirely different mechanism, the higher opacity of unburned matter; the terminology has led to some confusion such as Mitalas' (1973) statement that semiconvection can never occur in horizontal branch stars. We propose a slightly different structure for the semiconvective zone which guarantees mixing of helium into the core at the required rate. Consider a series of small, fully convective zones separated by narrow radiative regions and/or sharp μ-barriers; the helium abundance $Y(M)$ has a staircase shape as shown in Figure 3a. These zones move outwards on an overshooting timescale, occasionally merging with one another; the time average of $Y(M)$ over an intermediate timescale will be identical with Castellani's model. If the deceleration zone above M_{min} becomes unstable, it will engulf the adjacent zones, eventually neutralizing M_{min} as Y_c increases; a new, small zone above M_{min} will be formed with slightly lower Y than before. Should too much helium be mixed into the core so that M_{min} becomes stable by a finite amount, then no further mixing will occur until burning causes a large enough opacity rise to destabilize M_{min}. Clearly, this "bucket brigade" of small convective zones can impose neutrality at M_{min} quite precisely, by adding small amounts of helium to the core at each mixing.

The proper gradient of Y (time-averaged) in the

semiconvective zone is not immediately clear from the above
discussion. First we will discuss this problem for
Castellani's (incorrect) model with a continuous abundance
distribution, because there is great confusion on this
point in the literature: see Spiegel (1969) for a review.
The Schwarzschild (1906) criterion for neutral stability
against convective mixing is $\nabla_{rad} = \nabla_{ad}$; this means that a
parcel of fluid displaced adiabatically from its initial
position remains at the same temperature as its surround-
ings. In a region where μ decreases outwards, the parcel
will suffer a buoyant restoring force from the μ-barrier.
Ledoux (1947) suggested that mixing will not occur unless
this buoyant force is zero, and the correct criterion is
equal density of the parcel and its environment:

$$\nabla_{rad} = \nabla_{ad} + \frac{\beta}{4 - 3\beta} \frac{d \log \mu}{d \log P}, \qquad (2.31)$$

where β is the ratio of gas to total pressure. However, a
parcel displaced in a Ledoux-stable environment will oscil-
late about its origin with increasing amplitude, because
heat flow near the turning points tends to increase the
buoyant restoring force above its initial value. This
overstability has been analyzed by Moore and Spiegel (1966)
and Baines and Gill (1969), among others. The latter au-
thors show that growing oscillations will occur in the
stellar case if the Schwarzschild criterion is exceeded by
a tiny amount,

$$\nabla_{rad} \geq \nabla_{ad} + O(10^{-5})\frac{d \log \mu}{d \log P}. \qquad (2.32)$$

The effectiveness of these oscillations in causing mixing, however, is not apparent.

Fortunately, these problems have been studied intensively because of their importance in oceanography and meteorology (Turner 1973). Shirtcliffe (1967; 1969a; 1969b) prepared a tank of salt water with a Ledoux-stable density gradient (salt concentration decreasing vertically); it was then heated from below to become Schwarzschild-unstable. The initial oscillations rapidly changed to fully developed convection which occurred in a series of well-mixed layers and persisted throughout the experiment; layering occurred so rapidly that the oscillations were difficult to observe and were not seen in the first experiment of this type by Turner and Stommel (1964). When averaged over the layers, the density gradient always remained Ledoux-stable. These results show that local mixing will occur if the Schwarzschild criterion is violated by a tiny amount, and a bucket brigade structure will result. In the stellar case, helium (analagous to cool, fresh water) is continually added from the top of the semiconvective zone and carried down by mixing between adjacent layers; therefore, we expect that the average composition profile will satisfy the Schwarzschild criterion very accurately.

Another interesting confirmation of our model of

the semiconvective zone is provided by the observations of Lake Vanda, Antarctica, by Wilson and Wellman (1962) and Hoare (1966), which stimulated Shirtcliffe's experiments in the first place. This is an ice-covered, brackish lake with no outlet; heating by solar radiation causes an unstable temperature gradient which opposes the Ledoux-stable density gradient due to dissolved salt. The layered structure of the resulting semiconvection is shown in Figure 4, reproduced from Hoare. Remarkable persistence of this configuration is shown by the excellent agreement of observations made four years apart. Turner (1973) mentions examples of semiconvective zones observed beneath Arctic ice islands and other brackish lakes. If a solar thermometer can be built deep in a South Dakota gold mine, then perhaps it is not so surprising that the assay of the Big Bang is to be found in an Antarctic lake!

Our model for "normal semiconvection" has a homogeneous adiabatic core extending to M_{min}, where it is neutrally stable, a small homogeneous deceleration zone, a semiconvective zone obeying the Schwarzschild criterion, and a second fully convective zone overshooting into unburned matter through a sharp μ-barrier. We assume that each layer in the semiconvective zone is a small fraction of the entire zone; this may not be true (see Figure 4), but we have no quantitative basis for an alternative in the stellar case. One final problem remains; the overshooting

rate $\dot{M}_{pen}$ of the second convective zone may be insufficient to provide helium to stabilize M_{min} and the semiconvective zone. If so, the semiconvective zone will not develop, and the two convective zones will exchange matter through a small region near M_{min} which is approximately neutral. This structure is shown schematically in Figure 3. The evolutionary track HB2 of Chapter 3 has been computed with this structure. Table 3 compares the overshooting rate of the upper convective zone in these models with the minimum rate needed to establish normal semiconvection. For a brief period after M_{min} is reached at $Y_c = 0.6$, the rates are comparable, but normal semiconvection will certainly be established and maintained for $Y_c \leq 0.45$. Other aspects of this model sequence will be discussed in Chapter 3.

3. EVOLUTION OF HORIZONTAL BRANCH STARS

3.1. INTRODUCTION

Six evolutionary sequences of models for horizontal branch stars have been computed. The purposes are: to determine the effects of overshooting and semiconvection, previously neglected by Iben and Rood (1970b), on observable characteristics of horizontal branch stars; to see whether models consistent in the sense of Section 2.1 can be made during all stages of horizontal branch evolution; to assess the effects of the revised helium-burning reaction rates (Fowler et al. 1975) on the models; and, to set limits on the primordial helium abundance of globular cluster stars. We also note that the Yale University stellar evolution group of P. Demarque has concurrently been studying horizontal branch evolution (Sweigart and Gross 1974 and references therein); comparison with their results gives confidence in our (common) fundamental assumptions about globular cluster stars and also points out remaining uncertainties in the details of horizontal branch evolution.

The defining characteristics of the sequences HB1 – HB6 are given in Table 2. Each star's total mass M_* (solar mass units), helium core mass M_c, initial helium abundance Y_0, and heavy element abundance Z are chosen to represent typical stars in the extensively observed cluster M3, according to the most reliable estimates available (Rood

1973). Normal semiconvection, assumed for HB1, HB3 and HB4 was described at length in Section 2.3; HB2 uses the double convective zone model mentioned at the end of that section. Sequence HB5 terminates at the end of the over-shooting phase; it employs a finite size for the deceleration zone, which is neglected in the other models. HB6 is computed with precisely the same methods as those of Iben and Rood (1970b), i.e., with no allowance for overshooting or semiconvection, and is directly comparable with their models.

Each evolutionary sequence is a solution of the time-dependent stellar structure equations:

$$\frac{dP}{dM} = \frac{-GM}{4\pi r^4} \; ; \qquad (3.1)$$

$$\frac{dr}{dM} = \frac{1}{4\pi r^2 \rho} \; ; \qquad (3.2)$$

$$\frac{dL}{dM} = \varepsilon_N + \varepsilon_g ; \qquad (3.3)$$

$$\frac{dT}{dM} = \frac{dP}{dM} \cdot \min(\nabla_{ad}, \nabla_{rad}) \cdot \qquad (3.4)$$

Here, M is the mass interior to r (spherical symmetry is assumed); ε_N is the nuclear energy generation rate per unit mass, and ε_g is the gravitational counterpart, given by

$$\varepsilon_g = -T \frac{dS}{dt}$$

$$= -c_P \frac{dT}{dt} - T \left(\frac{\partial S}{\partial P}\right)_T \frac{dP}{dt} \; , \qquad (3.5)$$

where S is the entropy per unit mass and c_p is the specific heat at constant pressure. The equations for composition changes (expressed as mass fractions),

$$\frac{dX_i(M)}{dt} = \left(\frac{\partial X_i}{\partial t}\right)_{Nuc} + \left(\frac{\partial X_i}{\partial t}\right)_{Mix} \qquad (3.6)$$

are solved simultaneously with the structure equations; the terms on the right hand side represent changes caused by nuclear burning and mixing, respectively, and are described in detail in Section 3.2 and Appendix B. Typically, about 150 time-steps are included in each evolutionary sequence. At each time step, the solution is a table of the dependent variables P, T, L, r, and X_i evaluated at approximately 400 values of M between the center and surface.

Computer programs for calculating initial stellar models and evolutionary sequences were most generously provided to the author by Dr. R. T. Rood. They were written by Dr. I. Iben, Jr., and Dr. Rood between 1964 and 1971 and have been used in several important studies of stellar evolution (see Iben 1967, 1974). Input physics and numerical methods are described in Appendices A and B. The author's contributions are the addition of important mixing algorithms to make self-consistent horizontal branch models and numerous minor changes to ensure convergence, improve accuracy, update reaction rates, etc.

In the next section, we describe the mixing algorithms in detail. The structure and observable

characteristics of the models are discussed in Section 3.3,
with emphasis on the effects of overshooting and semicon-
vection. Problems in the construction of consistent models
near core-helium exhaustion (Y_c < 0.08) are treated in Sec-
tion 3.4. Finally, we derive the primordial helium abun-
dance and discuss its uncertainty in the last section.

3.2. MIXING ALGORITHMS

Self-consistent models are calculated by the iter-
ation procedure described in Section 2.1. Figure 13 is a
flowchart of the operations at each time-step. During the
overshooting phase, the algorithm is very simple, and two
passes always produce consistency. The algorithm examines
points outside the convective core boundary and decides
whether or not they will become unstable if given core com-
position by overshooting. A neutral opacity κ_N is computed
for each point by the relation

$$\kappa_N(M) = \frac{\nabla_{ad}\, \kappa(M)}{\nabla_{rad}(M)} ;$$

(3.7)

here, ∇_{ad} is the adiabatic gradient just inside the core
boundary. If the opacity at point M after complete mixing
with the core exceeds $\kappa_N(M)$, then the Schwarzschild cri-
terion for instability is satisfied, and the mass zone
centered on M is added to the convective core.

To estimate the change in $\kappa(M)$ after mixing, we
consider composition and density effects. Derivatives of

κ with respect to composition are routinely computed and stored for each point, and we have

$$\Delta\kappa(M) = \sum_i \left(\frac{\partial\kappa}{\partial X_i}\right)_{\rho,\ T} [X_{ic} - X_i(M)]; \qquad (3.8)$$

^{4}He, ^{12}C and ^{16}O are included in the summation. For density effects, we assume the classical formula

$$\left(\frac{\partial\kappa}{\partial\rho}\right)_{T,\ X_i} = \frac{\kappa - 0.20}{\rho}; \qquad (3.9)$$

exact evaluation of the derivative from the opacity tables is slower and no more accurate for this purpose. The equation of state is

$$P = \frac{\alpha\rho}{\mu}\, RT, \qquad (3.10)$$

where the factor α represents the extra pressure due to partially degenerate electrons ($\alpha = 1.1$, typically). P changes very little after mixing because hydrostatic equilibrium must be maintained, and changes in T are also found to be small. Thus the density change $\Delta\rho$ is

$$\frac{\Delta\rho}{\rho(M)} = \frac{\alpha(M)\mu_c}{\alpha_c\mu(M)} - 1. \qquad (3.11)$$

The final criterion for mixing the point M into the core is, in obvious notation,

$$(1 + \delta)\ \kappa_N(M) \leq \kappa(M) + \sum_i \partial_i\kappa\ \Delta X_i \qquad (3.12)$$
$$+ [\kappa(M) - 0.2]\left(\frac{\alpha\mu_c}{\alpha_c\mu} - 1\right).$$

The tolerance δ prevents excessive mixing and is equal to

0.003 and 0.0007 on the first and second passes through the mixing algorithm, respectively. Occasionally, when a shell is found to be radiative ($\nabla_{rad} < \nabla_{ad}$) after mixing, it is removed from the adiabatic core and given exterior abundances again. Mass shells outside the boundary are thinner than 0.2% of the convective core mass M_{cc}, and so the neutrality criterion is always satisfied at the boundary to an accuracy better than 0.1%.

No deceleration zone is allowed in the above algorithm. In all models of HB5, the convective core extends a distance 0.05 H_p beyond the point where $\nabla_{rad} = \nabla_{ad}$; H_p is the pressure scale height at that point. The adiabatic gradient is used in the deceleration zone, following the treatment of Shaviv and Salpeter (1973). The only noticeable difference between HB5 and HB1 is that semiconvection appears at a slightly higher value of Y_c in the former, but the core masses M_{cc} are identical at this point. Typically, the deceleration zone contains 0.008 $M_\odot$ or less than 10% of M_{cc}.

Semiconvection is recognized when the minimum of ∇_{rad} occurs several zones inside the core boundary. The overshooting algorithm is discontinued, and abundances in the core and the semiconvective zone are calculated by techniques similar to those of Robertson and Faulkner (1972).

Helium burning during each time-step raises the opacity of the core, causing the point M_{min} to be unstable at the start of the mixing algorithm. Usually, much of the semiconvective zone is also superadiabatic. The neutral opacity, $\kappa_N(M)$ (the opacity for which $\nabla_{rad} = \nabla_{ad}$), is computed for each point using (3.7). We want to compute the "neutral helium abundance" $Y_N(M)$ (the abundance for which $\kappa = \kappa_N$). If the convective core is given the abundance $Y_N(M_{min})$ and if each point M in the semiconvective zone is given $Y_N(M)$, then the core boundary M_{min} and the entire semiconvective zone will have $\nabla_{rad} = \nabla_{ad}$ within a given tolerance. The detailed discussion of Section 2.3 showed that this is the correct criterion for a consistent model. $Y_N(M)$ is most easily computed by assuming that the final (post-mixing) ratio $S \equiv X_{16}/X_{12}$ is given. Then we find from (3.12) that

$$Y_N(M) = \frac{(1 + \delta)\kappa_N - \kappa + D}{B_4 + \dfrac{B_{12}}{1 + S} + \dfrac{SB_{16}}{1 + S}} ,$$

$$D = B_4 Y + B_{12}\left(X_{12} - \frac{1}{1 + S}\right) + B_{16}\left(X_{16} - \frac{S}{1 + S}\right).$$

(3.13)

In these equations, δ is the tolerance defined after (3.12); Y, X_{12} and X_{16} are the abundances at M before mixing; and B_i is the total derivative of κ with respect to X_i, upon mixing:

$$B_i = \left(\frac{\partial \kappa}{\partial X_i}\right)_{\rho, T} + \frac{(\kappa - 0.2)}{\mu} \frac{\partial \mu}{\partial X_i} . \qquad (3.14)$$

Degeneracy is neglected because only small changes in abundances are made.

In principle, (3.13) evaluated at $M = M_{min}$ gives the value of Y_c which will neutralize M_{min}. In fact, it is not always accurate, and we use instead the lesser of $Y_N(M_{min})$ and

$$Y_N' = Y_c + A[(\nabla_{rad}/\nabla_{ad})_{min} - (1 + \delta)]. \qquad (3.15)$$

The slope A was found by trial and error and is varied between 0.8 and 1.0 as evolution proceeds. When Y_N' is used, values of Y_N for points near M_{min} are adjusted slightly to ensure a smooth composition profile.

Equations (3.13 - 15) enable us to compute the abundances at each point necessary for a consistent model. The mixing algorithm sets these abundances, maintaining exact conservation of nuclei, and determines the extent of the semiconvective zone. An imaginary reservoir of mass M_r is created by mixing mass zones beyond M_{min} with the convective core, one at a time; reservoir abundances are updated every time a zone is added:

$$X_{ir} = \frac{1}{M_r} \int_0^{M_r} X_i(M) dM. \qquad (3.16)$$

As soon as the helium abundance of the reservoir exceeds the neutral helium abundance for M_{min}, core abundances are set equal to those of the reservoir for all nuclei, and M_{min} is subtracted from M_r; core abundances are also given

to the first few mass zones beyond M_{min} to simulate the deceleration zone, and its mass is subtracted. Thereafter, each mass shell above the deceleration zone is neutralized in turn. $Y_N(M)$ is calculated, using the oxygen-to-carbon ratio of the reservoir; if $Y_N(M) > Y_r$, zones are mixed into the reservoir, increasing Y_r. Eventually, Y_r exceeds $Y_N(M)$ and reservoir abundances are given to the shell centered on M, and the process repeats to neutralize the next shell at $M + \Delta M$. When the size of the reservoir shrinks to zero (the last zone neutralized is also the last zone to have been mixed into the reservoir), the upper boundary of the semiconvective zone M_{sc} has been reached; a jump in Y to the unburned value (0.969) is left here. In practice, the last several zones have uniform composition and represent the fully convective region which provides fresh helium for the whole process by overshooting.

Two iterations of this procedure at each time-step provide acceptable consistency as long as $Y_c > 0.08$. When $Y_c < 0.08$, it is not always possible to make a consistent model for reasons discussed in Section 3.4. The convective core boundary at M_{min} always satisfies

$$| \frac{\nabla_{rad}}{\nabla_{ad}} - 1 | < 0.001; \qquad (3.17)$$

the residual error rises gradually throughout the semiconvective zone, occasionally becoming as large as 0.01 at the

outermost point, M_{sc}. Figure 5 shows $Y(M)$ and ∇_{rad}/∇_{ad} in the semiconvective zone of HB1 when $Y_c = 0.353$. The adiabatic temperature gradient is used for $M < M_{sc}$, with a discontinuous change to ∇_{rad} at that point. Fine zoning is crucial in and around the region of varying composition. We require that $\Delta M < 0.0025M$ near M_{min} and that Y change by less than 0.015 from point to point in the entire semiconvective zone. Near M_{sc}, ΔM is limited by the constraint

$$\frac{0.969 \, \Delta M + Y_c M_{min}}{\Delta M + M_{min}} < Y_c + 0.0004; \qquad (3.18)$$

the purpose is to ensure that the reservoir helium abundance does not change too much when one shell of unburned helium is added to it.

The above algorithm is the normal treatment of semiconvection. In models of HB2, the same procedure is followed until the point M_{min} is neutralized, $Y_r \geq Y_N(M_{min})$. Then reservoir abundances are given to every point M, $0 \leq M \leq M_r$, so that we have two fully convective zones, with identical abundances, in the intervals $(0, M_{min})$ and (M_{min}, M_r). As before, the point M_{min} is neutral to an accuracy of 0.1%.

3.3. PROPERTIES OF THE EVOLUTIONARY SEQUENCES

Once the mixing algorithms have been chosen (and debugged!), it is straightforward to compute consistent models as long as $Y_c \geq 0.08$. Summaries of the interior and

surface properties of all six sequences are given in Tables
6 - 17. At this point, the reader is urged to look briefly
at Tables 6 and 7 to familiarize himself with the important
physical properties of horizontal branch stars. The
Hertzsprung-Russell diagram is shown in Figure 6; there are
no surprises here. Although overshooting and semiconvection
cause a longer track in log T_e, none of the tracks covers as
wide an interval as observed in M3 or M5. Rood (1973) has
shown that a dispersion in total mass (or core mass) is al-
ways necessary to fit the observed H-R diagram, and the de-
tailed shape of the track is not important for this purpose.
In Figure 7, we see the straight evolutionary tracks in the
log g - log T_e plane, which are quite sensitive to the
initial helium abundance. Gross (1973) has used this fact
to determine that $Y_0 \geq 0.30$, using initial models which
agree well with ours. As we shall see in Chapter 4, the
possibility of systematic errors in the observed values of
log g renders this result uncertain by perhaps $\pm$ 0.10.

We will discuss the physical reasons for differences
among the sequences, without repeating all the details of
the interior evolution, well summarized in Iben and Rood
(1970b). HB1 is our standard star, and HB5 is virtually
identical in all properties: the only importance of the
deceleration zone is that no superadiabatic gradient can be
allowed at the core boundary. Exploratory models of
Sweigart and Gross (1974) and of Castellani et al. (1972)

computed using $\nabla_{rad} > \nabla_{ad}$ at the boundary cannot give accurate lifetimes.

Comparing HB6 (no overshooting) with HB1, we see that the obvious effect of internal mixing is to increase the horizontal branch lifetime t_{HB} by at least 75% because additional fuel is made available. The helium core luminosity, L_{He}, is also larger in HB1, by about 50% at $Y_c = 0.1$, because of the higher central temperature. Burning at high temperature in HB1 decreases the final ^{12}C abundance and enhances the longer lifetime because the reaction $^{12}C(\alpha, \gamma)^{16}O$ yields three times as much energy per ^{4}He nucleus consumed as the triple-alpha process.

Turning to the surface properties, we see that both stars evolve toward higher T_e for $0.8 > Y_c \gtrsim 0.3$; HB1 spends more time in this phase and thus its maximum value of $\log T_e$ is greater by 0.028. The central density is actually decreasing during this phase of HB1, and the star obeys the "rule of thumb" that central expansion implies surface contraction, and vice-versa. Redward evolution begins when central density rises to maintain energy generation. HB1 displays surface expansion and contraction for roughly equal lengths of time, and this fact may be reflected in the observed period changes of cluster variables. The pulsation period P obeys

$$P = kM_*^{-1/2}R_*^{3/2}, \qquad (3.19)$$

where k is constant for a given mode (fundamental or first harmonic). Nearly equal numbers of positive and negative period changes dP/dt are observed for M3. Although HB1 is too blue to pulsate, slightly more massive models would trace out similar loops in the instability strip.

HB4 uses new reaction rates (Fowler et al. 1974) and intermediate screening (DeWitt et al. 1973) for which $\varepsilon_{3\alpha}/\varepsilon_{412}$ is increased by a factor of about three compared with the old rates (see Appendix B). This causes a lower L_{He} and shorter t_{HB} for two reasons: less ^{16}O is produced, implying less energy liberated per ^{4}He; and, the semiconvective zone is smaller because of the decreased opacity of burned matter. Semiconvection appears later, at $Y_c = 0.575$ (Table 5), in HB4, again an opacity effect. Its track in the H-R diagram shows a much smaller variation in $\log T_e$ (.044 vs. .079), partly because of the shorter lifetime, and occurs at systematically lower luminosity.

At the end of Section 2.3, we noted that the models of HB2 are not self-consistent for $Y_c \lesssim 0.45$; they are still interesting for comparison. The surface characteristics are indistinguishable from those of HB1. Surprisingly, in the interior, the mass of the second convective zone is greater than or equal to the mass of the semiconvective zone in HB1; inefficient overshooting in the second zone provides more fuel to burn than the efficient overshooting assumed in HB1! Naturally, this lengthens

t_{HB}, although the effect is partially cancelled by a larger L_{He}. This result is also relevant to the uncertainty introduced by the unknown sizes of the "bucket brigade" convective zones which comprise the normal semiconvection model; it suggests that t_{HB} may increase if only a few of these zones are present. If a sequence were computed using the Ledoux criterion in the semiconvective zone, its helium distribution $Y(M)$ would lie between the curves of HB1 and HB2; thus its lifetime would be bracketed by the results for these two sequences.

Finally, we come to the effects of the initial helium abundance, seen by comparing HB1 and HB3. The major change is a larger value of M_c for lower Y_0; M_c is assumed to be the critical helium core mass at the core flash, computed by Rood (1972). The hydrogen shell source weakens because it is further out in the star and because μ is smaller in the envelope, both causing lower values of T and ρ at the shell; therefore, L_H and log L are lower in HB3. In the H-R diagram, HB3 remains nearly stationary during the overshooting phase and then moves redward; it shows no observable differences from the tracks in Iben and Rood (1971).

The lifetime of HB3 is only slightly (4%) shorter than that of HB1, and it is interesting to see why. Our result implies $t_{HB} \propto M_c^{-1.7}$ whereas Rood (1973) assumed $t_{HB} \propto M_c^{-4}$, derived in the following way. It is natural to

compare the evolution of the helium core with that of a pure helium main sequence star. For the latter, t_{MS} α EM_{cc}/L, where E is the energy released per ^{4}He burned, which is constant if all stars have the same final ^{16}O abundance. The homology relation for pure helium stars is roughly L α $\bar{\mu}^{-4}M^5$, where $\bar{\mu}$ is the mass-averaged mean molecular weight, and Rood's result follows, assuming M_{cc} lies at a fixed mass-fraction. In our cores, however, the fuel supply is determined by M_{sc}, and this is identical in HB1 and HB3 because it is determined by the local properties of the opacity. Furthermore, $L_{He}(3)$ approaches $L_{He}(1)$ rather closely for $Y_c \lesssim 0.5$, and so the weaker dependence is explained.

We can generalize this result by applying the homology relation to the mass interior to M_{sc}. In Figures 8 and 9, log L_{He} is plotted against log M_{sc} and log $\bar{\mu}$, respectively, for HB1 - 4. We see that HB1, HB2 and HB4 define a common, homologous curve, and HB3 approaches this curve asymptotically from above. This suggests that all cores evolve through the same structural sequence in terms of these variables. Then the lifetime in the semiconvective phase is determined by the rates of increase of M_{sc} and $\bar{\mu}$; therefore, the critical variables are the stability criterion in the zone and the rate of ^{16}O production by ^{12}C(α, γ)^{16}O, which determines $\bar{\mu}$ and the local opacities.

We can make the sweeping conjecture that all evolutionary sequences, computed with a given stability criterion and reaction rates, will have nearly the same t_{HB}; naturally, a weaker dependence on M_c remains, because L_{He} does not relax immediately to the common curve.

We can compare our results with those of other workers to check the validity of our conjecture. Evolutionary sequences with some treatment of semiconvection have been published by Paczynski (1970), Castellani et al. (1971b, 1972), Robertson and Faulkner (1972), Eggleton (1972), and Sweigart and Gross (1974); of these, only the last authors present detailed results for comparison with globular cluster stars. Earlier papers by the Yale group (Demarque and Mengel 1972; Sweigart and Demarque 1972a) represent early stages of program development and will not be compared here. Sequence S of Sweigart and Gross has initial parameters (M_*, M_c, Y, Z) of (0.66, 0.475, 0.30, 0.001); in general, its interior evolution is similar to our HB1 or HB3. Its lifetime at $Y_c = 0.1$ is 96.3 (10^6 years) compared with 91.8 and 87.6 for HB1 and HB3. In their reaction rates, $\varepsilon_{3\alpha}/\varepsilon_{412}$ has a value 1.20 compared to our old rates. If we interpolate $t_{HB}(S)$ to the rates and core mass of HB1 (this procedure will be described in detail in Section 3.5), the result is 93.9, a discrepancy with $t_{HB}(1)$ of only 2.3%. The uniform nature of semiconvective evolution is apparent, although certain differences

remain. As shown in Table 5, semiconvection appears earlier in sequence S; the homology invariants show that opacity differences are at least partly responsible. Also, M_{sc} is slightly larger in their models, partly because we allow a small convective zone just below M_{sc}; this probably accounts for the residual difference in t_{HB}.

3.4. PROBLEMS NEAR CORE HELIUM EXHAUSTION

In the sequence HB1, it becomes very difficult to make self-consistent models with our mixing algorithms when $Y_c \leq 0.061$. Up to four iterations of the mixing algorithms were tried, and after each iteration the following results appeared: ∇_{rad}/∇_{ad} at the core boundary increased from the previous iteration; M_{min} increased; T_c decreased; ε_N became less centrally concentrated, but L_{He} still increased. Occasionally, the point M_{min} could be neutralized if M_{sc} was increased, mixing stable fluid into the semiconvective zone. Clearly, the local opacity near M_{min} no longer determines the mixing rate; we will call this phenomenon the composition instability. It also occurred in HB3 and HB4 at $Y_c = 0.063$ and 0.073, respectively. In HB2, Y_c became constant in time and M_{min} rather erratic at $Y_c = .040$. Sweigart and Demarque (1972b) have studied this instability in more detail, finding it at $Y_c = 0.12$ in a sequence with $\varepsilon_{412} = 0$. They impose a perturbation on Y_c, growing on an overshooting timescale as the core mixes into the

semiconvective zone; for $Y_c \le 0.12$, this leads to a similar growth of ∇_{rad}/∇_{ad} at the core boundary. The entire semi-convective zone is mixed in about 10^6 years, causing rapid evolution to the blue and adding several million years to t_{HB}, before Y_c reaches 0.12 again by means of nuclear burning. This situation is reminiscent of Shirtcliffe's (1969b) experiments (see Section 2.3), where a tank of stable salt water was heated from below. He observed a well-mixed convective layer form at the bottom, whose upper boundary rose as overlying fluid became unstable. In the terminology of Section 2.1, the composition instability prevents the construction of a consistent model because the intermediate timescale no longer exists. Mixing on an overshooting time-scale causes simultaneous structural changes, and no time-averaged composition profile can be defined. The instability is caused by the sensitive (Y^3) dependence of $\varepsilon_{3\alpha}$ on composition and does not occur if Y^2 dependence is artificially imposed (Demarque 1975); this explains the different critical values of Y_c found because of different reaction rates.

Our first attempt to treat the composition instability was to ignore it, hoping that dominance of ε_N by $^{12}C(\alpha, \gamma)^{16}O$ would suppress it quickly. Models were made stable by increasing M_{sc}, still allowing only two iterations per time-step. This was a failure: after Y_c reached 0.025, it rose rapidly anyway. Our second attempt is more

realistic; starting with a model just before instability
(Y_c = .069), HB1 is gradually converted to the two-zone
scheme. At each time-step, the convective core mixes out-
ward until M_{min} is neutralized, and no readjustment of the
semiconvective zone is made. Properties of these models
are shown in Tables 18 and 19. The timescale is about four
times slower than the actual overshooting rate (for ease of
convergence), and so the surface response is not computed
realistically; these models should be adequate for a rough
estimate of the increase in t_{HB}, however. The entire semi-
convective zone is mixed in 3.7 million years, reaching
Y_c = .106; subsequent evolution proceeds smoothly on a
nuclear timescale. The sequence is terminated at Y_c = .063,
at which time it is identical to the corresponding model of
HB2.

A second sequence has been computed to see the
effects of rapid mixing. Starting with a model of HB2 at
Y_c = 0.043, the outer boundary M_{sc} is arbitrarily extended
by 0.0044 over one time-step. Y_c rises to 0.074, and a
small increase in log T_e (0.01) is seen after several time-
steps; Tables 20 and 21 contain the details. After mixing,
a radiative region develops around M_{min}, and evolution pro-
ceeds smoothly with the convective core overshooting into
that region. After Y_c becomes less than 0.016, no more
overshooting is permitted, so that we may see the star

approach core helium exhaustion without computer fund exhaustion. Several convective zones of varying composition appear between M_{cc} and M_{sc}, mimicking normal semiconvection. In the H-R diagram (Figure 6), the star rapidly approaches the red giant branch along a track similar to those of Iben and Rood (1970b).

The sequence is finally terminated by extremely slow convergence, 60 models after the imposed mixing. At this time, $Y_c = 2.2 \times 10^{-5}$ and yet the center still produces $L_{He} = 24.3\ L_\odot$; the surface properties are log L = 2.009 and log T_e = 3.697, well removed from the horizontal branch. Neutrino losses due to the universal Fermi interaction, not included in the models, are beginning to be important. The dominant process is the photoneutrino reaction, $\gamma + e^- \to e^- + \nu_e + \bar{\nu}_e$; using the rate of Petrosian et al. (1967), we calculate $L_\nu \simeq 2.0\ L_\odot$ in the last model. This cooling process at the stellar center is not negligible, and so further evolution with our program would not be realistic.

3.5. THE PRIMORDIAL HELIUM ABUNDANCE

In this section, we derive the initial helium abundance Y_0 of the similar globular clusters M3 and M5. Our method is to compare relative lifetimes of horizontal branch and red giant stars with relative numbers observed in star counts. Introduced by Iben (1968a), this method is

potentially quite accurate because of the simplicity of the observational data used; in practice, it must be calibrated using a number of technical assumptions of varying accuracy. Fortunately, we have devised a simple variant of Iben's technique which avoids some of the largest systematic errors.

The first task is to derive the horizontal branch lifetime, $t_{HB}(Y_0)$. This is defined as the elapsed time (unit = 10^6 years) between the initial model and the model with $Y_c = 0.01$. The latter model is brighter than the star's mean horizontal branch luminosity by 0.3 - 0.4 magnitudes and is evolving rapidly toward the red giant branch; it should be distinguishable photometrically as an early asymptotic branch star. t_{HB} is considered to be independent of M_*, Y_0 and Z, <u>for a given core mass</u>, because of the work of Iben and Rood (1970b) and the arguments of Section 3.3. The core mass M_c is determined uniquely by Y_0 and Z, which is approximately known from observations. Butler (1975) has summarized recent measurements of the iron abundances of globular clusters, relative to the solar abundance; he finds deficiency factors of 8 to 37 for M3 and 5 to 16 for M5, the range representing different measurement techniques. We adopt $Z = 0.001$ for both clusters, since the sensitivity of our final results is not great. An implicit assumption is that the CNO abundances in

globular clusters are normal (solar) relative to the iron abundance. This has been questioned (Hartwick and McClure 1972) but definitive observational evidence either way is lacking.

We actually derive three values of t_{HB} to illustrate the uncertainties introduced by semiconvection and the composition instability; the effects of new reaction rates will be considered shortly. Graphs of $Y_c(t)$ are shown in Figure 10. Let $t_L(Y_0)$ be a lower limit to t_{HB}, where normal semiconvection with no composition instability is assumed. Extrapolating the curves for HB1 and HB3 to $Y_c = 0.01$, we find $t_L(.25) = 110.1$ and $t_L(.20) = 106.2$. For an extreme upper limit to $t_{HB}(Y_0)$, we take the lifetime of HB2 with imposed mixing; this gives $t_U(.25) = 133.9$ and $t_U(.20) = 129.2$, where we have used the ratio $t_L(.20)/t_L(.25)$ to approximate the core mass dependence. Our "best" value of $t_{HB}(Y_0)$ assumes normal semiconvection with one occurence of the composition instability. Inspecting Figure 10, we see that the imposed, sudden mixing adds about 10 million years to the lifetime of HB2; a slightly larger increase is found for the mixing episode of HB1, although the actual composition instability develops more rapidly than assumed in these models. Reasonable estimates are $t_{HB}(.25) = 121.$ and $t_{HB}(.20) = 116.7$. By comparison with HB6, overshooting and semiconvection increase t_{HB} by a factor of 1.87 ± 0.17.

Helium-burning reaction rates affect t_{HB} in two ways. The obvious effect is ^{16}O production, quantified by comparing HB1 and HB4. If $r \equiv \varepsilon_{3\alpha}/\varepsilon_{412}$ relative to the old rates, then for new rates we have $r = 2.94$ at $T_6 = 150$ and $t_{HB} \propto r^{-0.16}$. After HB4 was finished, Fowler et al. (1975) reported a "most recent" rate for the triple-alpha process, larger than the rate of HB4 by a factor of 1.20; the most recent rate has been confirmed by three independent groups of nuclear physicists (Chamberlin et al. 1974; Davids et al. 1975; Mak et al. 1975). This decreases t_{HB} by a factor of 0.814. The second effect of the triple-alpha rate on t_{HB} is its influence on the helium core flash which determines $M_c(Y_0)$. Stability of a degenerate helium core has been carefully analyzed by Tarbell and Rood (1975; reproduced as Appendix C), and the correct $M_c(Y_0)$ for any rate is compu- ted there. Most recent rates give $M_c(.25) = .479$ $M_\odot$ and $M_c(.20) = .490$ $M_\odot$ for typical horizontal branch stars in M3 or M5. Assuming $t_{HB} \propto M_c^{-1.5}$ as above, the final horizontal branch lifetimes are

$$t_{HB}(.25) = 92.2, \ 101.3, \ 112.1; \qquad (3.20)$$

$$t_{HB}(.20) = 89.1, \ 97.9, \ 108.4 . \qquad (3.21)$$

Next, we must determine $t_{RG}(Y_0)$, the lifetime of a cluster star on its first ascent up the red giant branch. This is defined, following Iben et al. (1969), as the time for which the visual magnitude is less than M_{VRR}, that of

the RR Lyrae variables of the cluster. In a comprehensive

study of M3, Rood (1973) has found, for the variables,

$< \log L > = 1.66$ and 1.59 for $Y = .25$ and $.20$, respectively.

He used evolutionary tracks computed with old rates, and we

may subtract 0.01 from log L (compare HB1 and HB4) without

doing violence to his fitting techniques. Using bolometric

corrections from Schlesinger (1969), we get $\log L_{RG} = 1.69$

and 1.62 at the same visual magnitude. By interpolation in

the evolutionary sequences of Rood (1972), $t_{RG}(Y_0)$ is found

to be 66.7 and 83.3 for typical red giants of M3. t_{RG} has

the dependence

$$t_{RG} \propto L_{RG}^{-0.84} \, Z^{-0.04} \, M_*^{-0.27}, \qquad (3.22)$$

which will be used in the error analysis.

The first observed quantity from which we determine

Y_0 is the ratio R,

$$R \equiv \frac{N_{HB}}{N_{RG}}, \qquad (3.23)$$

where N_{HB} and N_{RG} are the numbers of horizontal branch and

red giant stars in an unbiased selection of cluster stars;

naturally, red giants are counted down to M_{VRR} in visual

magnitude. On the basis of sixteen different data-sets,

Iben et al. (1969) found that R_{obs} lies in the range 0.80 –

0.95. However, at high luminosity, asymptotic branch stars,

which should not be included in N_{RG}, are indistinguishable

by photometry from (helium-core) red giants; the authors

were able to recognize and exclude early asymptotic branch stars. Gingold (1974) has computed an evolutionary sequence of an asymptotic branch star with initial parameters (M_*, Y, Z) equal to (.60, .30, .001); after careful comparison of relative lifetimes and color differences, he concludes

$$R_{obs} = 1.2 \pm 0.15 \qquad\qquad (3.24)$$

(our estimate of standard error). Using the theoretical values of $R(Y_0)$ shown in Table 22, we find

$$Y = 0.207 \pm 0.015, \qquad\qquad (3.25)$$

where the uncertainty includes only the effects of different treatments of semiconvection. This value has been anticipated by Demarque et al. (1972), who guessed the result before careful calibration became possible.

Before we estimate a realistic uncertainty for Y_0, a variant of the R method will be introduced. Define a new number ratio

$$Q \equiv \frac{N_{HB}}{\Delta N_{RG}}, \qquad\qquad (3.26)$$

where ΔN_{RG} is the number of red giants with visual magnitudes between M_{VRR} and $M_{VRR} + 0.4$. This defines a narrow horizontal band in the H-R diagram at the luminosity of the horizontal branch, but it still contains enough stars for reasonable counting statistics. The measurement of Q avoids several systematic errors which may affect R. First, no asymptotic branch stars contaminate the sample. Second,

no selection effect in M_v (brighter giants being more likely to be counted) should be present in ΔN_{RG}. In the theoretical calibration, where Δt_{RG} is the time spent between log L_{RG} - 0.16 and log L_{RG}, uncertainties in the neutrino energy loss rates from the red giant core have a negligible effect on Δt_{RG}. The same is probably true for rotation of the core, although both of these can influence t_{HB} because of its dependence on the core mass at the helium flash. Both methods, Q and R, show equal sensitivity to the reference luminosity level, L_{RG}.

Cubic polynomial interpolation has been used in the tables of Rood (1972) to find $\Delta t_{RG}(Y_0)$, and the resulting values of Q are given in Table 22. For the cluster M3, the three data-sets listed by Iben et al. (1969) give Q = 3.65, 2.90, and 3.27; for M5, one data-set gives 3.02. A simple average is misleading because of the different sizes of data-sets; instead, we combine the sets to find

$$Q_{obs} = \frac{\Sigma N_{HB}}{\Sigma \Delta N_{RG}} = 3.09. \qquad (3.27)$$

In deriving the standard error, if we assume $\sigma(N) = N^{1/2}$, i.e., Poisson statistics govern the occurence of a given star in the sample, the result is $\sigma(Q) = 0.20$. This is smaller than the sample standard deviation of the data-sets and than the error in R, quoted by the authors, which was based on a much larger number of stars. We assume there is

bias in some of the data-sets and use the sample standard deviation, which gives a fractional error similar to that of R; thus, $\sigma(Q) = 0.33$. Referring to Table 22, we see that

$$Y_0 = 0.187 \pm 0.015, \qquad\qquad (3.28)$$

where, again, the uncertainty includes <u>only</u> the limits on $t_{HB}(Y_0)$.

At this point, the reader may be justifiably uneasy about the large number of assumptions, correction factors, interpolations and extrapolations in the calculation. Unfortunately, they are virtually always necessary in stellar evolution, unless the answers are known beforehand or unlimited time (human and computer) is available. We will not attempt a detailed error analysis of every step. Instead, we note that R and Q are sensitive to Y_0 mainly through t_{RG}, and it is in turn strongly dependent on L_{RG}. A generous estimate will be made for the standard error in $\log L_{RG}$, and its effect will be combined with the uncertainties due to R_{obs}, Q_{obs}, semiconvection and reaction rates (as they affect t_{HB}). The results for the two methods will be combined with no reduction in standard error, because they are not statistically independent.

Realizing that both theoretical and observational uncertainties are involved, we adopt a standard error in $\log L_{RG}$ of 0.10 (0.25 in visual magnitude). The

calculations have been repeated twice, using log L_{RG} varied by $\pm$ 0.1; Q and R method abundances change by $\mp$ 0.030. The upper and lower limits for t_{HB} depending on semiconvection are considered to be two standard error limits; thus, they contribute $\pm$ 0.01 for the R method and $\pm$ 0.008 for the Q method. Fowler et al. (1974) tell us that the reaction rates for the triple-alpha process and for $^{12}C(\alpha, \gamma)^{16}O$ both have standard errors of about 30%; these cause uncertainties in the ratio r and t_{HB} of 42% and 6%, respectively. Using the variations from Table 22,

$$\frac{\partial Y_0}{\partial R} \simeq 0.15, \quad \frac{\partial Y_0}{\partial Q} = 0.045, \qquad (3.29)$$

we find that reaction rates cause standard errors in the R and Q methods of $\pm$ 0.011 and $\pm$ 0.008. The errors in R_{obs} and Q_{obs} become $\pm$ 0.023 and $\pm$ 0.015 in terms of Y_0. Combining all of these in quadrature, the standard errors in Y_0 become

$$\sigma_R(Y_0) = 0.041, \quad \sigma_Q(Y_0) = 0.035. \qquad (3.30)$$

Taking a weighted average and rounding, our conclusion is

$$Y_0 = 0.20 \pm 0.04. \qquad (3.31)$$

A glance at Table 1 shows that our result is the lowest recent measurement of Y_0 but is consistent with several others employing stellar evolution and pulsation theory. Perhaps we have been too generous in increasing t_{HB} because of the composition instability. Two other

assumptions must be mentioned before we pass on to more
general comments. First, we have assumed that every red
giant becomes a horizontal branch star. Rood (1970a) has
shown that mixing of hydrogen to the stellar center at the
helium flash causes a star to return near the main se-
quence. Caloi and Castellani (1975) have made more exten-
sive calculations, showing that blue stragglers and some
cluster B stars may be explained this way. Although no
model calculations have found mixing to occur at the flash,
relatively small numbers of blue stragglers are observed in
M3. As we shall see in Chapter 4, excessive mass loss at
the flash results in stars too blue to be considered hori-
zontal branch members. If not negligible, "non-conservation
of stars" causes us to underestimate Y_0. The second as-
sumption we have made is that red giants have approximately
the mass they had on the main sequence ($M_* \sim 0.8$); if they
lose mass sufficiently early, then t_{RG} increases according
to (3.22) and our Y_0 values are too low. It seems unlikely
that this could affect the Q method, however, because sur-
face gravities at log L_{RG} are several hundred times their
values at the helium flash.

Our value $Y_0 = 0.2$ agrees with the prediction of
"standard" Big Bang nucleosynthesis. The implied age, ~ 16
billion years, is consistent with the Hubble time if the
universe is nearly empty. The most interesting implication
is for the chemical evolution of the galaxy: model-

builders must address themselves to an increase in Y

($\Delta Y \sim .05 - 0.1$) between the formation of globular clusters

and of young stars here and now. This problem can and

surely will be solved in as many ways as there are theorists

who attack it.

4. MODELS FOR SUBDWARF B STARS

4.1. INTRODUCTION

The subdwarf B (sdB) stars of the galactic halo pose a challenge to stellar evolution theory: their interior structure and evolutionary status have remained unknown since their discovery. For classification purposes, Sargent and Searle (1968) have given the following definition:

> A star which has colors corresponding to
> those of a B star and in which the Balmer
> lines are abnormally broad for the color,
> as compared to Population I main-sequence
> B stars. Such stars may also be recognized
> by the early confluence of the Balmer
> series, which is only seen up to n ≃ 12.
> Some, but not all, subdwarf B stars have
> He I lines that are weak for their color.

These stars occupy a compact region of the surface gravity-effective temperature plane, given by

$$4.3 < \log T_e < 4.6,$$
$$4.5 < \log g < 6.0. \qquad (4.1)$$

This region is collinear with the locus of horizontal branch stars, which has led Greenstein (1971) to call it the "extended horizontal branch." Hotter, subdwarf O stars are found with effective temperatures at least as high as $50,000^\circ K$.

Published evolutionary tracks avoid the region of the sdB stars, as shown strikingly in Figure 16 of Greenstein and Sargent (1974; hereafter, GS). In brief,

horizontal branch stars are too cool; pure helium stars are too hot, and hydrogen lines are clearly present in sdB spectra, anyway; helium shell-burning stars are too luminous; nuclei of planetary nebulae are too luminous or too hot. Petersen (1972) and Caloi and Castellani (1975) have evolved stars assuming mixing during the helium core flash; their models are too cool or they show no tendency to cluster in the sdB region. Trimble (1973) has studied models with inert helium cores and thin hydrogen envelopes; these suffer the same drawbacks and also evolve too rapidly.

Cox and Salpeter (1961) first suggested that the hot subdwarfs might be burning helium in their cores, with inert hydrogen envelopes making up a small fraction of the mass. Faulkner (1972) and Caloi (1972) attempted to fit the observed properties with models of this kind. Both found that this could be done only by assuming a large helium core mass, about $0.6 \, M_{\odot}$. Core masses of this size imply an initial helium abundance very close to zero, in conflict with a great mass of data for globular clusters. Additional problems with this structure, some of which will be discussed later, have been pointed out by Sweigart et al. (1974).

The observational data for sdB stars are described in more detail in Section 4.2. In Section 4.3, we present evolutionary sequences with semiconvection for models of the Cox - Salpeter type, and we show that the observations

are reproduced very well. The core mass and initial helium abundance are estimated in the last section, and remaining problems are briefly pointed out.

4.2. OBSERVATIONAL DATA

A sample of thirty-one sdB stars in the halo field has been analyzed by GS. This supersedes the earlier compilation of twenty-one stars by Newell (1973), most of which were drawn from Greenstein (1971). For the sake of homogeneity, Newell's data will not be considered here. GS have measured effective temperatures from UBV photometry, corrected for reddening. Surface gravities were found from measured widths of the hydrogen Balmer lines, calibrated with a large grid of recent model atmospheres. We prefer to consider log L/M, given by

$$\log L/M = 4 \log T_e - \log g - 10.615. \quad (4.2)$$

All stars of GS are plotted in the log L/M - log T_e plane, Figure 11. The mean and median values of log L/M are 1.9 and 1.8, respectively. Note that the stars with the smallest light-to-mass ratios are also the coolest of the sample (with one uncertain exception). This could be a selection effect, hotter stars being fainter in visual magnitude and less likely to be included in the sample.

Helium lines are systematically weak, implying deficiency factors of 2.5 - 100 relative to normal (Population I) helium abundances; similar deficiencies are seen in blue

horizontal branch stars. They are not considered to re-
flect a low primordial helium abundance (Searle and Sargent
1972). The metallicity of the sdB stars is not well known.
In general, GS find upper limits for the carbon and magne-
sium abundances to be normal or deficient by a factor of
two. Some peculiar abundances are seen: the star FB 103
(Feige 66) shows strong sulfur and helium lines. A few sdB
stars have been analyzed at higher dispersion by other au-
thors. In a differential analysis of HD 4539 with respect
to a normal B star, Baschek et al. (1972) found nitrogen
overabundant by a factor of three, oxygen underabundant by
a factor of at least ten, and other heavy elements erratic
but roughly normal. Baschek and Norris (1970) found that
metal abundances "may be approximately normal" in HD 205805.
The same authors (1975) found sulfur enhanced by a factor
of ten and the CNO abundances low by factors between four
and forty in HD 149382.

Hot subdwarfs seem to be very rare in globular clus-
ters, although two sdB stars are known in M13. This sug-
gests membership in the Intermediate Population II, which is
consistent with the metal abundances given above. Newell
(1973) has found a distinction between sdB and blue hori-
zontal branch stars which is relevant to the problems of
their origin and interior structure. He shows that there is
a statistically significant lack of stars in the interval
$4.31 < \log T_e < 4.34$ rather than a continuous distribution

in color. The data of GS also suggest this gap, although too few stars are present for a definite test. We offer a speculative explanation of this gap in Section 4.4.

Finally, we mention that GS also analyze a sample of thirty sdO stars. Although these measurements are more uncertain because of the higher atmospheric temperatures, most sdO stars lie in the intervals

$$1.5 < \log L/M < 3.5,$$
$$4.55 < \log T_e \leq 4.7.$$

(4.3)

Helium lines are much stronger than in the sdB stars (this is one of the defining characteristics of the type sdO), and many of these are nuclei of planetary nebulae.

4.3. EVOLUTIONARY MODELS FOR sdB STARS

Our hypothesis (see also Faulkner 1972) is that catastrophic mass loss during the helium core flash has oc- curred in sdB stars. The resulting structure is burning helium at the center of a helium core, with a thin, inert envelope of hydrogen and helium. From our knowledge of horizontal branch stars, we expect the core mass M_c to be about 0.5 $M_{\odot}$. The envelope mass $M_e = M_* - M_c$ is deter- mined by the observed effective temperatures and by the envelope composition. Contamination of the envelope with products of hydrogen burning on the red giant branch may have occurred, so we do not restrict ourselves to primordial envelope abundances.

It is straightforward to compute initial models for sdB stars, with homogeneous helium cores, using the program described in Appendix A. New helium-burning reaction rates have been used in all sdB models. Table 23 gives the properties of a set of models with initial parameters (M_c, X_e, Z) of (.488, .75, .001) as M_e is varied; X_e is the envelope hydrogen abundance. The trend of decreasing luminosity and increasing effective temperature for lower values of M_e is evident. For this composition, M_e must be less than 0.02 $M_\odot$ to reproduce the observed values of log T_e for sdB stars; hydrogen burning is negligible in such models. The region of varying abundances in the hydrogen-burning shell is 0.002 $M_\odot$ thick in all models. Decreasing this parameter to 0.001 $M_\odot$ (in better agreement with the red giant models of Rood 1972) has a negligible effect.

The effects of varying M_c with fixed envelope mass and composition are illustrated in Table 24 for (M_e, X_e, Z) = (.012, .75, .001). Log L/M is determined uniquely by the core mass, for all models hot enough to represent sdB stars. The relation is

$$\log L_0/M = 2.574 + 3.36 \log M_c, \qquad (4.4)$$

where the subscript reminds us that these are initial models only. In agreement with previous workers, an uncomfortably large value, $M_c = 0.6$, is needed to obtain the mean observed value of log L/M. According to Appendix C, this is larger

than the core mass at the helium flash even if the primordial helium abundance is zero.

Envelope compositions are varied in the models of Table 25. If mixing occurs simultaneously with mass loss at the helium flash, then ^{4}He and ^{12}C abundances in the envelope will increase. Log L/M is not affected, but log T_e decreases as X_e or Z is increased. This is readily understood because hydrogen and heavy elements are both more opaque than helium; a steeper temperature gradient and lower surface temperature result. Even the model with the extremely low value X_e = 0.20 and log T_e = 4.557 is not hot enough to represent the majority of sdO stars, however.

Next, we consider evolutionary tracks in the log L/M - log T_e plane. Interior evolution should be very similar to that of pure helium stars (Paczynski 1971) or horizontal branch cores. In order to study many stars without requiring excessive computer time, we have computed "quasi-evolutionary" sequences for sdB stars. These are sequences of static stellar models with identical parameters (M_*, M_c, X_e, Z) which have helium-depleted convective cores and semiconvective zones. The gravitational term in the luminosity equation (3.3) has a small effect on the observable properties of horizontal branch stars prior to the composition instability, and this should also be true for sdB stars. For a given value of central helium abundance Y_c, we compute a static model using the program of Appendix A, modified to

use the following abundance distribution in the core:

$$Y(M) = Y_c \text{ for } M < M_{cc};$$

$$Y(M) = Y_c + \frac{(Y_{sc} - Y_c)(M - M_{cc})^2}{(M_{sc} - M_{cc})^2}$$

(4.5)

$$\text{for } M_{cc} < M < M_{sc};$$

$$Y(M) = 0.969 \text{ for } M_{sc} < M < M_c.$$

The parabolic profile for Y in the semiconvective zone is a reasonable approximation to the models of HB4. M_{sc}, the mass at the upper boundary of the semiconvective zone, and Y_{sc}, the helium abundance at that point, are taken from the models of HB4. M_{cc}, the mass of the convective core, is varied until $\nabla_{rad} = \nabla_{ad}$ at that point. A constant ratio X_{16}/X_{12} (also taken from HB4) is assumed. These models should be sufficiently realistic to show the general features of sdB evolution.

One evolutionary sequence is given in Table 26 for Y_c = .969, .6, .3, and .1, and for $(M_*, M_c, X_e, Z) = (.510, .500, .75, .001)$. The star brightens rapidly and steadily at nearly constant color. It is essential to include convective overshooting and semiconvection to obtain correct luminosities: L_{He} did not increase so markedly in HB6, with no internal mixing. Also given in the table are estimates for the elapsed time since the initial model. These are obtained from the times of HB4 by using

$$t(Y_c) = \frac{L_{He}(4)\ t_4(Y_c)}{L_{He}(sdB)}. \tag{4.6}$$

The sdB lifetime is only slightly less than horizontal branch lifetimes.

Initial model parameters for eight sequences are given in Table 27, and all tracks are plotted in Figure 11. Every star considered, except the coolest sequence with $X_e = 0.99$, spends its entire core-helium burning life in the region of observed sdB stars. The rapid brightening shows that stars with $M_c \sim 0.5\ M_\odot$ can fit the observations. Again, the star with $X_e = 0.20$ is too cool to enter the region of sdO stars. Clearly, our hypothesis provides a viable explanation for sdB stars.

Convergence problems prevent construction of static models for $Y_c < 0.1$, and time-dependent evolution would be exceedingly expensive with our computer programs. We can guess the nature of subsequent evolution by analogy with horizontal branch cores and with Paczynski's helium stars. The luminosity will continue to rise until $Y_c \leq 0.01$; it may drop briefly during core helium exhaustion, but will rise again as the helium-shell source ignites. From Paczynski's $0.5\ M_\odot$ sequence, a rough estimate of the time between our last model ($Y_c = .10$) and the decline of the shell source is 30 million years. In log T_e, our tracks have the same shape as Paczynski's but are shifted redwards because of the envelope. If the evolution toward higher

temperatures in Figure 11 continues (as it does in his models), then the models will become sdO stars. In all probability, our hypothesis can account for the more luminous sdB stars and at least some of the sdO stars. The author hopes that this matter will be decided conclusively by someone with a faster stellar evolution program.

4.4. THE HELIUM ABUNDANCE AND FINAL PROBLEMS

The observed stars plotted in Figure 11 are distributed at random along their evolutionary tracks. This explains the failure to fit the observed values of log L/M with reasonable core masses by earlier workers, who apparently thought the evolutionary tracks would be horizontal, as they are for stars with larger envelopes. We know that the observed stars are uniformly distributed as a function of the time since arrival in the sdB region after the helium flash, i.e., the time variable listed in Table 26. Since sdB stars brighten steadily between t = 0 and $t \geq 80 \times 10^6$ years, the lower envelope of the star positions in Figure 11 gives us a lower limit to the initial value, log L_0/M. If this can be measured in the presence of observational errors, then the core mass-luminosity relation (4.4) provides a lower limit to M_c. Then the calibration of M_c with initial helium abundance Y_0 (Appendix C) gives an upper limit to Y_0 which is fairly insensitive to the (unknown) metallicity of the stars.

We have carried out this procedure in the following way. For a given observed star, a standard error σ_* is assigned to the measured value of log $(L/M)_*$; the probability distribution for the true light-to-mass ratio is assumed to be a normalized Gaussian with mean log $(L/M)_*$ and standard deviation σ_*. The summation of these Gaussians over all stars in the sample gives the smooth "observed" distribution N_*(log L/M). This distribution must be compared with a predicted distribution to obtain the initial value, log L_0/M. Since the number of stars predicted in a luminosity interval is proportional to the time spent in that interval, we have

$$N_P(\log L/M) \ \alpha \ \frac{dt}{d \log L/M}, \qquad (4.6)$$

which is easily found if an evolutionary sequence is available. Naturally, N_P depends on the luminosity of the initial model ($N_P = 0$ for log L/M < log L_0/M). We assume that the shape of N_P is independent of log L_0/M, and so we have a one-parameter family of predicted distributions which differ only by a shift in the independent variable, log L/M. N_P(log L/M) is folded with a Gaussian (with standard deviation equal to the sample mean of σ_*) to make it directly comparable with N_*(log L/M).

GS have discussed their observational errors in some detail. We have computed several curves of N_*, using $\sigma_* = 0.15$ and 0.25; those stars listed as uncertain by GS

are given larger errors or excluded in the various treat-
ments. N_p is derived from the evolution of the helium core
of HB4. This curve is extrapolated to the higher luminos-
ities of core-helium exhaustion in several different ways;
the final result is insensitive to this extrapolation be-
cause log L/M in this phase is about two standard deviations
larger than log L_0/M. N_* and N_p, before and after folding
with a Gaussian, are plotted in Figure 12.

Best values of log L_0/M have been determined graphi-
cally by overlaying plots of N_* and N_p. From sixteen fits,
we find the lower limit to be

$$\log L_0/M = 1.488 \pm 0.019, \qquad (4.7)$$

or, using (4.4),

$$M_c = 0.474 \pm 0.006 \, M_\odot; \qquad (4.8)$$

the errors are standard deviations from the _fitting_ _only_.
The calibration of Appendix C implies

$$Y_0 = 0.25 - 0.05(\log Z + 2) \qquad (4.9)$$

and

$$\frac{\partial Y_0}{\partial \log L_0/M} = -1.42. \qquad (4.10)$$

We emphasize that this is an upper limit to the primordial
helium abundance, and it is really very uncertain. Fewer
than 20 stars lie within one standard deviation of log L_0/M,
and these determine the final result. If we assume a real-
istic standard error in log L_0/M of $\pm 0.25/4$, then Y_0 has an

uncertainty of ∓ 0.09. Furthermore, a systematic observational error of ± 0.05 in log L/M leads to an error in Y_0 of ∓ 0.07; in view of the difficulty of the observations, systematic errors twice as large are possible.

It is obvious that we cannot claim to have measured the primordial helium abundance by this technique. A much larger sample of stars is needed; it will not be available anytime soon because Greenstein has been assembling the present sample for over twenty years. A selection effect against fainter sdB stars and systematic errors in the model atmospheres may also be present. Our conclusion is that the observations and theoretical models of sdB stars are consistent with the primordial helium abundance found for M3, $Y_0 = 0.2$; because of the uncertainties, they are also consistent with a "normal" abundance, $Y_0 = 0.3$.

Finally, we discuss some of the objections raised by Sweigart et al. (1974) to our hypothesis of an extended horizontal branch caused by mass loss. These last paragraphs are necessarily speculative. First, how can mass loss give rise to a discontinuous distribution of number of stars vs. effective temperature (or envelope mass M_e)? We mentioned in Section 4.2 that Newell (1973) found a "forbidden region" nearly devoid of stars near log $T_e = 4.33$, corresponding to $M_e \approx 0.03$. Both Newell and GS found another gap in the distribution of field horizontal branch stars near log $T_e = 4.1$ or $M_e \approx 0.1$. Newell claimed to

find a similar feature at $\log T_e = 4.07$ in the distribution of globular cluster stars; the presence of a gap at this temperature (not apparent in the data) may be obscured by his use of stars from six clusters of varying metallicity in the sample.

A tentative explanation of these gaps proceeds as follows. We know that individual stars lose different amounts of mass on the red giant branch; this has been shown observationally by Norris (1974). Suppose that critical values of the envelope mass on the red giant branch exist; if gradual mass loss (by a stellar wind, perhaps) decreases M_e below a critical value, then a new mechanism begins to operate which guarantees further ejection of a finite mass. This scenario predicts a range of forbidden values of M_e, bounded above by the critical value. The observed gaps require two critical values of M_e, each corresponding to the onset of a new instability causing mass loss. Candidates for these mechanisms include pulsational instability of the envelope (Feast 1974), photospheric instabilities (similar to the solar five-minute oscillation, perhaps) and dynamical effects of the helium core flash. The last candidate seems necessary to explain the small values of M_e in sdB stars.

Can mass loss occur at the helium flash? Tomasko (1970) has studied the hydrodynamics of the flash using unpublished models of Schwarzschild and Härm. He argues

convincingly that very little mass loss can occur in those models. On the other hand, Edwards (1969) has computed models for the flash in which the core explodes, disrupting the star considerably. While his results are controversial and cannot represent the behavior of most stars, they suggest that the violence of the flash is model-dependent and not completely understood. Furthermore, most red giants do not become sdB stars, so mass loss at the flash is rare in the real world as it is in evolutionary models. Perhaps the high temperature gap at $M_e \simeq 0.03$ represents the critical envelope mass for a catastrophic flash.

Why are sdB stars rarer in globular clusters than in the halo field? This question has a simple answer if we assume that the field stars have larger metal abundances, on the average, than cluster stars. The observations of Section 4.2 support this assumption, but more abundance measurements of sdB stars are needed. The red giant models of Rood (1972) show that larger metal abundances lead to lower surface gravities at the helium flash. Thus, field stars lose mass more easily and are more likely to become sdB stars.

Finally, Sweigert et al. (1974) and Baschek and Norris (1975) have suggested that mass transfer to a close binary companion may cause the low values of M_e in sdB stars. The latter authors note possible radial velocity variations in several sdB stars. This hypothesis would explain their

rarity in globular clusters, because close binaries are practically nonexistent among extreme Population II stars. However, the explanation of gaps in the color distribution becomes extremely puzzling. Critical values of M_e (or stellar radius) for mass transfer would depend on the separation and relative masses of the binary system; thus, the gaps would be smeared beyond recognition in a large sample of stars. Sweigert et al. (1974) also point out that the mass transfer must occur at precisely the proper rate to leave a small envelope mass at the helium flash; more rapid transfer would prevent the flash from occurring, causing the star to become a helium white dwarf with a thin hydrogen envelope. Special initial parameters for the binary system are needed, which seems unlikely, in view of the sizable percentage of sdB stars among the blue halo stars of GS. The binary hypothesis must be considered a less satisfactory competitor to our hypothesis of mass loss at the helium flash.

In conclusion, we believe that the agreement between theory and observation is compelling evidence for the assumed interior structure of sdB stars. The fact that puzzling questions remain attests to the true complexity of real stars and the naiveté of our attempts to understand them theoretically.

APPENDIX A - THE STELLAR EVOLUTION PROGRAM

R. T. Rood made available to the author two FORTRAN programs for calculating static stellar models and evolutionary sequences of models, respectively. The evolution program was described in some detail by Iben (1965a); revisions are noted in the papers by Iben (1965b), Iben and Rood (1970a, 1970b) and Rood (1970b, 1972, 1973). Input physics and numerical methods are described briefly here, except for nuclear reaction rates which are given in Appendix B. More details about the programs are available from the author on request.

The static model program computes a solution of the stellar structure equations (3.1-4) for a given total mass M_* (solar masses) and composition distributions $X_i(M)$; the gravitational energy term in (3.3) is taken to be 0. For an initial horizontal branch model, the helium core mass M_c and primordial compositions X, Y, and Z are given along with M_*. A homogeneous core composition is assumed for $M \leq M_c$: $Y = 0.969$, $X(^{12}C) = X_{12} = 0.030$, and $X(^{14}N) = X_{14} = 0.607 Z$, the remainder being unspecified heavy elements. In the envelope, the primordial composition is used, with the assumptions $X_{12} = 0.141 Z$, $X_{14} = 0.046 Z$ and $X(^{16}O) = X_{16} = 0.420 Z$. Compositions in the hydrogen-burning shell between M_c and $M_c + 0.002 M_\theta$ are smoothly interpolated between core and envelope values, with a small buildup of

[3]He allowed.

Solutions are computed by fourth order Runge-Kutta integration as follows: guesses are provided for P and T at the center, L and T at the surface, and P, T, L, r at M_c. Integrations outward from the center, inward from the surface, and in both directions from M_c, are matched at the points M = 0.1 and M = M_c + 0.01; this is repeated, varying the initial guesses, until continuity at the matching points is achieved to an accuracy of 0.1%. Minor modifications to this procedure used in calculating evolved models for sdB stars are described in Section 4.3. Input physics is identical for static and evolutionary models and is described below.

Time-dependent solutions of the structure equations are computed by the evolution program using Iben's (1965a) variation of the Henyey method (Henyey et al. 1964). A flowchart of the algorithm is shown in Figure 13. Difference equations corresponding to (3.1-4) are expanded for first order variations in lnP, lnT, lnr, and arcsinh L, given an initial guess at the solution for time t. Since the guess is not an exact solution, the resulting inhomogeneous linear equations for corrections to the dependent variables are solved by the usual technique for a band matrix. After adding these corrections, the procedure is iterated until the corrections are less than a preset tolerance. Usually three iterations are sufficient for

convergence; periodically, five iterations are allowed to maintain accuracy. Model atmospheres are computed and stored for a rectangular grid in the log L - log T_e plane; accurate surface boundary conditions are obtained by interpolation at each iteration. The grid of atmospheres is enlarged as necessary during evolution. Consistent models are obtained by repeated application of the mixing algorithms and Henyey iteration, as shown in the flowchart and discussed in Section 3.2. Printout of the model, composition profiles, changes in structural variables from the preceding time-step, and selected physical properties of the model are provided in varying degrees of detail. Approximately every tenth pair of models is saved on magnetic tape.

When a self-consistent model has been generated, another subroutine redefines the grid of the independent variable M, changing the zone sizes and interpolating P, T, L, r, and X_i accordingly. Fine zoning is inserted in regions of rapidly changing variables or compositions, especially near the center, the hydrogen-burning shell, and upper boundaries of the convective core and semiconvective zone. Adjacent shells in uninteresting regions may be merged to increase speed. In general, P, T, L, and r may change by at most 10% across one shell, and X and Y, by 0.015.

An initial guess for the next time-step, t + Δt, is

extrapolated linearly from the two preceding models. The time-step is chosen as large as possible, with the constraint that no variable change by more than 10% in any mass zone. Composition changes due to nuclear reactions are computed by second order Runge-Kutta integration of the rate equations given in Appendix B. No mixing is allowed in radiative or semiconvective regions. In a fully convective zone, abundances and reaction rates are averaged, weighted by mass, over the entire zone. Because the mixing algorithms subsequently change the abundances in the convective core, a small error is introduced: the final core abundances in a consistent model are correct, but the amount of helium burned during each time-step is underestimated slightly. The size of this error has been checked periodically, and even its cumulative effect on the lifetime of the star is negligible. Abundances of ^{1}H, ^{3}He, ^{4}He, ^{12}C, ^{14}N, ^{16}O, ^{18}O and ^{22}Ne are followed. In the hydrogen-burning shell, abundances of ^{3}He, ^{12}C, ^{14}N and ^{16}O are computed from the rate equations until equilibrium is reached; thereafter, equilibrium abundances are used with proper conservation of the total CNO abundance.

Model atmospheres contain the outermost 0.5% of the star's total mass. These are constructed by inward integration from the point where $T = 2^{-1/4} T_e$ and P is assumed to be 1.5 P_{rad}. Given T and P, ionization fractions of H and He and the density ρ are calculated by iterating the

Saha equations and the ideal gas law with radiation pressure added. The temperature gradient in convective regions is found from the mixing-length theory (Mihalas 1970) with a mixing-length of one-half the pressure scale height.

Rosseland mean radiative opacities are taken from the tables of Cox and Stewart (1970). Interpolation in log ρ and log T is performed by the cubic polynomial method described in Rood (1971). In regions containing hydrogen, log κ is interpolated linearly in X from tables for X = 0, 0.2, 0.5, and X_e, each table containing the contribution of the heavy elements of abundance Z. In the helium core, opacities for pure ^{12}C and ^{16}O are added to those for X = 0.0 in proportion to the mass fractions X_{12}, X_{16} and Y. Conductive opacities, although unimportant, are taken from tables of Iben (1968b), as modified by Rood (1972). Derivatives of the total opacity with respect to Y, X_{12} and X_{16} are also returned for use in the mixing algorithms.

The equation of state used at interior points includes contributions of the ideal ion gas, radiation, and electrons, which may be relativistically degenerate to an arbitrary degree; total ionization is assumed. Given T, P, and the composition variables, the subroutine computes ρ, ∇_{ad}, and several other thermodynamic derivatives necessary at various stages. Rational approximations to the Fermi integrals for degenerate electrons are taken from Divine (1965).

APPENDIX B – NUCLEAR REACTION RATES

The nuclear reaction rates used to compute energy generation and composition changes are described here using the notation of Iben (1965a, 1965b). With the exception of star HB4, all reaction rates for horizontal branch computations are identical with those of Rood (1972); although more accurate expressions are available (Fowler et al. 1975), they were intentionally disregarded to maintain consistency with previous work. Revised expressions including intermediate screening factors ("new rates") for the triple-alpha process and for $^{12}C(\alpha, \gamma)^{16}O$ have been used in all models of sdB stars and of HB4.

For any two-body reaction, let r_{ij} be the number of reactions per gram per second. For non-resonant reactions, we have

$$r_{ij} = \rho T_6^{-2/3} X_i X_j \exp(A_{ij} - B_{ij}T_6^{-1/3} + S_{ij}),$$

$$\text{(B.1)}$$

where ρ is the density in gm/cm^3, $T_6 = T/10^{6}{}^{\circ}K$, X_i and X_j are the mass fractions of the reacting nuclei, and S_{ij} is the screening function. The constants A_{ij} and B_{ij} for all non-resonant reactions considered are given in Table 28. Screening functions are expressed in terms of S_0, the Salpeter (1954) result for a reaction of two helium nuclei:

$$S_0 = 0.752 (\rho/T_6{}^3)^{1/2} \left(X_1 + \frac{4}{3}X_3 + Y + 3X_{12} \right.$$

$$\left. + 3.5X_{14} + 4X_{16} + \frac{1}{\mu_e} \right)^{1/2}, \qquad (B.2)$$

where μ_e is the mean molecular weight (in amu) per electron. Also listed in Table 28 is E_{ij}, the energy released per reaction, excluding neutrino losses; when subsequent reactions or β-decays follow immediately, their energy release is included in E_{ij}. The overall result is

$$\varepsilon_N = \Sigma E_{ij} r_{ij}. \qquad (B.3)$$

In the extensive compilation of reaction rates by Fowler et al. (1975), the quantity $N_A <\sigma v>_{ij}$ is tabulated for two-body reactions; N_A is Avogadro's number (6.0222 x 10^{23}) and $<\sigma v>_{ij}$ is the thermal average of cross-section times speed. To facilitate comparison, we give the relation (Fowler et al. 1967)

$$N_A <\sigma v>_{ij} = \frac{A_i A_j (1 + \delta_{ij})}{\rho X_i X_j N_A} r_{ij}. \qquad (B.4)$$

E_{ij} is related to Fowler's Q-values by

$$E_{ij} (\text{ergs}) = 1.6022 \times 10^{-6} \Sigma Q_{ex} (M_e v) \qquad (B.5)$$

where Q_{ex} refers to the value exclusive of neutrino energy and the summation extends over the primary and all subsequent reactions. Fowler's rates should be used in any future studies of stellar evolution. In all cases, our new rates agree well with the dominant terms of Fowler's

expressions.

With the addition of two branching ratios, the reactions of Table 28 specify the complete network for hydrogen burning. For the CNO bi-cycle, we assume the ratio of $^{15}N(p, \gamma)^{16}O$ to $^{15}N(p, \alpha)^{12}C$ reaction rates to be 0.000514. For the PP-II and PP-III chains, let γ be the ratio of $^{7}Be(p, \gamma)^{8}B (e^{+}\nu) \ ^{8}Be^{*}(\alpha)^{4}He$ to $^{7}Be(e^{-}, \nu\gamma)^{7}Li (p, \alpha)^{4}He$ reaction rates; we assume

$$\gamma = 0.09118 \ X_1 \mu_e T_6^{-1/6} \exp(39.1440 - 102.639/T_6^{1/3} + S_0). \qquad (B.6)$$

Then E_{34} must be replaced by

$$E_{34}' = E_{34} + (\gamma E_{17} + E_{e7})/(1 + \gamma), \qquad (B.7)$$

where

$$E_{17} = 1.737 \times 10^{-5} \text{ergs}, \ E_{e7} = 2.786 \times 10^{-5} \text{ergs}. \qquad (B.8)$$

The helium-burning reaction $^{14}N(\alpha, \gamma)^{18}F(e^{+}\nu)^{18}O$ has two resonances which dominate the reaction rate. We use the expressions

$$r_{414} = \rho Y \ X_{14} \ T_6^{-3/2} \ \exp(1.75S_0)(R_1 + R_2),$$

$$R_1 = \exp(37.6896 - 2798./T_6), \qquad (B.9)$$

$$R_2 = \exp(61.5178 - 5054./T_6),$$

$$E_{414} = 1.057 \times 10^{-5} \text{ergs}. \qquad (B.10)$$

The <u>old</u> rate for $^{12}C(\alpha, \gamma)^{16}O$, used in all horizontal branch models except those of HB4, is given by

$$r_{412} = \rho Y X_{12} T_6^{-2} \exp(83.877605 + 1.5 S_0$$

$$- 321.4854/T_6^{1/3} - 8.929241/T_6^{2/3}),$$

$$(B.11)$$

$$E_{412} = 1.145 \times 10^{-5} \text{ergs.} \qquad (B.12)$$

This is numerically equal to the rate of Fowler <u>et al.</u> (1967) at $T_6 = 150$ when the reduced width parameter θ_α^2 is taken to be 0.079. For the triple-alpha process, the <u>old</u> rate is

$$r_{444} = \rho^2 Y^3 T_6^{-3} \exp(51.687468 -$$

$$4434.032/T_6 + S_0), \qquad (B.13)$$

$$E_{444} = 1.166 \times 10^{-5} \text{ergs.} \qquad (B.14)$$

To aid comparison, Fowler <u>et al.</u> (1975) tabulate

$$N_A^2 <\sigma v>_{444} = \frac{384}{\rho^2 Y^3 N_A} r_{444}. \qquad (B.15)$$

Before discussing the new rates, we point out that the screening function S_{444} is smaller than the correct, weak screening result by a factor of three, and all other S_{ij} for helium burning are off by a factor of two. However, the criterion for applicability of weak screening, as shown by DeWitt <u>et al.</u> (1973) and Graboske <u>et al.</u> (1974), is

$$S_{ij}^{W} \; (\rho, \; T) \; \leq \; 0.10, \qquad\qquad\qquad (B.16)$$

and this is violated at the center of a horizontal branch star; typically, the correct value for S_{44}^{W} is 0.35 there. Intermediate screening functions have been evaluated for relevant densities, temperatures and compositions using the recipe on p. 465 of the latter paper; these are shown in Table 29 along with the old and correct weak screening results. The adopted <u>new</u> screening functions are

$$S'_{444} = 1.83 \; S_0, \; S'_{412} = 1.73 \; S_0. \qquad (B.17)$$

Fowler <u>et al</u>. (1974) have provided new rates for the triple-alpha process and $^{12}C(\alpha, \gamma)^{16}O$, based on nuclear experiments described by Barnes and Nichols (1973) and Dyer and Barnes (1973). Fowler's expressions have been evaluated and their ratios to the old rates are shown in the second and third columns of Table 30. Total changes to the energy generation including intermediate screening are also shown. We approximate the new value of r_{412} by 0.62 times the old. Thus, the <u>new</u> rates are given by

$$r_{444} = \rho^2 Y^3 T_6^{-3} \exp(52.08759 - 4410.9/T_6 +$$

$$1.83 \; S_0) \qquad\qquad\qquad (B.18)$$

and

$$r_{412} = \rho Y \; X_{12} \; T_6^{-2} \exp(83.39957 + 1.73 \; S_0$$

$$- \; 321.4854/T_6^{1/3} - 8.929241/T_6^{2/3}).$$

$$(B.19)$$

No neutrino loss rates except those in β-decays are included in the calculation of ε_N; they are completely negligible as long as helium burning continues at the stellar center, with $Y_c > 0.001$.

The rate equations for abundance changes are those of Iben (1965a, b). In hydrogen-burning zones, we use:

$$\frac{dX_1}{dt} = m_H[(2r_{33} - 3r_{11} - r_{34}) - 2(r_{112} + r_{114} + r_{116})],$$

$$\frac{dX_3}{dt} = 2.993 \, m_H(r_{11} - 2r_{33} - r_{34}),$$

$$\frac{dX_4}{dt} = 3.972 \, m_H(r_{33} + r_{34} + r_{116} + 0.999486r_{114})$$

$$\frac{dX_{12}}{dt} = 11.907 \, m_H(-r_{112} + 0.999486r_{114}),$$

$$\frac{dX_{14}}{dt} = 13.894 \, m_H(-r_{114} + r_{112} + r_{116}),$$

$$\frac{dX_{16}}{dt} = 15.871 \, m_H(-r_{116} + 0.000514r_{114}),$$

$$(B.20)$$

where m_H is the mass of the hydrogen <u>atom</u> in gm. In helium-burning regions, we have

$$\frac{dX_4}{dt} = -3.972m_H(3r_{444} + r_{412} + r_{414} + r_{418}),$$

$$\frac{dX_{12}}{dt} = 11.907 \, m_H(r_{444} - r_{412}),$$

$$\frac{dX_{14}}{dt} = -13.894 \, m_H r_{414}, \qquad\qquad (B.21)$$

$$\frac{dX_{16}}{dt} = 15.871 \ m_H r_{412},$$

$$\frac{dX_{18}}{dt} = 17.860 \ m_H (r_{414} - r_{418}),$$

$$\frac{dX_{22}}{dt} = 21.821 \ m_H r_{418}.$$

Iben's equations differ trivially because his definition of r_{444} is three times larger than ours.

APPENDIX C

THE TRIPLE-ALPHA RATE, SCREENING FACTORS, AND THE HELIUM FLASH*

T. D. TARBELL AND R. T. ROOD
California Institute of Technology
Received 1974 December 19

ABSTRACT

A simple but accurate stability analysis is presented for a degenerate stellar core containing a temperature-sensitive nuclear fuel. It is used to study the dependence of the helium core mass at the helium flash M_{cf} on the triple-α rate and its screening factor. Updated values of M_{cf} are computed, and a sizable discrepancy between the results of different workers is removed.

Subject headings: interiors, stellar — late-type stars — nuclear reactions — stellar evolution

I. INTRODUCTION

It has long been known that a degenerate stellar core containing a temperature-sensitive nuclear fuel may be unstable to runaway ignition (Mestel 1952): this fact is most convincingly demonstrated by calculations through the helium flash in low-mass red giants (Schwarzschild and Härm 1962). The origin of the instability is clearly seen in the weak dependence of pressure on temperature in a degenerate gas. This property of the equation of state allows us to simplify greatly the stability analysis of a degenerate stellar core and to obtain a simple second-order boundary value problem for perturbations to the temperature distribution. The analysis presented in § II shows clearly the competition between heating by nuclear burning and cooling by neutrino losses and electron conduction in producing stability or instability; it is applicable to the helium flash and degenerate carbon ignition, as long as nuclear reaction rates are much more sensitive to temperature than to density.

The precise value of the core mass M_{cf} at the time of the helium flash is crucial for understanding the horizontal branch in globular clusters (Faulkner 1966) and its counterpart in old open clusters (Faulkner and Cannon 1973). In a previous paper (Rood 1972, hereafter RTR), six evolutionary tracks were computed from main sequence to helium flash to determine M_{cf} and its dependence on initial mass and composition. Similar computations by Demarque and Mengel (1971, 1973a) using different expressions for the triple-α rate and electron screening factor yield systematically lower values of M_{cf}. They have commented on this but conclude that uncertainties as large as 0.02 $M_\odot$ may remain (Demarque and Mengel 1973b, hereafter DM).

In addition to this discrepancy, three more recent developments have prompted us to reexamine the determination of M_{cf}. First, a detailed theory of degenerate intermediate electron screening has appeared (DeWitt, Graboske, and Cooper 1973;

Graboske *et al.* 1973); neither weak nor strong screening is applicable to the helium flash. Second, the radiation width of the 7.655 MeV state in ^{12}C has been remeasured (Chamberlin *et al.* 1974) with the result that the "best" value for the triple-α rate has increased by nearly 50 percent over that used in RTR (Fowler, Caughlan, and Zimmerman 1974). Finally, Barnes and Nichols (1973) have reanalyzed the measurements of the precise excitation energy of the 7.655 MeV state, so that the temperature dependence of the rate is now known more accurately than the rate itself.

In § III, we use the stability analysis of § II to find new best values for M_{cf} as a function of initial mass, composition, triple-α rate, and screening; a large part of the discrepancy between RTR and DM is also resolved.

II. STABILITY ANALYSIS

We will calculate the stability of a red giant core to a perturbation in its temperature distribution. The pressure and density structure is assumed to be completely determined by the usual equations of hydrostatic equilibrium and mass conservation and by the equation of state for a zero-temperature electron gas; the accuracy of our neglect of ion pressure will be established below. Thus, $P(M)$, $r(M)$, and $\rho(M)$ are unaffected by a temperature perturbation.

The remaining two equations of stellar structure determine the unperturbed temperature $T_0(M, t)$ and luminosity $L_0(M, t)$:

$$T\frac{\partial s}{\partial t} = \epsilon_N - \epsilon_\nu - \frac{\partial L}{\partial M}, \qquad (1)$$

$$L(M) = -\frac{Ar^4T^3}{\kappa}\frac{\partial T}{\partial M}, \qquad (2)$$

where $A = 64\pi^2 ac/3$, and ϵ_N, ϵ_ν, and s are the nuclear energy generation, neutrino loss, and entropy per unit mass (all positive).

Now we introduce a small temperature perturbation $T_1(M)$ and assume exponential time dependence, so

that the complete temperature distribution

$$T(M, t) = T_0(M, t) + T_1(M) e^{\lambda t},\qquad (3)$$

where

$$T_1 \ll T_0 .$$

Equations (1) and (2) may be expanded to first order in T_1 (taking all derivatives with respect to temperature at constant density), and the results combine to give a single equation for T_1:

$$FT_1'' + (G + F')T_1'$$
$$+ \left[\frac{\partial}{\partial T}(\epsilon_N - \epsilon_v) + G' - \lambda C_v\right]T_1 = 0 , \quad (4)$$

where

$$F = A r^4 T_0{}^3/\kappa ,$$

$$G = F \frac{\partial \ln T_0}{\partial M}\left(3 - \frac{\partial \ln \kappa}{\partial \ln T}\right) , \qquad (5)$$

and the prime means d/dM.

Detailed evolutionary calculations for models in which neutrino losses are included generally show that the thermal runaway begins in a thin shell away from the center. Therefore, the precise boundary conditions chosen at the center and edge of the core are unimportant, and we make the simplest possible choice, namely,

$$T_1(0) = T_1(M_c) = 0 . \qquad (6)$$

Equations (4) and (6) define a Sturm-Liouville boundary value problem, and the eigenvalues (all real) and eigenfunctions may be found numerically using standard techniques. A positive eigenvalue implies instability to thermal runaway with an e-folding time of $\tau = \lambda^{-1}$. The flash will take place when τ is of the same order as the evolutionary time scale.

We now derive an approximate expression for the largest eigenvalue, using qualitative results of the evolutionary calculations. The unperturbed model for a star approaching the flash has a temperature maximum away from the center at M_{T0}, because of the central concentration of neutrino losses during prior evolution. Consequently, ϵ_N is sharply peaked in this region and the flash will begin when neutrino losses and conduction fail to dissipate the heat generated in this shell. The eigenfunction $T_1(M)$ corresponding to the largest eigenvalue has no nodes and therefore one maximum in the core, at M_{T1}; physically, we expect $M_{T1} \approx M_{T0}$. Evaluating equation (4) at this point and using the approximation

$$T_1' \approx T_0' = 0 \quad \text{at} \quad M = M_{T0} \approx M_{T1} , \qquad (7)$$

we obtain

$$\lambda = \frac{1}{C_v}\frac{\partial}{\partial T}(\epsilon_N - \epsilon_v)$$
$$+ \frac{F}{C_v}\left[\frac{T_1''}{T_1} + \frac{T_0''}{T_0}\left(3 - \frac{\partial \ln \kappa}{\partial \ln T}\right)\right]. \qquad (8)$$

The perturbation T_1 is expected to be more sharply peaked than T_0, and we parametrize this by writing

$$T_1''/T_1 \equiv \sigma(T_0''/T_0) . \qquad (9)$$

Then the approximation may be written compactly as

$$\lambda = \tau^{-1} = \frac{1}{C_vT_0}\left[\frac{\partial}{\partial \ln T}(\epsilon_N - \epsilon_v) - \epsilon_c\right]_{M=M_{T0}} \qquad (10)$$

where

$$\epsilon_c \equiv -FT_0''\left(3 + \sigma - \frac{\partial \ln \kappa}{\partial \ln T}\right)_{M=M_{T0}} . \qquad (11)$$

The correct value of σ is not known a $priori$ but may be estimated by solving equation (4) for a few cases; it falls in the range 2 to 4, but precise values are not necessary for the study of different reaction rates in § III.

We see that the criterion for a runaway, $\lambda > 0$, is much more complicated than the relation $\epsilon_N > \epsilon_v$ that one might have naïvely guessed. Recent studies of degenerate carbon ignition (e.g., Graboske 1973) have made use of the latter criterion to determine the ignition line in the (ρ, T)-plane. In this case the stability may be seriously overestimated since ϵ_N is highly temperature-sensitive.

To estimate the influence of pressure and density perturbations, we use the following result of Kippenhahn, Thomas, and Weigert (1966; see also Cowling 1934), derived by assuming homologous perturbations and averaging over the core:

$$\epsilon_c = \frac{L_c}{M_c}\left[4 - \left(\frac{\partial \ln \kappa}{\partial \ln T}\right)_P - \varphi - \varphi\left(\frac{\partial \ln \kappa}{\partial \ln P}\right)_T\right] \qquad (12)$$

where

$$\varphi = -4\left(\frac{\partial \ln \rho}{\partial \ln T}\right)_P \bigg/ \left[4\left(\frac{\partial \ln \rho}{\partial \ln P}\right)_T - 3\right]. \qquad (13)$$

If the extra terms proportional to φ are introduced into equation (11), ϵ_c is increased by not more than 15 percent for the values of ρ and T of interest in low-mass red giants; again, this is unimportant for the differential effects to be studied next.

III. APPLICATION TO THE HELIUM FLASH

Before the appearance of instability, helium burning has a negligible effect on the temperature distribution of a red giant core; in the models of RTR, $\epsilon_v \geq 4\epsilon_N$ at the temperature maximum, and gravitational heating is larger by at least an order of magnitude. Therefore, given an evolutionary sequence of models computed with a known energy generation rate, ϵ_{N0}, we can solve equations (4) and (6) using any expression $\epsilon_N \geq \epsilon_{N0}$ and calculate accurately the core mass at onset of instability $M_{ci}(\epsilon_N)$. With the additional assumption that the flash will develop equally rapidly for the different rates, we obtain $M_{cf}(\epsilon_N)$, the core mass at the helium flash (defined, following RTR, as the onset

of convection in the helium-burning region). We have

$$M_{cf}(\epsilon_N) = M_{cf}(\epsilon_{N0}) + \Delta M_{cl} \qquad (14)$$

where

$$\Delta M_{cl} = M_{cl}(\epsilon_N) - M_{cl}(\epsilon_{N0}) . \qquad (15)$$

This procedure has been applied to the four evolutionary tracks RG2–RG5 of RTR. The growth rates $\lambda(M_c, \epsilon_N)$ for each available model of RG5 were found by solving equations (4) and (6) using the different rates and screenings described in the Appendix and neutrino losses and conductive opacities identical to those of RTR. Some of the results are plotted in Figure 1; we see in the figure that the growth rates have similar shapes as a function of M_c for all the rates studied. So ΔM_{cl} can be determined simply by reading off the horizontal shift in the curves at any convenient λ. In fact, the growth rates can be fitted quite well by a function of the form

$$\lambda(M_c, \epsilon_N) = \lambda_0 \exp\{B[M_c - M_{cl}(\epsilon_N)]\} - \lambda_0 , \quad (16)$$

where λ_0 and B are parameters determined graphically; this was used to interpolate accurate values of $M_{cl}(\epsilon_N)$.

Next, the models of RG5 were reanalyzed using the approximate formulae (10) and (11). A value of 2.5

for the parameter σ gave excellent agreement with the exact results. This value was used to study the stability of RG2–RG4 for different rates and screenings with the result that $\Delta M_{cl}(\epsilon_N)$ did not vary significantly from one star to the next.

Our numerical results can be stated concisely as follows. The energy generation rate from the triple-α reaction is, for pure helium,

$$\epsilon_{3\alpha} = E_0 \rho^2 T_9{}^{-3} \exp\left(-\frac{E_r}{T_9} + S_{3\alpha}\right) \text{ergs g}^{-1}\text{s}^{-1}, \quad (17)$$

where E_0 and E_r are derived from the nuclear measurements and $S_{3\alpha}$ is the screening function. Then we find

$$\left(\frac{\partial M_{cf}}{\partial \log_{10} E_0}\right)_{E_r, S_{3\alpha}} = -0.018 \ M_\odot \qquad (18)$$

and

$$\left(\frac{\partial M_{cf}}{\partial E_r}\right)_{E_0, S_{3\alpha}} = +0.057 \frac{M_\odot}{T_9} . \qquad (19)$$

On changing $S_{3\alpha}$ from the formula of RTR to degenerate intermediate screening, we obtain

$$\Delta M_{cf} = -0.0045 \ M_\odot . \qquad (20)$$
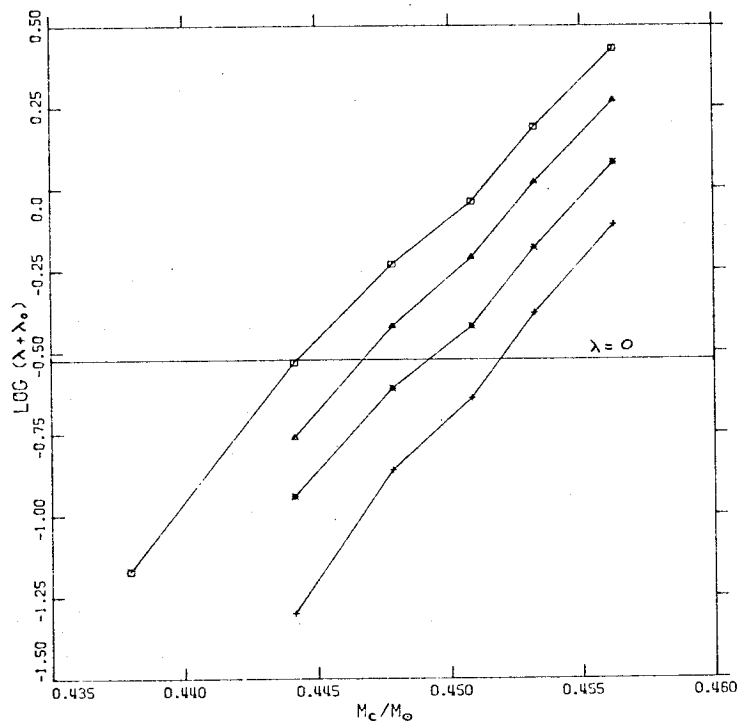
FIG. 1.—Growth rates of the most unstable mode versus core mass $M_c/M_\odot$. The plotted points are log $(\lambda + \lambda_0)$, where λ_0 is defined by equation (16) and is equal to 0.30 $(10^6 \text{ yr})^{-1}$. All are exact results for RG5. +, RTR rate, RTR screening; *, new rate, RTR screening; $\triangle$, RTR rate, intermediate screening; $\square$, new rate, intermediate screening. RTR found the flash at $M_c = 0.467 \ M_\odot$.

Each numerical result is an average of several determinations, with highest weight given to the exact results from RG5. *Using the new unscreened rate (see Appendix) and degenerate intermediate screening, the core masses of RTR should be decreased by 0.008 $M_\odot$, i.e.,*

$$\frac{M_{cf}}{M_\odot} = 0.467 + 0.23(X - 0.7) - 0.01(\log Z + 3)$$

$$+ 0.035(M/M_\odot - 0.8). \qquad (21)$$

We have also performed the stability analyses using weak and strong screening *to compare with the results of DM.* On changing from Reeves's rate and weak screening to the "DM" rate and strong screening, they find $\Delta M_{cf} = +0.010\ M_\odot$, and our method agrees precisely. Small discrepancies remain in the absolute values of M_{cf}. For the initial parameters $(M/M_\odot, X, Z) = (0.85, 0.732, 0.001)$, DM find $M_{cf} = 0.461\ M_\odot$ for the former rate and 0.471 $M_\odot$ for the latter; our results for the same parameters and rates are 0.465 and 0.475 $M_\odot$, respectively (RTR found 0.480 $M_\odot$). The remaining difference of 0.004 $M_\odot$ must be caused

by differences in the evolution codes and other input physics, such as conductive opacities.

IV. CONCLUSION

A simple secular stability criterion has been presented for stellar cores supported primarily by degenerate electron pressure. It shows clearly that stability is determined by competition between the temperature derivatives of the heating and cooling rates, as in equation (10). The stability theory has been applied to calculate the critical helium core mass used in studies of post–helium-flash evolution; our best values are given by equation (21) and may be corrected for any future changes in the triple-α rate by the formulae provided. Most of the disagreement on core masses between RTR and DM is explained by the different rates used.

We wish to thank P. Demarque and J. G. Mengel for providing their results prior to publication, and Professor William A. Fowler for advice and encouragement.

APPENDIX

REACTION RATES AND SCREENING FACTORS

The general expression for energy generation from the triple-α reaction is given in equation (17); the constants for the unscreened rate are given in Table A1.

Following DeWitt *et al.* (1973), we parametrize the screening function $S_{3\alpha}$ by the dimensionless quantities

$$\Lambda_0 = 5.95 \times 10^{-6}\left(\frac{\rho}{\mu_I T_9{}^3}\right)^{1/2}, \qquad (A1)$$

$$\tilde{Z} = \left(\bar{Z}\theta_e + \sum_{\text{ions}} f_i Z_i{}^2\right)^{1/2}, \qquad (A2)$$

$$\bar{Z} = \sum_{\text{ions}} f_i Z_i. \qquad (A3)$$

Here, μ_I is the mean molecular weight per ion, f_i is the number fraction of the ith ion, and θ_e is an electron degeneracy parameter given below. Then we have

RTR screening:

$$S_{3\alpha} = 4\tilde{Z}\Lambda_0, \quad \theta_e = 1; \qquad (A4)$$

Degenerate weak screening:

$$S_{3\alpha} = 12\tilde{Z}\Lambda_0, \quad \theta_e = 0; \qquad (A5)$$

Degenerate intermediate screening, assuming $Y = 1.0$:

$$S_{3\alpha} = 8.7055(\tilde{Z}\Lambda_0)^{0.860}, \quad \theta_e = 0. \qquad (A6)$$

TABLE A1
CONSTANTS IN THE TRIPLE-ALPHA RATE

Label	E_0	E_r	Reference
RTR	3.18 E+8	4.43395	RTR
Reeves	3.46 E+8	4.36188	Reeves 1965
DM	3.88 E+8	4.432	DM
New	4.72 E+8	4.4109	Fowler et al. 1974

In addition, DM used the strong screening function given by Reeves (1965):

$$S_{3\alpha} = 2.04 \times 10^{-3} \left(\frac{\rho}{\mu_e}\right)^{1/3} T_9^{-1} .$$

REFERENCES

Barnes, C. A., and Nichols, D. B. 1973, *Nucl. Phys.*, **A217**, 125.

Chamberlin, D., Bodansky, D., Jacobs, W. W., and Oberg, D. L. 1974, *Phys. Rev.*, **C9**, No. 1, 69.

Cowling, T. G. 1934, *M.N.R.A.S.*, **94**, 768.

Demarque, P., and Mengel, J. G. 1971, *Ap. J.*, **164**, 317.

———. 1973a, *Astr. and Ap.*, **22**, 121.

———. 1973b, preprint (DM).

DeWitt, H. E., Graboske, H. C., and Cooper, M. S. 1973, *Ap. J.*, **181**, 439.

Faulkner, D. J., and Cannon, R. D. 1973, *Ap. J.*, **180**, 435.

Faulkner, J. 1966, *Ap. J.*, **144**, 978.

Fowler, W. A., Caughlan, G. R., and Zimmerman, B. A. 1967, *Ann. Rev. Astr. and Ap.*, **5**, 525.

———. 1974, private communication.

Graboske, H. C. 1973, *Ap. J.*, **183**, 177.

Graboske, H. C., DeWitt, H. E., Grossman, A. S., and Cooper, M. S. 1973, *Ap. J.*, **181**, 457.

Kippenhahn, R., Thomas, H.-C., and Weigert, A. 1966, *Zs. f. Ap.*, **64**, 373.

Mestel, L. 1952, *M.N.R.A.S.*, **112**, 598.

Reeves, H. 1965, in *Stellar Structure*, ed. L. H. Aller and D. B. McLaughlin (Chicago: University of Chicago Press).

Rood, R. T. 1972, *Ap. J.*, **177**, 681 (RTR).

Schwarzschild, M., and Härm, R. 1962, *Ap. J.*, **136**, 158.

R. T. ROOD: Department of Astronomy, University of Virginia, Charlottesville, VA 22903

T. D. TARBELL: Kellogg Radiation Laboratory 106-38, California Institute of Technology, Pasadena, CA 91125

ERRATUM

In the paper "The Triple-Alpha Rate, Screening Factors, and the Helium Flash," by T. D. Tarbell and R. T. Rood (Ap. J., 199, 443, 1975), equation (A6) of the Appendix is incorrect for degenerate, intermediate screening. It should read

$$S_{3\alpha} = 5.905 \ (\tilde{Z}\Lambda_0)^{0.860}, \ \theta_e = 0.$$

Equation (21) should read

$$\frac{M_{cf}}{M_\odot} = 0.470 + 0.23 \ (X - 0.7) - 0.01 \ (\log Z + 3)$$

$$- 0.035 \ (M/M_\odot - 0.8).$$

[To appear in The Astrophysical Journal, Feb. 1, 1976.]

REFERENCES

G. Abraham and W. D. Eysink, J. Hydraulic Res. 7, 145 (1969).

L. H. Auer and J. Norris, Astrophys. J. 194, 87 (1974).

P. G. Baines and A. E. Gill, J. Fluid Mech. 37, 289 (1969).

C. A. Barnes and D. B. Nichols, Nucl. Phys. A217, 125 (1973).

B. Baschek and J. Norris, Astrophys. J. Suppl. 19, 327 (1970).

B. Baschek, W. L. W. Sargent and L. Searle, Astrophys. J. 173, 611 (1972).

B. Baschek and J. Norris, Astrophys. J. 199, 694 (1975).

E. Böhm-Vitense and P. Szkody, Astrophys. J. 184, 211 (1973).

D. Butler, Astrophys. J. 200, 68 (1975).

V. Caloi, Astron. and Astrophys. 20, 357 (1972).

V. Caloi and V. Castellani, Astron. and Astrophys. 39, 335 (1975).

V. Castellani, P. Giannone and A. Renzini, Astrophys. and Space Sci. 10, 340 (1971a).

V. Castellani, P. Giannone and A. Renzini, Astrophys. and Space Sci. 10, 355 (1971b).

V. Castellani, P. Giannone and A. Renzini, Astrophys. and Space Sci. 17, 80 (1972).

D. Chamberlin, D. Bodansky, W. W. Jacobs and D. L. Oberg, Phys. Rev. C9, 69 (1974).

S. Chandrasekhar, An Introduction to the Study of Stellar Structure (Univ. of Chicago Press, Chicago, 1939).

R. F. Christy, Astrophys. J. 144, 108 (1966).

I.-J. Christy-Sackmann, private communication (1975).

D. D. Clayton, Principles of Stellar Evolution and Nucleo-synthesis (McGraw-Hill, New York, 1968).

A. N. Cox and J. N. Stewart, Astrophys. J. Suppl. 19, 243 (1970).

J. P. Cox and E. E. Salpeter, Astrophys. J. 133, 764 (1961).

I. J. Danziger, Ann. Rev. Astr. and Ap. 8, 161 (1970).

C. N. Davids, R. C. Pardo and A. W. Obst, Phys. Rev. C11, 2063 (1975).

P. Demarque and J. G. Mengel, Astrophys. J. 171, 583 (1972).

P. Demarque, A. V. Sweigart and P. G. Gross, Nature Phys. Sci. 239, 85 (1972).

P. Demarque, private communication (1975).

K. H. Despain, Ph.D. Thesis, California Institute of Technology (1975).

H. E. DeWitt, H. C. Graboske and M. S. Cooper, Astrophys. J. 181, 439 (1973).

N. Divine, Astrophys. J. 142, 1652 (1965).

P. Dyer and C. A. Barnes, Nucl. Phys. A223, 495 (1974).

A. C. Edwards, Mon. Not. Roy. Astron. Soc. 146, 445 (1969).

O. J. Eggen, D. Lynden-Bell and A. R. Sandage, Astrophys. J. 136, 748 (1962).

P. P. Eggleton, Mon. Not. Roy. Astron. Soc. 156, 361 (1972).

J. Faulkner and I. Iben, Jr., Astrophys. J. 144, 995 (1966).

M. W. Feast, IAU Symposium #59, ed. P. Ledoux et al.
(D. Reidel, Dordrecht, 1974).

W. A. Fowler, G. R. Caughlan and B. A. Zimmerman, Ann. Rev.
Astr. and Ap. 5, 525 (1967).

W. A. Fowler, G. R. Caughlan and B. A. Zimmerman, private
communication (1974).

W. A. Fowler, G. R. Caughlan and B. A. Zimmerman, Ann. Rev.
Astr. and Ap. 13, 69 (1975).

R. A. Gingold, Astrophys. J. 193, 177 (1974).

H. C. Graboske, H. E. DeWitt, A. S. Grossman and M. S.
Cooper, Astrophys. J. 181, 457 (1973).

J. L. Greenstein, IAU Symposium #42, ed. W. J. Luyten (D.
Reidel, Dordrecht, 1971).

J. L. Greenstein and A. I. Sargent, Astrophys. J. Suppl.
28, 157 (1974; GS).

P. G. Gross, Mon. Not. Roy. Astron. Soc. 164, 65 (1973).

F. D. A. Hartwick and R. McClure, Astrophys. J. Lett. 176,
L57 (1972).

L. G. Henyey, J. E. Forbes and N. L. Gould, Astrophys. J.
139, 306 (1964).

R. A. Hoare, Nature 210, 787 (1966).

F. Hoyle and M. Schwarzschild, Astrophys. J. Suppl. 2, 1
(1955).

I. Iben, Jr., Astrophys. J. 141, 993 (1965a).

I. Iben, Jr., Astrophys. J. 142, 1447 (1965b).

I. Iben, Jr., Ann. Rev. Astr. and Ap. 5, 571 (1967).

I. Iben, Jr., Nature 220, 143 (1968a).

I. Iben, Jr., Astrophys. J. 154, 557 (1968b).

I. Iben, Jr., R. T. Rood, K. M. Strom and S. E. Strom, Nature 224, 1006 (1969).

I. Iben, Jr. and R. T. Rood, Astrophys. J. 159, 605 (1970a).

I. Iben, Jr. and R. T. Rood, Astrophys. J. 161, 587 (1970b).

I. Iben, Jr., Ann. Rev. Astr. and Ap. 12, 215 (1974).

R. H. Kraichnan, Phys. Fluids 5, 1374 (1962).

R. S. Kushwaha, Astrophys. J. 125, 242 (1957).

P. Ledoux, Astrophys. J. 105, 305 (1947).

A. Maeder, Astron. and Astrophys. 40, 303 (1974).

H. B. Mak, H. C. Evans, G. T. Ewan, A. B. McDonald and T. K. Alexander, Bull. Am. Phys. Soc. 20, 31 (1975).

D. Mihalas, Stellar Atmospheres (W. H. Freeman and Co., San Francisco, 1970).

R. Mitalas, Astrophys. J. 177, 693 (1973).

D. W. Moore and E. A. Spiegel, Astrophys. J. 143, 871 (1966).

E. B. Newell, Astrophys. J. 159, 443 (1970).

E. B. Newell, Astrophys. J. Suppl. 26, 37 (1973).

A. Nordlund, Astron. and Astrophys. 32, 407 (1974).

J. Norris, Astrophys. J. 194, 109 (1974).

B. Paczynski, Acta Astron. 20, 195 (1970).

B. Paczynski, Acta Astron. 21, 1 (1971).

M. Peimbert, Mem. Soc. Roy. Sci. Liege Ser. 6, 5, 307 (1973).

J. O. Petersen, Astron. and Astrophys. 19, 197 (1972).

V. Petrosian, G. Beaudet and E. Salpeter, Phys. Rev. 154, 1445 (1967).

M. J. Prather and P. Demarque, Astrophys. J. 193, 109 (1974).

C. H. B. Priestly, Turbulent Transfer in the Lower Atmosphere (Univ. of Chicago Press, Chicago, 1959).

A. Ralston, A First Course in Numerical Analysis (McGraw-Hill, New York, 1965).

L. F. Richardson, Proc. Roy. Soc. A97, 354 (1920).

J. W. Robertson and D. J. Faulkner, Astrophys. J. 171, 309 (1972).

R. T. Rood, Astrophys. J. 162, 939 (1970a).

R. T. Rood, Astrophys. J. 161, 145 (1970b).

R. T. Rood, Astrophys. J. 169, 191 (1971).

R. T. Rood, Astrophys. J. 177, 681 (1972).

R. T. Rood, Astrophys. J. 184, 815 (1973).

I. Roxburgh, Mon. Not. Roy. Astron. Soc. 130, 223 (1965).

E. E. Salpeter, Australian J. Phys. 7, 353 (1954).

A. Sandage, Astrophys. J. 157, 515 (1969).

A. Sandage, Astrophys. J. 162, 841 (1970).

W. L. W. Sargent, Astrophys. J. 148, 147 (1967).

W. L. W. Sargent and L. Searle, Astrophys. J. 152, 443 (1968).

W. C. Saslaw and M. Schwarzschild, Astrophys. J. 142, 1468 (1965).

P. M. Saunders, Tellus 14, 2 (1962).

B. M. Schlesinger, Astrophys. J. 157, 533 (1969).

K. Schwarzschild, Göttingen Nachr., 41 (1906).

M. Schwarzschild, Structure and Evolution of the Stars (Princeton Univ. Press, Princeton, 1958).

M. Schwarzschild and R. Härm, Astrophys. J. 128, 348 (1958).

M. Schwarzschild and R. Härm, Bull. Am. Astron. Soc. 1, 99 (1969).

M. Schwarzschild, Quart. J. Roy. Astron. Soc. 11, 12 (1970).

L. Searle and W. L. W. Sargent, Comm. Ap. and Space Phys. 4, 59 (1972).

G. Shaviv and E. E. Salpeter, Astrophys. J. 184, 191 (1973).

T. G. L. Shirtcliffe, Nature 213, 489 (1967).

T. G. L. Shirtcliffe, J. Fluid Mech. 35, 677 (1969a).

T. G. L. Shirtcliffe, Int. J. Heat Mass Transfer 12, 215 (1969b).

E. A. Spiegel, Comm. Ap. and Space Phys. 1, 57 (1969).

E. A. Spiegel, Comm. Ap. and Space Phys. 3, 53 (1971).

A. V. Sweigart and P. Demarque, Astron. and Astrophys. 20, 445 (1972a).

A. V. Sweigart and P. Demarque, IAU Colloquium #21, ed. J. D. Fernie (D. Reidel, Dordrecht, 1972b).

A. V. Sweigart and P. G. Gross, Astrophys. J. 190, 101 (1974).

A. V. Sweigart, J. G. Mengel and P. Demarque, Astron. and Astrophys. 30, 13 (1974).

T. D. Tarbell and R. T. Rood, Astrophys. J. 199, 443 (1975).

M. G. Tomasko, Astrophys. J. 162, 125 (1970).

A. A. Townsend, J. Fluid Mech. 5, 209 (1959).

A. A. Townsend, Quart. J. Roy. Met. Soc. 90, 248 (1964).

V. Trimble, Astron. and Astrophys. 23, 281 (1973).

R. S. Tuggle and I. Iben, Jr., Astrophys. J. 178, 455 (1972).

J. S. Turner, J. Fluid Mech. 16, 1 (1963).

J. S. Turner and H. Stommel, Proc. Nat. Acad. Sci. USA 52, 49 (1964).

J. S. Turner, Buoyancy Effects in Fluids (Cambridge Univ. Press, Cambridge, 1973).

J. Uchida, K. Suda and Z. Hitotuyanagi, Sci. Rep. Tohuku Univ. 50, 8 (1967).

R. K. Ulrich, Astrophys. and Space Sci. 7, 71 (1970).

A. T. Wilson and H. W. Wellman, Nature 196, 1171 (1962).

TABLE 1

Recent determinations of the primordial helium abundance of globular clusters and field halo stars. Standard errors for all but the first three rows are estimates by the author. All ages except those of M15 and M92 are based on the helium abundance alone, using the calibration of Rood (1973). The very low value of Y_0 in row two is generally believed not to be primordial (Danziger 1970); it is included to remind the reader that surface abundances of highly evolved objects can be misleading. The listing is not exhaustive but represents the most trustworthy data available, in the author's opinion. The global fitting method is a comprehensive comparison of the H-R diagram with evolutionary tracks, with special attention to the properties of RR Lyrae stars.

_

TABLE 1 header

TABLE 1

Stellar Sample	Method	Y_0	Standard Error	Age 10^9 yrs.	Reference
Planetary Nebula (K648) in M15	Spectroscopic He Lines	.29	.03	10.5	Peimbert (1973)
Blue HB Stars (several clusters)	Spectroscopic He Lines	<.03	—	—	Sargent (1967) Newell (1970)
Barnard 29 (B star in M13)	Spectroscopic He Lines	.315	.06	10	Auer and Norris (1974)
M3, M5	R Method, Q Method	.20	.05	16	Iben et al. (1969) This Work
M3	Global Fit	.20–.25	—	11–16	Rood (1973)
M15	Global Fit	.26	.05	14.1	Böhm-Vitense and Szkody (1973)
M92	Global Fit	.23	.05	13.2	Böhm-Vitense and Szkody (1973)
Blue HB Stars (several clusters)	Log g – Log T_e Plane	>.30	<.10	<10	Newell (1973) Gross (1973)
RR Lyrae Stars (M3)	Blue Boundary of Instability Strip	.22	.07	14	Tuggle and Iben (1972)
RR Lyrae Stars (M3)	Blue Boundary of Instability Strip	.30	.07	10.5	Christy (1966) Sandage (1969,1970)

TABLE 1 – (continued)

Stellar Sample	Method	Y_0	Standard Error	Age 10^9 yrs.	Reference
Several Clusters	Main Sequence Fitting, Luminosity Functions	>.20	—	<16	See Iben (1974)
Blue HB Stars in the Field	Log g – Log T_e Plane	.25	<.10	—	Newell (1973) Gross (1973)
sdB Stars in the Field	Log g – Log T_e Plane	<.30	>.10	—	Greenstein and Sargent (1974) This Work

TABLE 2

Properties of the evolutionary sequences for horizontal branch stars. Values of the total mass M_*, helium core mass M_c, envelope (initial) helium abundance Y_e, and initial heavy element abundance Z are chosen to represent stars in M3 or M5 (Rood 1973). Old and new helium-burning reaction rates are discussed in Appendix B. The different treatments of overshooting and semiconvection are described in Chapters 2 and 3.

TABLE 2

Name	$\frac{M_*}{M_\odot}$	$\frac{M_c}{M_\odot}$	Y_e	Z	Rates	Internal Mixing
HB1	.625	.488	.25	.001	Old	Normal Overshooting Normal Semiconvection
HB2	.625	.488	.25	.001	Old	Normal Overshooting Two Convective Zones
HB3	.625	.500	.20	.001	Old	Normal Normal
HB4	.625	.488	.25	.001	New	Normal Normal
HB5	.625	.488	.25	.001	Old	Enhanced Overshooting
HB6	.625	.488	.25	.001	Old	No Overshooting No Semiconvection

TABLE 3

Overshooting rates of selected horizontal branch models. The convective speed v_c is computed from (2.9), assuming $\delta = 0.25$. Mass-penetration rates $\dot{M}$ are given in units of $M_\odot$/s. No overshooting was allowed in HB6, so $\dot{M}_{req}$ is not defined. Numbers in parentheses give the exponent in scientific notation.

TABLE 3

Star	Y_c	v_c cm/s	$\dfrac{\dot{M}_{pen}}{M_\odot}$	$\dfrac{\dot{M}_{req}}{M_\odot}$	$\dfrac{\dot{M}_{pen}}{\dot{M}_{req}}$
HB1	.969	1600	—	—	—
HB1	.885	1700	2.6(−14)	4.9(−17)	530
HB1	.770	1700	1.3(−14)	5.5(−17)	240
HB1	.659	1800	9.6(−15)	6.0(−17)	160
HB2	.556	140	4.4(−17)	5.4(−17)	0.8
HB2	.457	560	2.4(−16)	3.8(−17)	6.3
HB2	.319	840	6.4(−16)	3.2(−17)	20
HB2	.120	1200	1.4(−15)	2.0(−17)	69
HB6	.969	1600	—	—	—
HB6	.879	1600	2.4(−14)	—	—
HB6	.668	1700	8.2(−15)	—	—
HB6	.489	1900	5.7(−15)	—	—

TABLE 4

Dimensionless extent of hydrogen-burning convective cores. Subscript "c" refers to the core boundary; the last column gives the prediction of (2.30), if a minimum of ∇_{rad} were to occur. Models are those of Kushwaha (1957).

TABLE 4

$\dfrac{M_*}{M_\odot}$	$\dfrac{M_c}{M_\odot}$	U_c	V_c	α_c	$\dfrac{3V_c}{5U_c}$	$\dfrac{3V}{5U_{min}}$
10	2.44	2.40	1.79	.293	.448	.768
5	1.01	2.48	1.55	.662	.375	.653
2.5	0.41	2.55	1.33	1.45	.313	.559

TABLE 5

Location of the minimum of ∇_{rad}/∇_{ad} for selected
models. The fourth column gives the actual value of 3V/5U
at the minimum, while column five is the value predicted
by (2.30). Values of $P_c^{3/2}/\rho_c^2$ are normalized to the first
one. The first model for HB1 and those for other sequences
represent the onset of semiconvection. Model S is taken
from Sweigart and Gross (1974) and uses the normal treat-
ment of overshooting and semiconvection.

TABLE 5

Star	Y_c	$\dfrac{M_{min}}{M_\odot}$	$\dfrac{3V}{5U}$	$\dfrac{3V}{5U_P}$	$\dfrac{P_c^{3/2}}{\rho_c^2}$
HB1	.608	.1720	.680	.683	1.00
HB1	.502	.1703	.676	.683	.999
HB1	.405	.1690	.671	.679	.994
HB1	.301	.1676	.669	.675	.987
HB1	.203	.1655	.664	.673	.979
HB1	.102	.1625	.657	.671	.970
HB3	.609	.1749	.684	.688	1.015
HB4	.575	.1711	.683	.684	.994
S	.742	.166	.651	—	1.007

TABLE 6

Interior properties of HB1. t is the elapsed time since the initial model in units of 10^6 years. The second and third columns list the central ^{4}He abundance, ^{12}C abundance, temperature (10^{6}°K), and density (10^4gm/cm^3). M_{cc} and M_{sc} are the masses at the fully convective core boundary and the semiconvective zone boundary, respectively. M_{sh} is the mass at the midpoint in luminosity of the hydrogen-burning shell; T_{sh} is the temperature at that point. The contributions of helium and hydrogen-burning to the luminosity are L_{He} and L_H; their sum is not precisely the total luminosity because of gravitational effects. All masses are in solar mass units (1.989 x 10^{33}gm) and likewise for luminosities (3.90 x 10^{33}erg/sec). The last row gives the structure immediately before the composition instability.

TABLE 6

t	Y_c	T_c	M_{cc}	M_{sh}	L_{He}
	X_{12c}	ρ_c	M_{sc}	T_{sh}	L_H
0.0	.969	120.3	.1129	.4918	17.55
	.030	1.99	–	27.2	24.13
7.5	.885	121.4	.1268	.4923	19.84
	.110	2.00	–	27.4	24.18
14.8	.770	123.1	.1430	.4937	21.55
	.210	1.98	–	27.4	23.76
25.2	.659	125.1	.1627	.4963	23.88
	.295	1.93	–	27.1	20.23
34.4	.576	126.9	.1720	.4987	26.00
	.350	1.88	.1813	26.8	16.86
42.7	.502	128.7	.1720	.5004	27.92
	.393	1.85	.1955	26.5	14.15
49.8	.438	130.4	.1700	.5016	29.62
	.425	1.84	.2059	26.2	12.23
56.8	.371	132.4	.1700	.5026	31.36
	.453	1.83	.2152	26.0	10.49
63.7	.316	134.4	.1683	.5035	33.12
	.466	1.83	.2229	25.8	9.06
70.2	.259	136.7	.1670	.5042	34.76
	.476	1.85	.2299	25.7	8.06
76.2	.208	139.1	.1661	.5048	36.28
	.475	1.89	.2358	25.6	7.46
83.1	.154	142.3	.1649	.5053	37.90
	.463	1.94	.2418	25.6	7.16
90.7	.105	146.2	.1627	.5059	39.55
	.431	2.04	.2471	25.8	7.26
98.2	.065	150.2	.1636	.5066	40.76
	.384	2.14	.2523	26.0	7.86

TABLE 7

Surface properties of HB1. t and Y_c identify the models in Table 5. Log L is the surface luminosity in solar units; log g, the surface gravity in units of cm/sec^2; and log T_e is the effective temperature (^OK). In the last column, R is the radius at the surface; the tabulated quantity is approximately equal to the logarithmic rate of change of the pulsation period, if the model lies in the instability strip. Note that there is no clear preference for positive or negative period changes. By definition, the surface of the star is the point where $T(R) = T_e/2^{1/4}$.

TABLE 7

t	Y_c	log L	log g	log T_e	$\frac{3}{2}\frac{1}{R}\frac{dR}{dt}$
0.0	.969	1.634	3.112	3.891	.091
7.5	.885	1.649	3.068	3.884	-.001
14.7	.770	1.655	3.092	3.892	-.017
25.2	.659	1.643	3.214	3.919	-.020
34.4	.576	1.631	3.317	3.942	-.016
42.7	.502	1.622	3.379	3.955	-.008
49.8	.438	1.620	3.404	3.961	-.004
56.8	.371	1.620	3.415	3.963	.002
63.7	.316	1.624	3.405	3.962	.004
70.2	.259	1.630	3.382	3.958	.008
76.2	.208	1.640	3.348	3.952	.011
83.1	.154	1.653	3.300	3.943	.015
90.7	.103	1.670	3.243	3.933	.016
98.2	.065	1.687	3.194	3.925	.009

TABLE 8

Interior properties of HB2. All quantities are defined in the caption to Table 6, although here M_{sc} is the mass at the upper boundary of the second convective zone. Models of HB2 before the onset of semiconvection are those of HB1, listed in Table 6. For $Y_c \leq 0.45$, these models are probably not consistent because overshooting should bring about normal semiconvection.

TABLE 8

t	Y_c	T_c	M_{cc}	M_{sh}	L_{He}
	X_{12c}	ρ_c	M_{sc}	T_{sh}	L_H
31.9	.578	126.9	.1714	.4987	25.99
	.348	1.88	.1813	26.8	16.80
43.9	.500	128.8	.1707	.5006	28.05
	.392	1.85	.1959	26.4	13.79
51.0	.441	130.4	.1703	.5019	29.73
	.421	1.83	.2057	26.2	11.87
58.9	.374	132.4	.1693	.5029	31.69
	.449	1.82	.2153	25.9	10.05
65.7	.319	134.3	.1686	.5038	33.39
	.464	1.82	.2227	25.7	7.69
73.4	.258	136.8	.1679	.5046	35.44
	.474	1.84	.2303	25.6	7.61
79.9	.209	139.2	.1667	.5051	37.05
	.473	1.87	.2361	25.5	6.85
87.6	.156	142.4	.1658	.5057	39.07
	.459	1.92	.2426	25.5	6.50
96.1	.106	146.3	.1649	.5063	41.07
	.427	2.00	.2484	25.6	6.39
106.3	.062	150.9	.1660	.5071	42.99
	.370	2.12	.2542	25.8	6.89
115.5	.040	154.4	.1668	.5078	44.30
	.312	2.23	.2591	26.1	7.65

TABLE 9

Surface properties of HB2. All quantities are de-
fined in the caption of Table 7. The models of HB2 prior
to the onset of semiconvection are identical to those of
HB1.

TABLE 9

t	Y_c	log L	log g	log T_e	$\frac{3}{2} \frac{1}{R} \frac{dR}{dt}$
31.9	.578	1.631	3.318	3.942	-.015
43.9	.500	1.620	3.385	3.956	-.008
51.0	.441	1.618	3.411	3.962	-.002
58.9	.374	1.619	3.414	3.963	.001
65.7	.319	1.623	3.402	3.961	.007
73.4	.258	1.633	3.376	3.957	.014
79.9	.209	1.642	3.331	3.948	.012
87.6	.156	1.658	3.279	3.939	.013
96.1	.106	1.676	3.213	3.927	.012
106.3	.062	1.698	3.139	3.914	.009
115.5	.040	1.716	3.089	3.906	.014

TABLE 10

Interior properties of HB3. All quantities are defined in the caption of Table 6.

TABLE 10

t	Y_C / X_{12c}	T_C / ρ_C	M_{CC} / M_{sc}	M_{sh} / T_{sh}	L_{He} / L_H
0.	.969 / .030	121.0 / 1.89	.1117 / –	.5039 / 26.1	19.84 / 14.41
4.8	.889 / .106	121.7 / 1.95	.1297 / –	.5041 / 26.2	22.18 / 14.55
13.8	.764 / .215	123.8 / 1.89	.1470 / –	.5046 / 26.0	23.89 / 12.55
23.0	.663 / .293	125.5 / 1.87	.1648 / –	.5052 / 25.8	25.72 / 10.73
31.8	.577 / .351	127.3 / 1.84	.1744 / .1833	.5059 / 25.5	27.53 / 8.95
39.8	.503 / .394	129.0 / 1.82	.1730 / .1970	.5064 / 25.3	29.18 / 7.46
46.7	.439 / .425	130.7 / 1.81	.1717 / .2071	.5069 / 25.0	30.68 / 6.20
53.6	.374 / .453	132.5 / 1.81	.1707 / .2156	.5073 / 24.8	32.27 / 5.34
60.3	.314 / .470	134.6 / 1.82	.1696 / .2237	.5076 / 24.7	33.84 / 4.57
66.1	.262 / .478	136.7 / 1.84	.1680 / .2302	.5079 / 24.5	35.20 / 4.06
72.0	.210 / .481	139.0 / 1.88	.1666 / .2360	.5081 / 24.5	36.58 / 3.71
79.6	.154 / .464	142.3 / 1.94	.1650 / .2422	.5083 / 24.5	38.28 / 3.49
86.7	.107 / .434	145.8 / 2.03	.1637 / .2478	.5084 / 24.6	39.73 / 3.54
94.3	.068 / .388	149.8 / 2.13	.1639 / .2524	.5086 / 24.8	40.93 / 3.87

TABLE 11

Surface properties of HB3. All quantities are
defined in the caption of Table 7.

TABLE 11

t	Y_c	log L	log g	log T_e	$\frac{3}{2}\frac{1}{R}\frac{dR}{dt}$
0.0	.969	1.552	3.378	3.937	.059
4.8	.889	1.562	3.344	3.931	-.012
13.8	.764	1.560	3.370	3.937	.000
23.0	.663	1.559	3.376	3.939	.000
31.8	.577	1.560	3.375	3.938	.002
39.8	.503	1.562	3.362	3.936	.007
46.7	.439	1.565	3.334	3.929	.007
53.6	.374	1.573	3.298	3.923	.012
60.3	.314	1.583	3.248	3.913	.015
66.1	.262	1.592	3.196	3.902	.017
72.0	.210	1.604	3.137	3.890	.018
79.6	.154	1.620	3.057	3.874	.019
86.7	.107	1.636	2.985	3.860	.017
94.3	.068	1.652	2.921	3.848	.020

TABLE 12

Interior properties of HB4. All quantities are defined in the caption of Table 6. Note that this sequence is identical to HB1 except for the reaction rates.

TABLE 12

t	Y_c	T_c	M_{cc}	M_{sh}	L_{He}
	X_{12c}	ρ_c	M_{sc}	T_{sh}	L_H
0.0	.969	118.5	.1194	.4919	17.85
	.030	1.88	–	26.9	21.31
5.2	.887	119.6	.1277	.4923	20.11
	.110	1.89	–	27.0	21.58
13.8	.769	121.3	.1421	.4933	21.74
	.222	1.88	–	27.0	20.29
23.7	.660	123.3	.1588	.4950	23.78
	.319	1.85	–	26.8	17.88
31.6	.575	125.1	.1711	.4966	25.59
	.391	1.83	.1730	26.5	15.34
39.2	.503	126.8	.1702	.4980	27.40
	.448	1.80	.1854	26.3	13.08
45.3	.441	128.5	.1693	.4990	28.91
	.494	1.80	.1951	26.1	11.42
52.0	.373	130.5	.1683	.5000	30.63
	.542	1.80	.2040	25.9	9.86
56.9	.320	132.3	.1673	.5006	31.95
	.576	1.81	.2098	25.7	8.92
63.2	.257	134.9	.1660	.5012	33.61
	.610	1.85	.2164	25.6	8.10
68.1	.206	137.4	.1651	.5016	34.98
	.633	1.89	.2212	25.7	7.91
73.7	.154	140.5	.1641	.5021	36.40
	.646	1.97	.2262	25.7	7.86
79.6	.105	144.4	.1631	.5025	37.74
	.645	2.08	.2307	26.0	8.40
83.6	.079	146.9	.1651	.5029	38.54
	.633	2.19	.2336	26.1	9.00

TABLE 13

Surface properties of HB4. All quantities are defined in the caption of Table 7.

TABLE 13

t	Y_c	log L	log g	log T_e	$\frac{3}{2}\frac{1}{R}\frac{dR}{dt}$
0.0	.969	1.607	3.238	3.916	.082
5.2	.887	1.618	3.207	3.911	.000
13.8	.769	1.622	3.219	3.915	-.008
23.7	.660	1.618	3.275	3.928	-.014
31.6	.575	1.610	3.339	3.942	-.011
39.2	.503	1.605	3.380	3.951	-.007
45.3	.441	1.604	3.399	3.955	-.002
52.0	.373	1.606	3.395	3.955	.003
56.9	.320	1.610	3.383	3.953	.009
63.2	.257	1.619	3.350	3.947	.012
68.1	.206	1.631	3.314	3.941	.016
73.7	.154	1.646	3.263	3.932	.023
79.6	.105	1.664	3.197	3.920	.019
83.6	.079	1.678	3.151	3.912	.026

TABLE 14

Interior properties of HB5. All quantities are
defined in the caption of Table 6. This sequence terminates
just before the onset of semiconvection.

TABLE 14

t	Y_c	T_c	M_{cc}	M_{sh}	L_{He}
	X_{12c}	ρ_c	M_{sc}	T_{sh}	L_H
0.0	.969	120.2	.1314	.4918	17.53
	.030	1.99	–	27.2	24.13
6.2	.879	121.5	.1355	.4924	19.91
	.115	1.99	–	27.4	24.69
14.4	.776	123.0	.1478	.4937	21.47
	.205	1.97	–	27.3	23.50
24.8	.668	125.0	.1662	.4962	23.71
	.289	1.92	–	27.1	20.20

TABLE 15

Surface properties of HB5. All quantities are
defined in the caption of Table 7.

TABLE 15

t	Y_c	log L	log g	log T_e	$\frac{3}{2} \frac{1}{R} \frac{dR}{dt}$
0.0	.969	1.634	3.112	3.891	.094
6.2	.879	1.647	3.070	3.884	−.001
14.4	.776	1.651	3.098	3.892	−.016
24.8	.668	1.641	3.212	3.918	−.020

TABLE 16

Interior properties of HB6. All quantities are defined in the caption of Table 6. No overshooting is allowed, so M_{sc} is not defined. The sequence terminates arbitrarily at $Y_c = 0.01$, although there is no composition instability to hamper further evolution.

TABLE 16

t	Y_c	T_c	M_{cc}	M_{sh}	L_{He}
	X_{12c}	ρ_c		T_{sh}	L_H
0.0	.969	120.3	.1129	.4918	17.55
	.030	1.99		27.2	24.13
5.6	.879	121.4	.1211	.4923	19.88
	.115	2.01		27.4	24.90
11.4	.783	122.8	.1211	.4931	21.01
	.200	1.99		27.3	23.84
18.2	.668	124.5	.1211	.4945	22.56
	.292	2.01		27.3	22.13
24.2	.563	126.4	.1211	.4960	24.07
	.367	2.03		27.1	19.92
34.8	.377	130.7	.1211	.4985	26.81
	.469	2.11		26.8	16.49
41.6	.259	134.5	.1211	.4999	28.49
	.507	2.23		26.7	15.47
47.9	.161	139.0	.1211	.5011	29.78
	.509	2.42		26.9	16.00
51.7	.108	142.6	.1211	.5018	30.38
	.490	2.58		27.1	17.43
56.3	.060	147.2	.1211	.5028	30.77
	.448	2.85		27.5	20.73
60.3	.030	151.8	.1211	.5040	30.86
	.402	3.15		28.0	25.16
62.8	.0173	155.2	.1211	.5049	30.72
	.372	3.39		28.4	29.25
64.8	.0098	158.3	.1211	.5057	30.39
	.361	3.63		28.8	33.63

TABLE 17

Surface properties of HB6. All quantities are
defined in the caption of Table 7.

TABLE 17

t	Y_c	log L	log g	log T_e	$\frac{3}{2}\frac{1}{R}\frac{dR}{dt}$
0.0	.969	1.634	3.112	3.891	+.100
5.6	.879	1.649	3.063	3.883	−.007
11.4	.783	1.650	3.087	3.889	−.009
18.2	.668	1.649	3.133	3.900	−.020
24.2	.563	1.642	3.201	3.916	−.018
34.8	.377	1.635	3.282	3.934	.000
41.6	.259	1.642	3.279	3.935	.008
47.9	.161	1.661	3.228	3.927	.024
51.7	.108	1.680	3.164	3.916	.039
56.3	.060	1.714	3.039	3.893	.058
60.3	.030	1.751	2.884	3.864	.092
62.8	.0173	1.781	2.741	3.836	.116
64.8	.0098	1.810	2.583	3.803	.166

TABLE 18

Interior properties of HB1 after imposed mixing.
All quantities are defined in the caption of Table 6. Just
before the composition instability appears, models are
gradually converted to the double-zone scheme of HB2; the
core is extended only until M_{min} is neutralized at each
time step. Eventually, the entire semiconvective zone is
mixed, and the model is identical in structure to HB2.
Here, $M_{cc} = M_{min}$ and M_{sc} is the mass at the upper boundary
of the second convective zone; initially, the jump to un-
burned composition occurs at M = .2523. t is the elapsed
time since the start of mixing, which occurred 97.65×10^6
years after the initial model. Before mixing, Y_c = .069.

TABLE 18

t	Y_c	T_c	M_{cc}	M_{sh}	L_{He}
	X_{12c}	ρ_c	M_{sc}	T_{sh}	L_H
0.0	.074	149.1	.1655	.5066	40.97
	.389	2.13	.2006	25.9	7.60
1.24	.077	149.0	.1655	.5067	41.36
	.382	2.10	.2225	25.8	7.20
2.53	.087	148.2	.1649	.5069	41.87
	.373	2.06	.2432	25.7	6.70
3.68	.106	146.7	.1659	.5070	41.91
	.362	1.99	.2543	25.5	6.09
5.08	.096	147.6	.1646	.5071	41.81
	.358	2.01	.2543	25.6	6.19
6.93	.083	148.9	.1646	.5072	42.43
	.352	2.05	.2543	25.7	6.35
9.09	.074	149.9	.1661	.5074	42.86
	.342	2.08	.2555	25.7	6.49
11.92	.063	151.2	.1665	.5076	43.36
	.327	2.12	.2569	25.8	6.73

TABLE 19

Surface properties of HBl after imposed mixing.
See the caption of Table 18 for explanation. The pulsation
period changes in the first four rows may be unphysical be-
cause the composition instability probably develops on a
faster time scale. The fourth row represents the end of
arbitrary mixing, after which the star evolves on a nuclear
time scale; therefore, subsequent period changes are more
realistic.

TABLE 19

t	Y_c	log L	log g	log T_e	$\frac{3}{2}\frac{1}{R}\frac{dR}{dt}$
0.0	.074	1.686	3.195	3.925	.004
1.24	.077	1.685	3.196	3.925	.003
2.53	.087	1.684	3.197	3.925	-.006
3.68	.106	1.678	3.207	3.926	-.030
5.08	.096	1.682	3.199	3.925	.031
6.93	.083	1.688	3.181	3.922	.017
9.09	.074	1.693	3.164	3.919	.020
11.92	.063	1.700	3.141	3.915	.009

TABLE 20

Interior properties of HB2 after imposed mixing.
All quantities are defined in the caption of Table 6. The
first row gives the structure before mixing, corresponding
to t = 117.20 in Table 8. The convection zone was arbi-
trarily extended, resulting in the model of row two (Y_c =
.074). Section 3.4 describes these models in greater de-
tail. No overshooting was permitted for models with Y_c <
.016; the sequence was terminated at the last model shown
because of extremely slow convergence. Negative numbers in
the second column give the exponent of Y_c in scientific
notation.

TABLE 20

t	Y_c	T_c	M_{cc}	M_{sh}	L_{He}
	X_{12}	ρ_c	M_{sc}	T_{sh}	L_H
0.0	.043	154.0	.1679	.5080	44.50
	.299	2.24	.2614	26.1	7.70
0.89	.074	152.8	.1800	.5082	45.44
	.285	2.23	.2658	26.0	6.93
2.32	.064	150.8	.1709	.5084	44.55
	.280	2.18	.2658	25.9	6.68
4.65	.049	154.2	.1660	.5087	44.23
	.267	2.08	.2658	25.8	6.46
11.0	.021	158.9	.1703	.5090	44.95
	.225	2.42	.2658	26.6	9.88
16.8	9.9 −3	163.3	.1640	.5098	44.72
	.196	2.59	.2658	27.1	12.60
21.3	2.8 −3	170.2	.1640	.5107	43.93
	.176	2.97	.2658	28.0	19.81
24.1	5.1 −4	180.8	.1640	.5115	41.50
	.169	3.36	.2658	29.0	30.78
24.9	1.0 −4	187.0	.1219	.5117	30.78
	.168	4.31	.2658	30.2	46.89
25.2	2.2 −5	195.7	.0934	.5116	24.30
	.168	5.15	.2658	31.2	62.68

TABLE 21

Surface properties of HB2 after imposed mixing.

See Tables 7 and 20 for explanation.

TABLE 21

t	Y_c	log L	log g	log T_e	$\frac{3}{2} \frac{1}{R} \frac{dR}{dt}$
0.0	.043	1.717	3.084	3.905	−.002
0.89	.074	1.717	3.080	3.904	−.040
2.32	.064	1.709	3.112	3.910	−.032
4.65	.049	1.704	3.137	3.915	.015
11.0	.021	1.740	3.025	3.896	.012
16.8	9.9 −3	1.762	2.963	3.886	.056
21.3	2.8 −3	1.808	2.765	3.848	.133
24.1	5.1 −4	1.867	2.414	3.775	.644
24.9	1.0 −4	1.943	2.090	3.713	.788
25.2	2.2 −5	2.009	1.960	3.697	1.162

TABLE 22

Ratios of horizontal branch and red giant lifetimes as a function of Y_0. $R = t_{HB}/t_{RG}$ and $Q = t_{HB}/\Delta t_{RG}$ as defined in (3.23) and (3.26). Three values are shown for each, using best values and lower and upper limits for t_{HB}.

TABLE 22

Y_0	0.25	0.20
R_L	1.36	1.05
R	1.49	1.15
R_u	1.65	1.28
Q_L	4.13	3.12
Q	4.53	3.42
Q_u	5.02	3.79

TABLE 23

Properties of sdB models as a function of envelope mass. All quantites are defined in the captions of Tables 6 and 7. Log L/M is the light-to-mass ratio, both expressed in solar units. All models have a surface composition of $Y_e = 0.25$ and $Z = 0.001$; core composition is $Y_c = 0.969$ and $X_{12c} = 0.03$. The helium core mass is 0.488 $M_\odot$ and the region of varying composition in the hydrogen-burning shell extends to M = 0.490 $M_\odot$. M_{cc}, the convective core mass, varies smoothly from .117 in the first row to .111 in the last. As usual, the units of T_c, T_e, ρ_c and g are $10^{6 \circ}K$, $^\circ K$, $10^4 gm/cm^3$, and cm/sec^2.

TABLE 23

M_*	T_c	L_{He}	$\log L$	$\log T_e$
	ρ_c	L_H	$\log g$	$\log (L/M)$
.600	118.8	19.4	1.547	4.020
	1.86	15.8	3.70	1.77
.575	118.8	19.5	1.458	4.121
	1.86	9.2	4.18	1.70
.550	118.8	19.3	1.351	4.208
	1.87	3.25	4.61	1.61
.525	118.5	18.4	1.277	4.284
	1.91	0.55	4.97	1.56
.510	118.2	17.6	1.248	4.340
	1.95	0.12	5.21	1.54
.500	118.0	17.0	1.230	4.391
	1.98	0.02	5.42	1.53
.495	117.9	16.6	1.219	4.426
	2.00	0.00	5.57	1.52
.4925	117.8	16.4	1.214	4.450
	2.01	0.00	5.67	1.52

TABLE 24

Properties of sdB models as a function of core
mass. See Tables 6, 7 and 23 for definitions. L_H is less
than 0.02 $L_\odot$ for all models. All models have surface
abundances $(X_e, Z) = (.75, .001)$.

TABLE 24

M_*	M_c	T_c	log L	log T_e
	M_{cc}	ρ_c	log g	log (L/M)
.487	.475	117.4	1.178	4.383
	.109	2.08	5.36	1.49
.512	.500	118.6	1.276	4.397
	.116	1.89	5.41	1.57
.537	.525	119.8	1.366	4.410
	.124	1.72	5.40	1.64
.562	.550	121.0	1.450	4.423
	.131	1.58	5.38	1.70

TABLE 25

Properties of sdB models as a function of envelope composition. See Tables 6, 7 and 23 for definitions. All models have $M_* = 0.5275$ and $M_c = 0.525$. The surface hydrogen abundance (mass fraction) is X_e; Z is the mass fraction of heavy elements. The interior properties of these models are predictable from Tables 23 and 24 and are not given.

TABLE 25

X_e	Z	log L	log g	log T_e	log (L/M)
.99	.001	1.347	5.63	4.465	1.63
.75	.001	1.348	5.76	4.499	1.63
.50	.001	1.348	5.90	4.533	1.63
.50	.010	1.350	5.83	4.515	1.63
.20	.010	1.350	5.99	4.557	1.63

TABLE 26

Quasi-evolutionary sequence for a sdB star. Surface and interior properties are shown for static models with helium-depleted convective cores and semiconvective zones, described in Section 4.3. t is the elapsed time (10^6 years) since the initial model, obtained by scaling the lifetimes of HB4 by the ratio of the helium luminosities. See Tables 6, 7 and 23 for other definitions. This star has initial parameters (M_*, M_c, X_e, Z) equal to (.510, .500, .75, .001).

TABLE 26

t	Y_c	M_{cc}	T_c	log L	log T_e
	X_{12c}	M_{sc}	ρ_c	log g	log (L/M)
0.	.969	.117	118.6	1.272	4.410
	.030	–	1.89	5.46	1.57
29.7	.600	.167	125.0	1.400	4.393
	.370	–	1.79	5.28	1.68
58.3	.300	.167	134.4	1.536	4.376
	.587	.212	1.73	5.06	1.83
78.0	.100	.164	147.8	1.618	4.385
	.645	.230	2.01	5.01	1.91

TABLE 27

Initial models for sdB quasi-evolutionary sequences.
The sequences plotted in Figure 11 started from these mod-
els and may be identified by comparing log (L/M) and log T_e.
Evolution is similar to that shown in Table 26, and the same
values of Y_c and X_{12c} were used in each sequence. See
previous tables for definitions.

TABLE 27

M_*	X_e	T_c	log L	log T_e
M_c	Z	ρ_c	log g	log (L/M)
.510	.75	118.6	1.272	4.410
.500	.001	1.89	5.46	1.57
.535	.75	119.8	1.363	4.423
.525	.001	1.73	5.45	1.64
.5275	.75	119.6	1.348	4.499
.525	.001	1.75	5.76	1.63
.560	.75	120.9	1.447	4.436
.550	.001	1.59	5.44	1.70
.5525	.75	120.7	1.433	4.511
.550	.001	1.61	5.74	1.69
.5275	.99	119.6	1.347	4.465
.525	.001	1.75	5.63	1.63
.560	.99	120.9	1.449	4.362
.550	.001	1.59	5.14	1.70
.560	.20	121.2	1.455	4.555
.550	.010	1.57	5.90	1.71

TABLE 28

Non-resonant reaction rates. All quantities are defined in (B.1 - 3) of Appendix B. The reactions in the last column are assumed to follow the primary reaction instantaneously.

TABLE 28

Primary Reaction	A_{ij}	B_{ij}	$\dfrac{S_{ij}}{S_0}$	$10^5 E_{ij}$ ergs	Subsequent Reactions
$^1H(p, e^+\nu)^2H$	25.45904	33.8077	0.25	1.070	$^2H(p, \gamma)^3He$
$^3He(^3He, 2p)^4He$	81.43872	122.737	1.0	2.059	
$^4He(^3He, \gamma)^7Be$	72.51508	128.266	1.0	0.253	$^7Be(p, \gamma)^8B(e^+\nu)^8Be^*(\alpha)^4He$ or $^7Be(e^-, \nu\gamma)^7Li(p, \alpha)^4He$
$^{12}C(p, \gamma)^{13}N$	73.64976	136.913	1.5	1.761	$^{13}N(e^+\nu)^{13}C(p, \gamma)^{14}N$
$^{14}N(p, \gamma)^{15}O$	74.35622	152.299	1.75	2.250	$^{15}O(e^+\nu)^{15}N(p, \alpha)^{12}C$ or $^{15}N(p, \gamma)^{16}O$
$^{16}O(p, \gamma)^{17}F$	75.47576	166.945	2.0	0.581	$^{17}F(e^+\nu)^{17}O(p, \alpha)^{14}N$
$^{18}O(\alpha, \gamma)^{22}Ne$	96.52073	400.5018	2.0	1.547	

TABLE 29

Screening functions for the triple-alpha process and $^{12}C(\alpha, \gamma)^{16}O$. The temperatures and compositions are appropriate for horizontal branch stars; we have assumed $X_{16} = 1 - Y - X_{12}$ and $\rho = 2 \times 10^4$ gm/cm^3. S_{444} and S_{412} are the old screening functions, S_w is the correct weak screening result for both reactions, and S_{444}^I and S_{412}^I are the intermediate (new) screening functions. Perhaps Iben (1965b) was anticipating the smaller values of S_{444}^I and S_{412}^I when he chose not to use S_w.

TABLE 29

T_6	Y	X_{12}	S_{444}	S_{412}	S_w	S^I_{444}	S^I_{412}
120.	.97	.03	.101	.152	.303	.186	.176
130.	.50	.40	.116	.174	.347	.209	.197
140.	.10	.70	.120	.180	.360	.220	.208
150.	.10	.70	.108	.162	.325	.201	.190
150.	.10	.45	.112	.168	.336	.206	.195

TABLE 30

Ratios of new to old reaction rates for helium burning. Density and compositions are those of the previous table. Column headings identify the quantities whose dimensionless ratios are tabulated, T_6 excepted. Thus the last column gives ε_{444}(new) ε_{412}(old)$/\varepsilon_{444}$(old) ε_{412}(new).

TABLE 30

T_6	$<\sigma v>_{444}$	$<\sigma v>_{412}$	ε_{444}	ε_{412}	$\dfrac{\varepsilon_{444}}{\varepsilon_{412}}$
120	1.786	.605	1.94	.620	3.13
130	1.762	.612	1.93	.626	3.08
140	1.741	.618	1.92	.636	3.02
150	1.723	.625	1.89	.643	2.94
150	1.723	.625	1.89	.642	2.94

FIGURE 1

Self-consistent abundance profiles during the overshooting phase. These are numerical solutions of (2.17) and (2.19) showing Y(Z) in the region of varying abundance above the deceleration zone of the convective core; $Y_c = 0.90$ and $Y_e = 0.969$. Curves are labeled with the value of n which determines the velocity distribution, (2.20). Z is measured in units of $\bar{v}^2 \mu_c / g \delta \mu$. The curve for $n = 0$ is concave down because the most probable velocity is zero in this case.
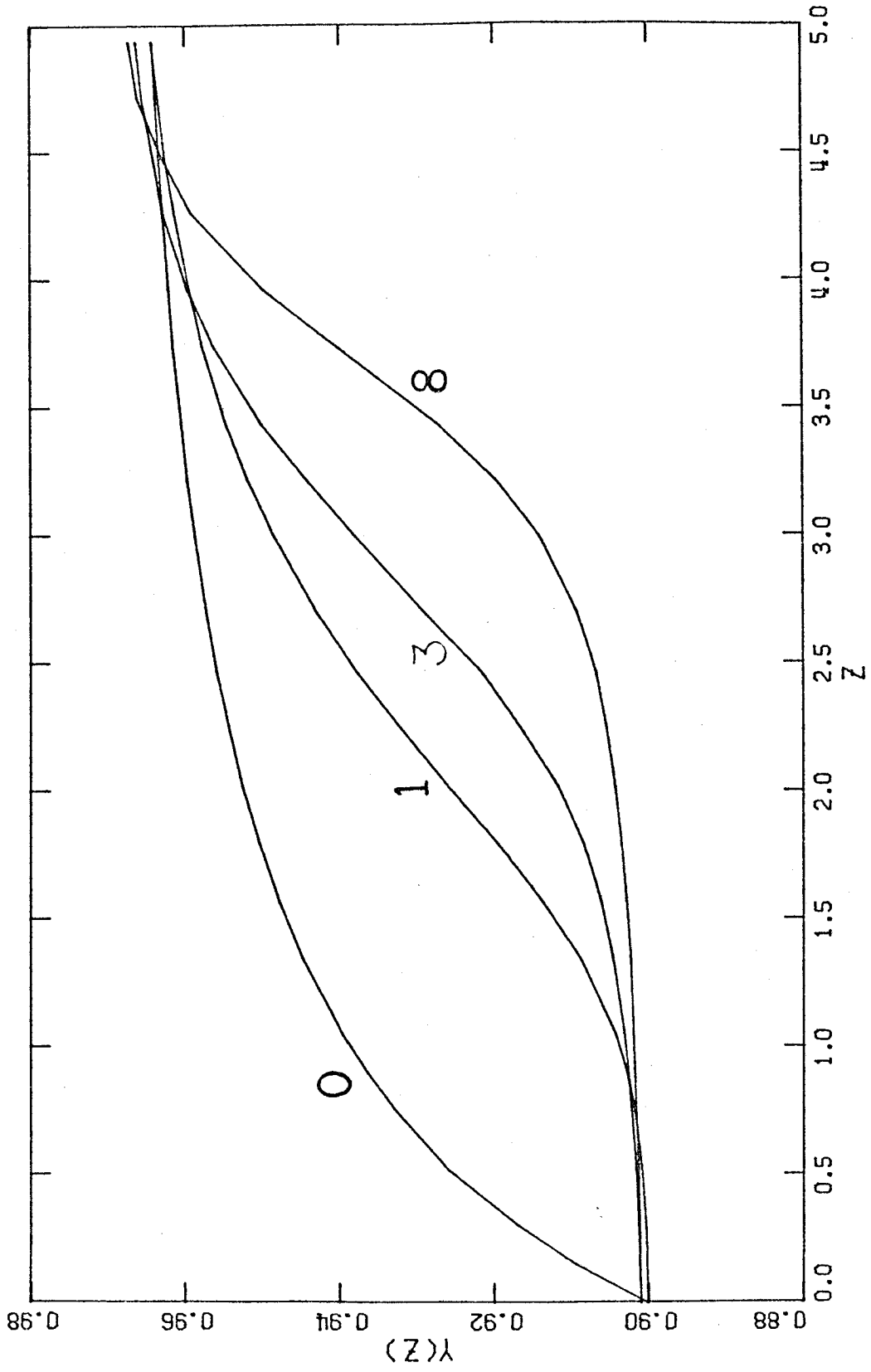
FIGURE 2

∇_{rad}/∇_{ad} vs. M during the overshooting phase.
Parts (a) and (b) refer to convective core masses less
than and greater than M_{min}, respectively. Uniform
Y is assumed for $0 \leq M \leq M_{cc}$.
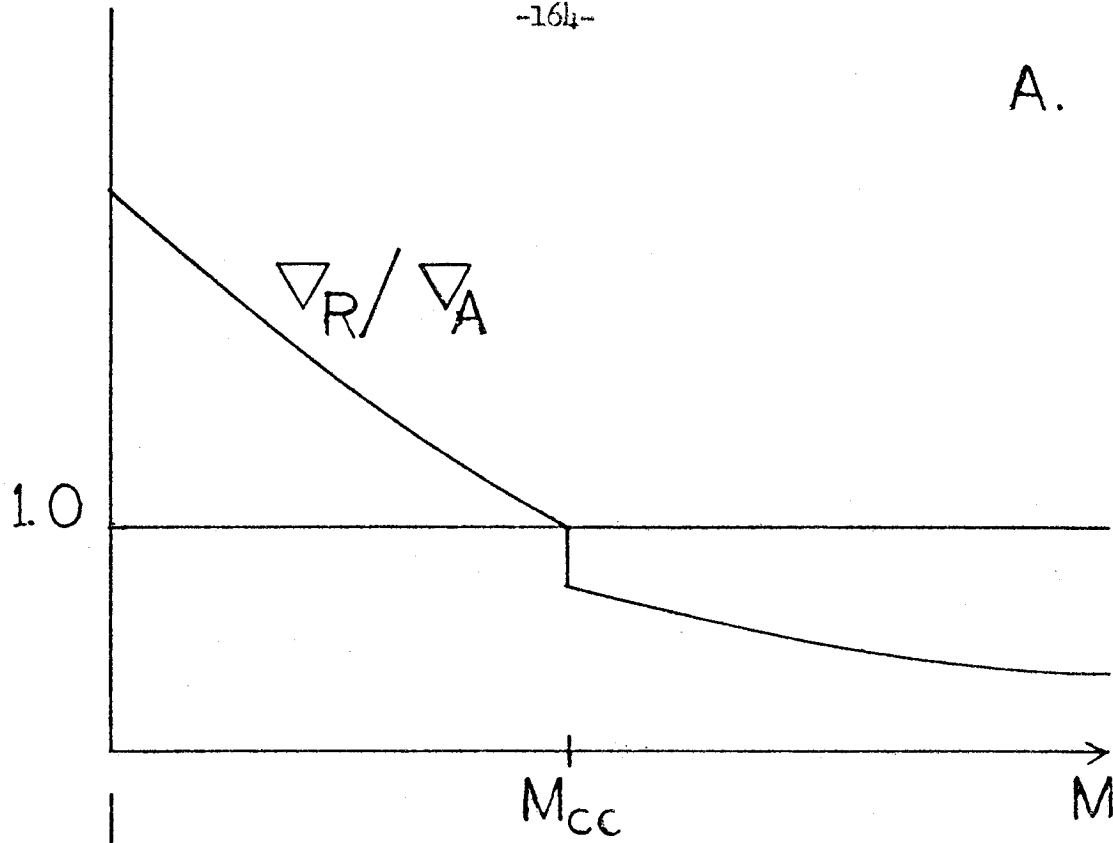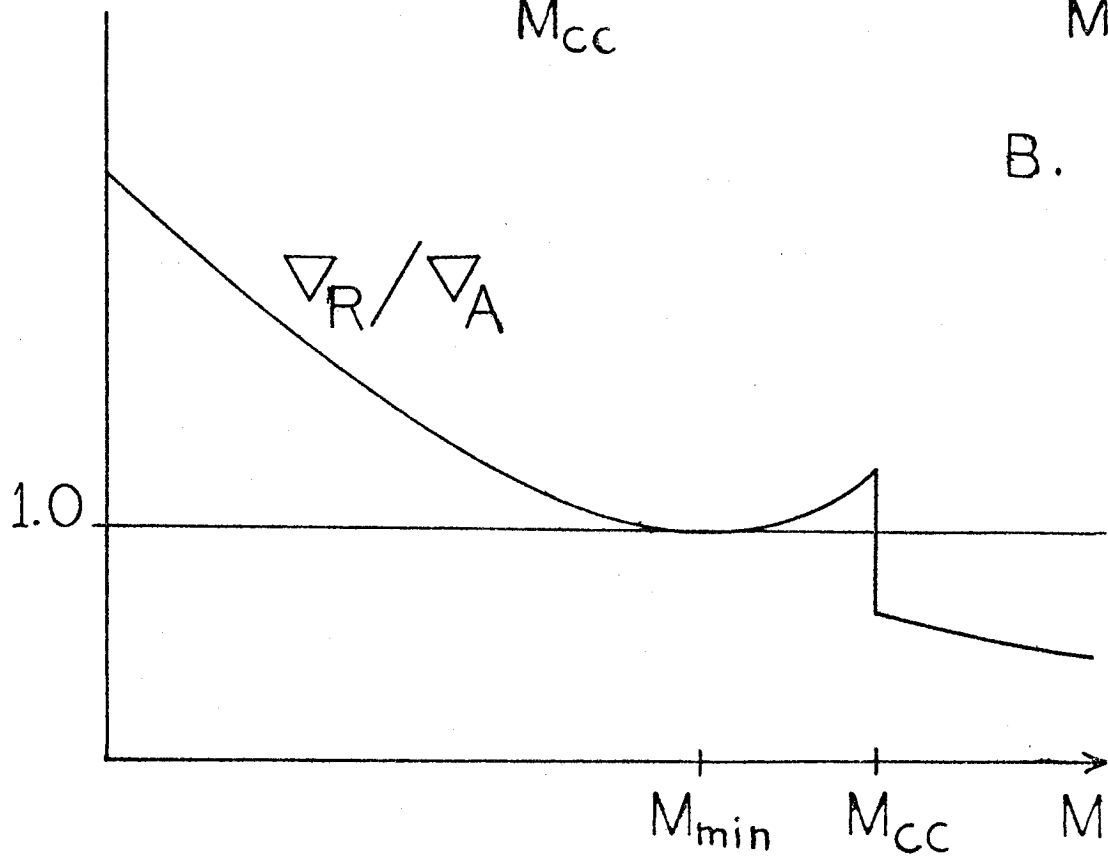
FIGURE 3(a)

Qualitative behavior of Y and ∇_{rad}/∇_{ad} vs. M during normal semiconvection. This "bucket brigade" model is described in Section 2.3.
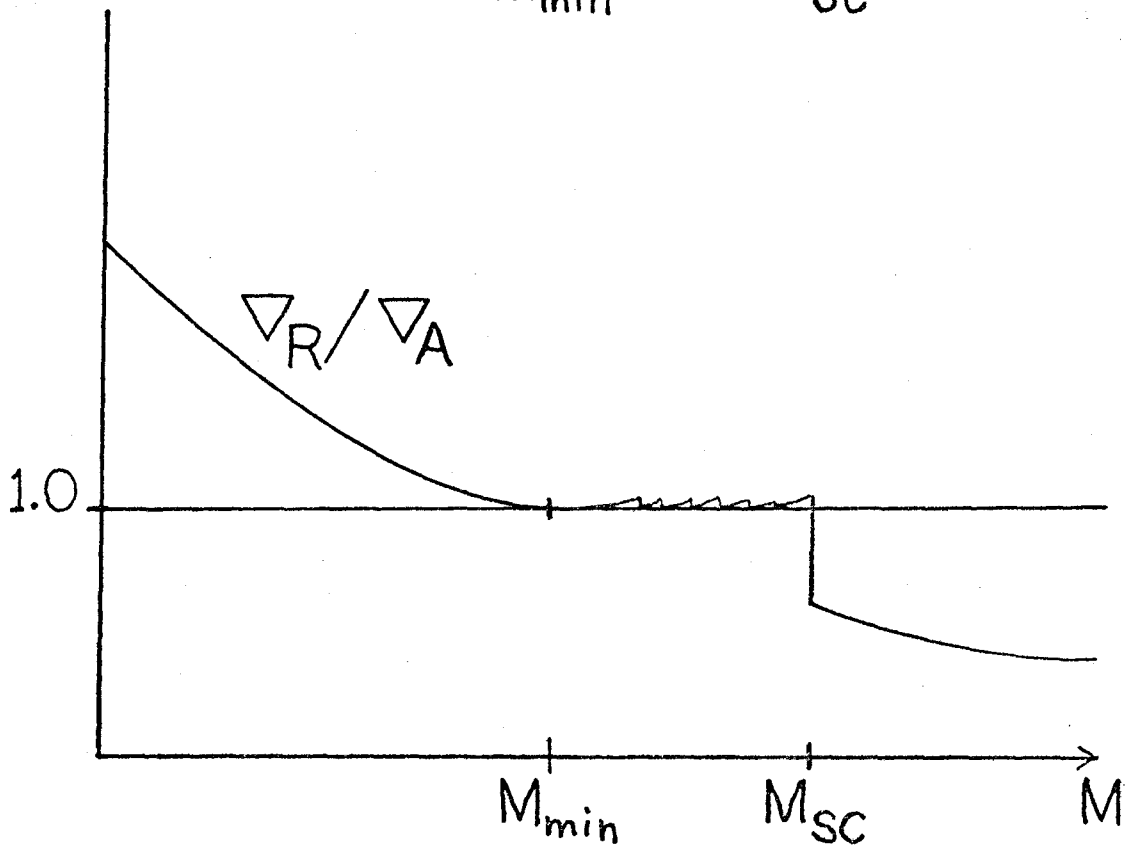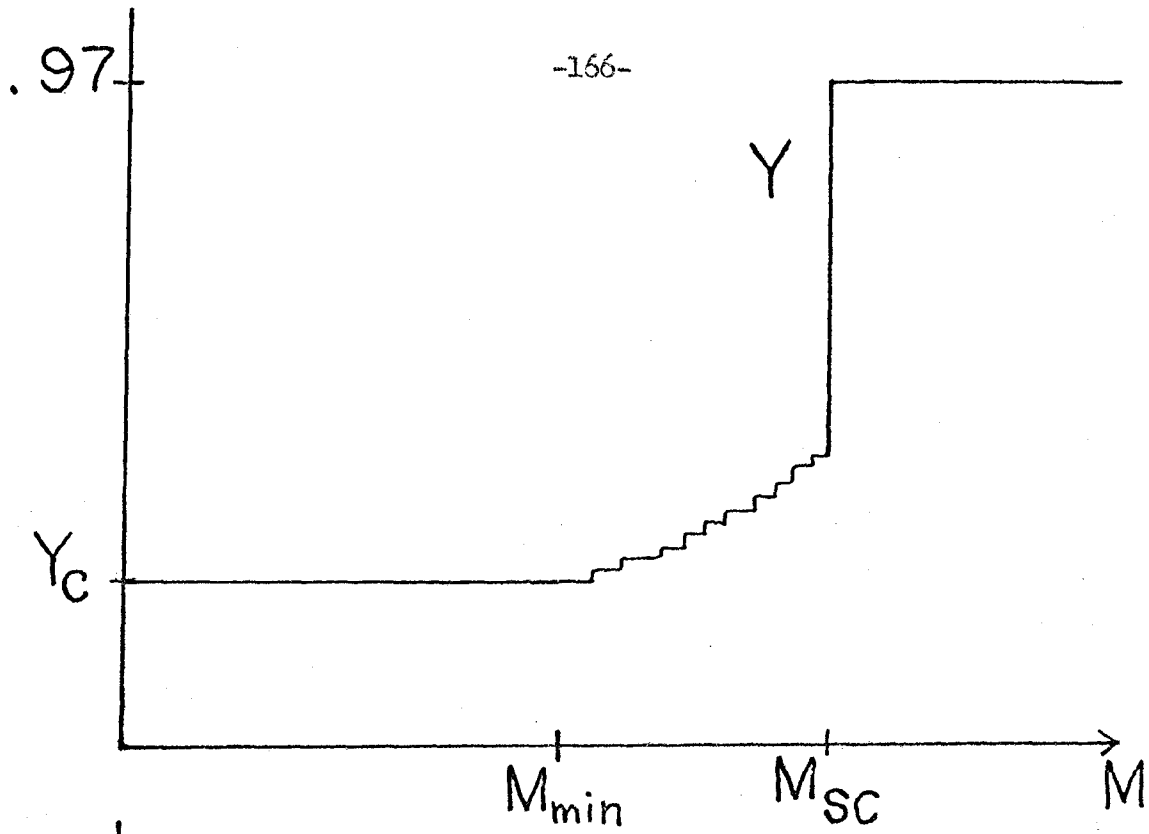
FIGURE 3(b)

Qualitative behavior of Y and ∇_{rad}/∇_{ad} vs. M for the double convection zone model. This model is described at the end of Section 2.3; it is probably unphysical for $Y_c < 0.45$.
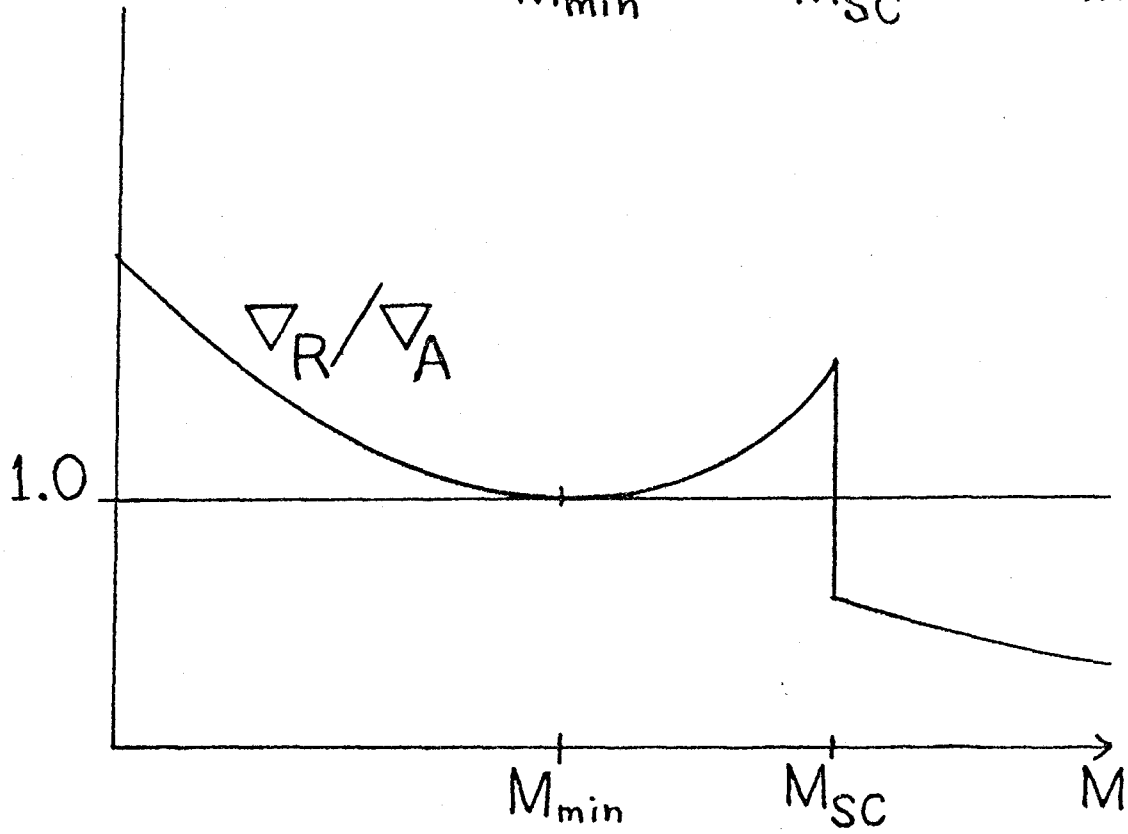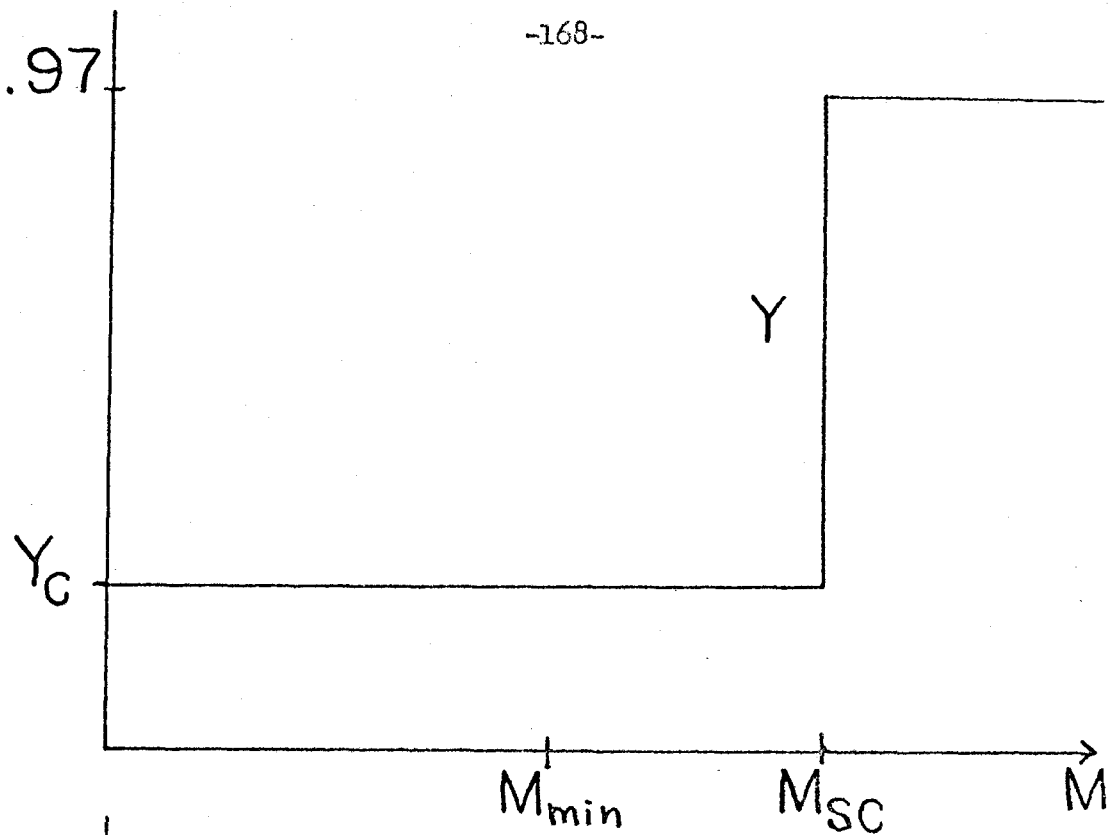
FIGURE 4

The semiconvective zone of Lake Vanda. This is
Figure 1 of the paper by Hoare (1966), reproduced with
permission of the author and the editor of <u>Nature</u>. Con-
ductivity is a measure of dissolved salt concentration.
The semiconvective zone extends to a depth of 155 feet.
It is density-stable because of dissolved salt, thermal
expansion being negligible. The small regions of constant
conductivity and temperature are convective zones trans-
porting heat vertically against the overall density
gradient.

Temperature, Conductivity, & Density of Lake Vanda
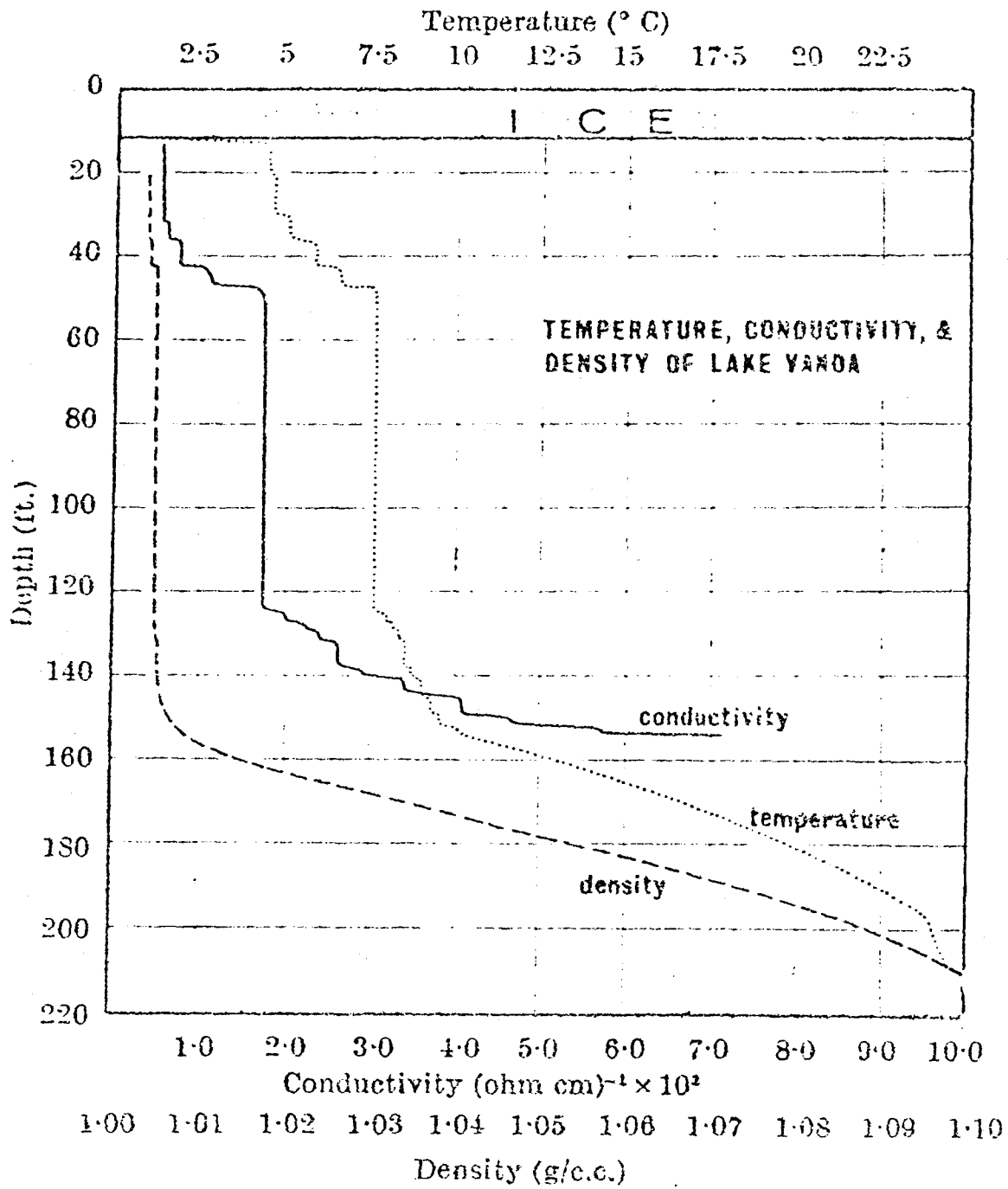
FIGURE 5

Y and ∇_{rad}/∇_{ad} vs. M in the semiconvective zone of HB1. In this model, $Y_c = 0.353$ and $M_{min} = 0.1681$. M_{min} is superadiabatic by 0.05%, and most of the semiconvective zone is subadiabatic by less than 0.4%.
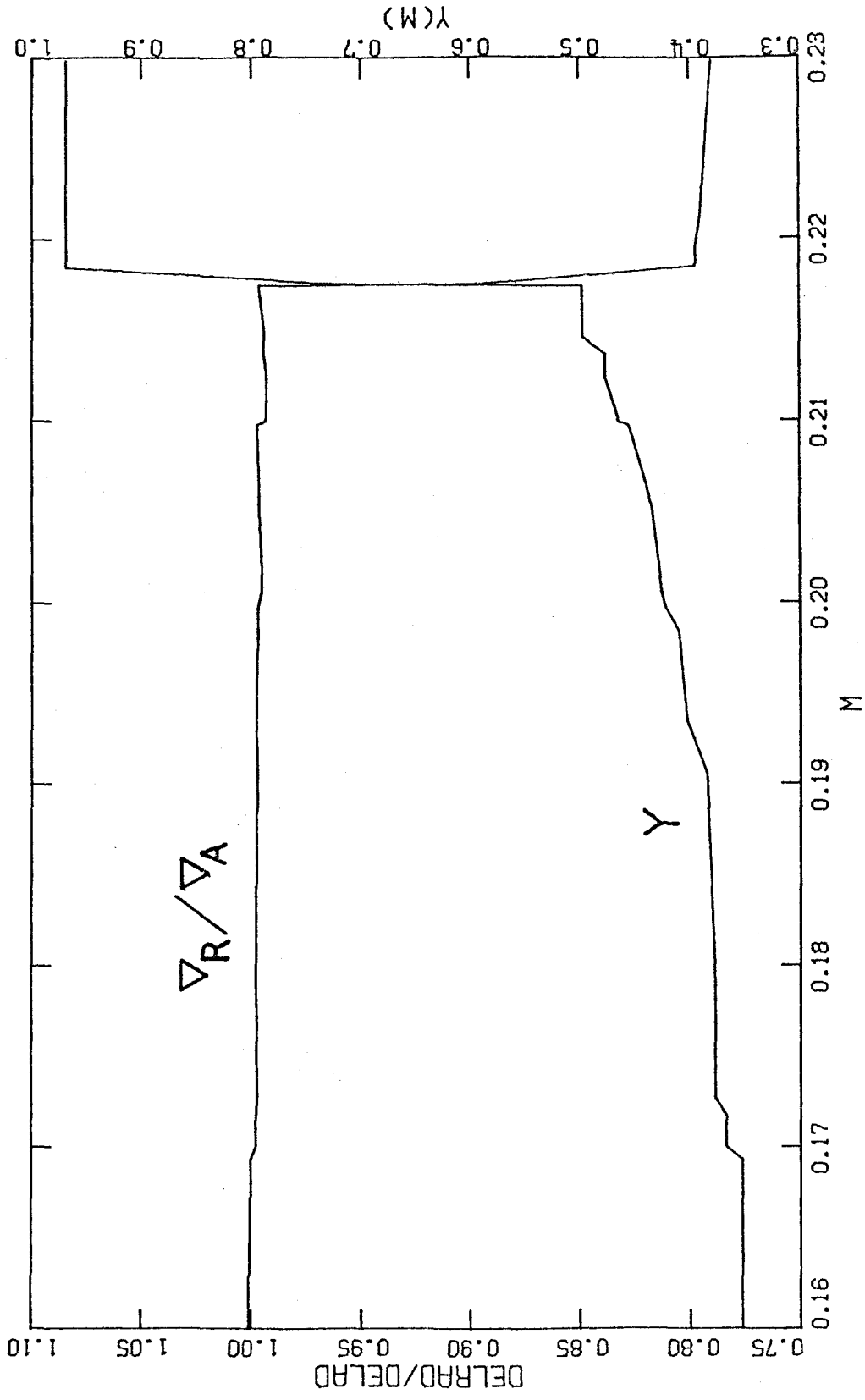
FIGURE 6

The Hertzsprung-Russell diagram for HB1 - 6.
Tracks for HB1, HB3 and HB4 end at the composition in-
stability. The path of HB5 coincides with that of HB1.
For HB2, the track begins at $Y_c = 0.081$, just before
sudden mixing; "noise" in this track following the blue-
ward loop is caused by erratic behavior of the small
convective zones outside the core, as described at the
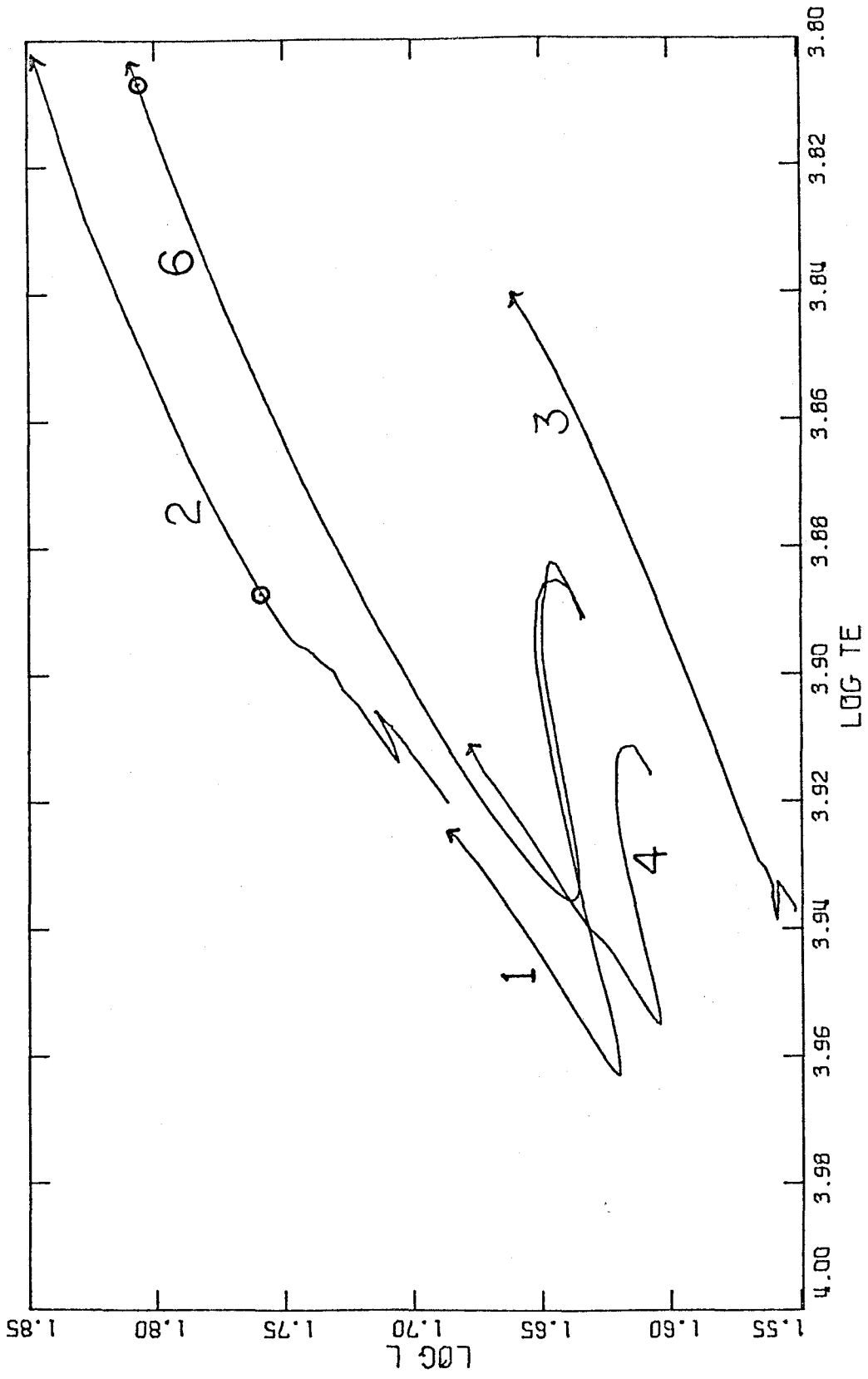end of Section 3.4. Circled points are models with $Y_c = 0.01$.

FIGURE 7

The log g - log T_e plane. Tracks for HB1 and
HB3 end at the composition instability. HB4 and HB5
follow the track of HB1 rather closely. See the previous
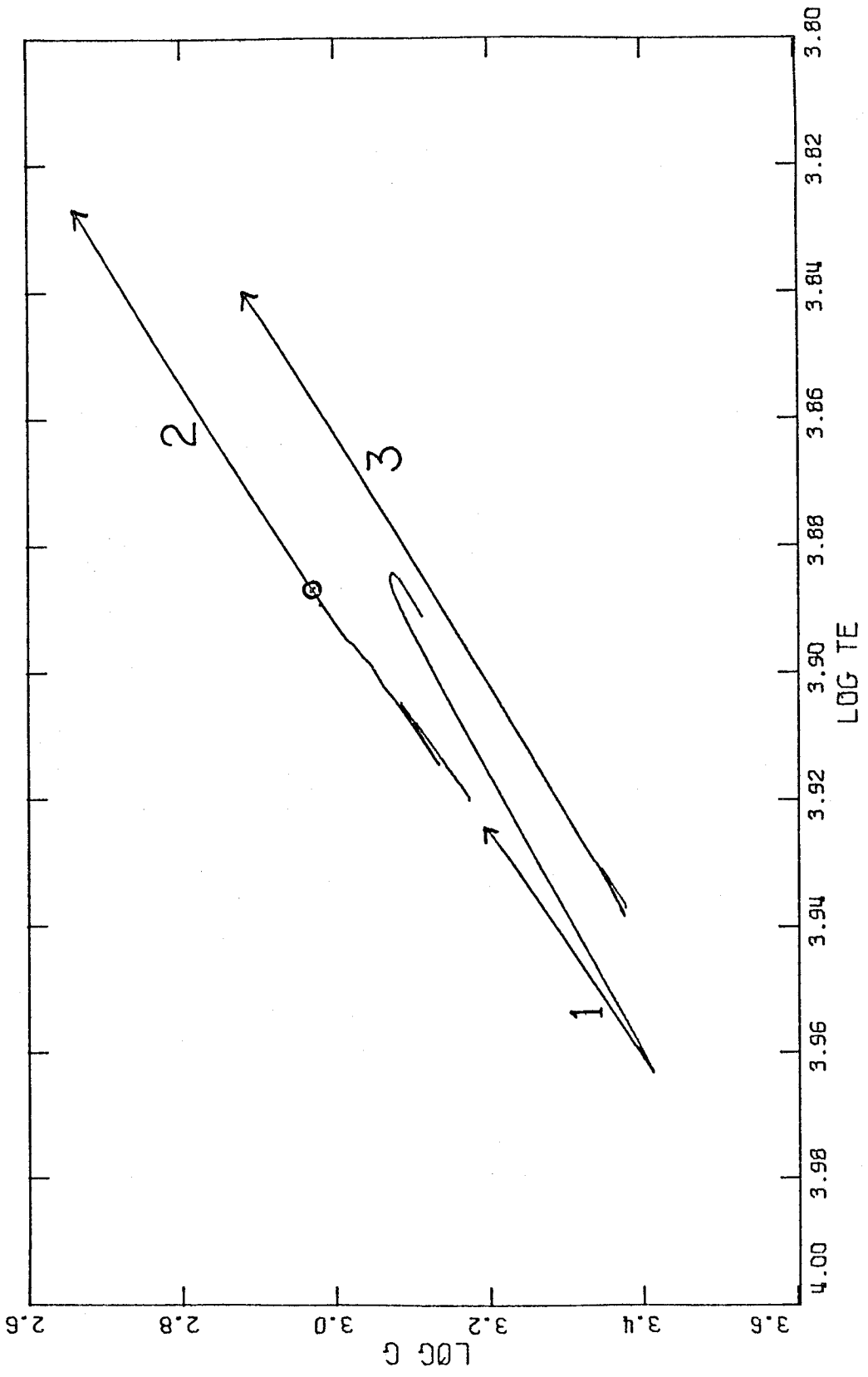caption for discussion of HB2.

FIGURE 8

Log L_{He} vs. log M_{sc} for HB1 - 4. Asterisks and squares are selected models of HB2 and HB4, respectively. M_{cc} is used in place of M_{sc} before the onset of semiconvection. The curve for HB3 approaches that of HB1 asymptotically, regardless of the helium-core mass difference.
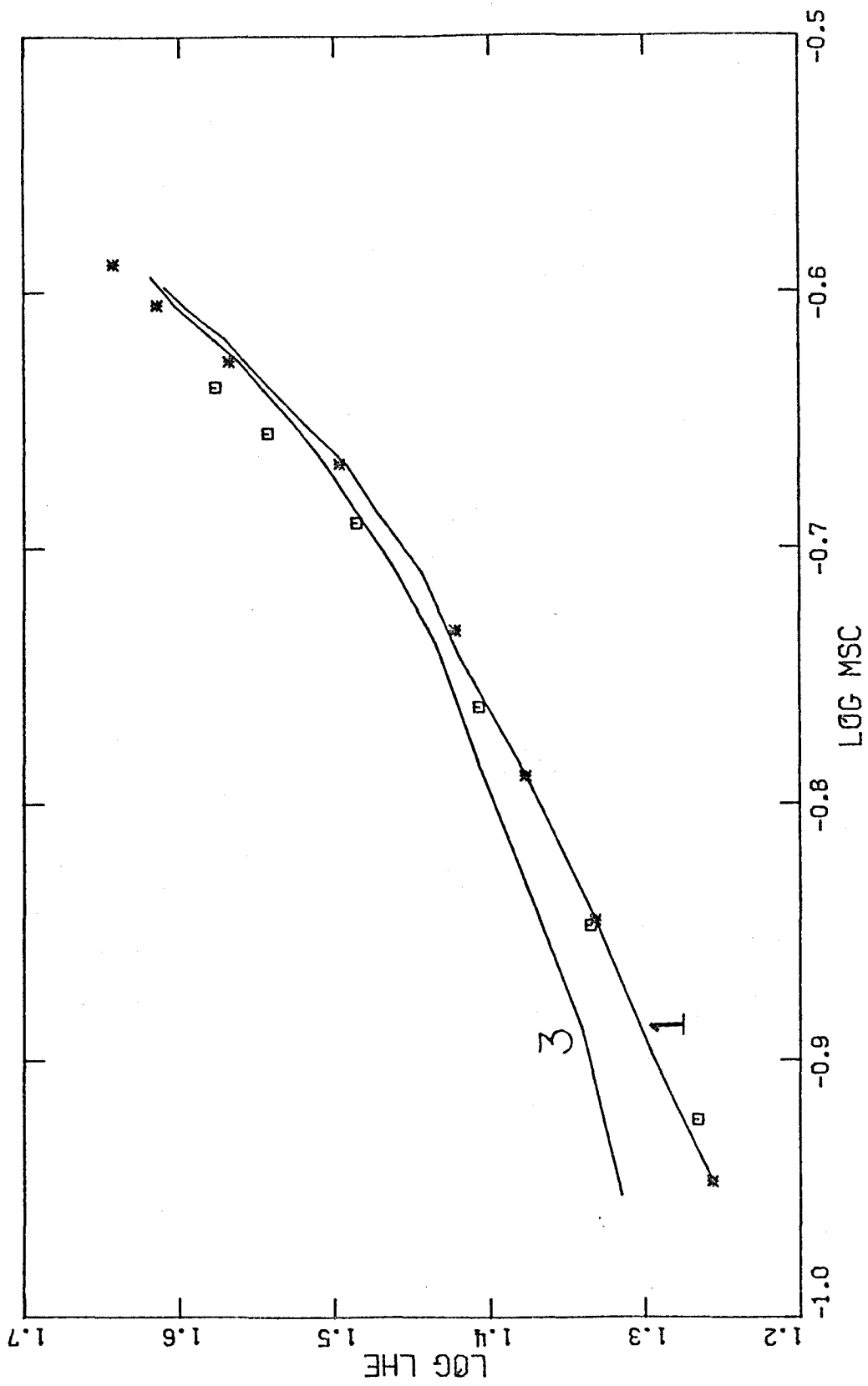
LOG MSC

LOG LHE

FIGURE 9

Log L_{He} vs. log $\bar{\mu}$ for HB1 - 4. See the previous caption for symbol definitions. $\bar{\mu}$ is the mean molecular weight, mass-averaged over the interval $0 < M < M_{sc}$.
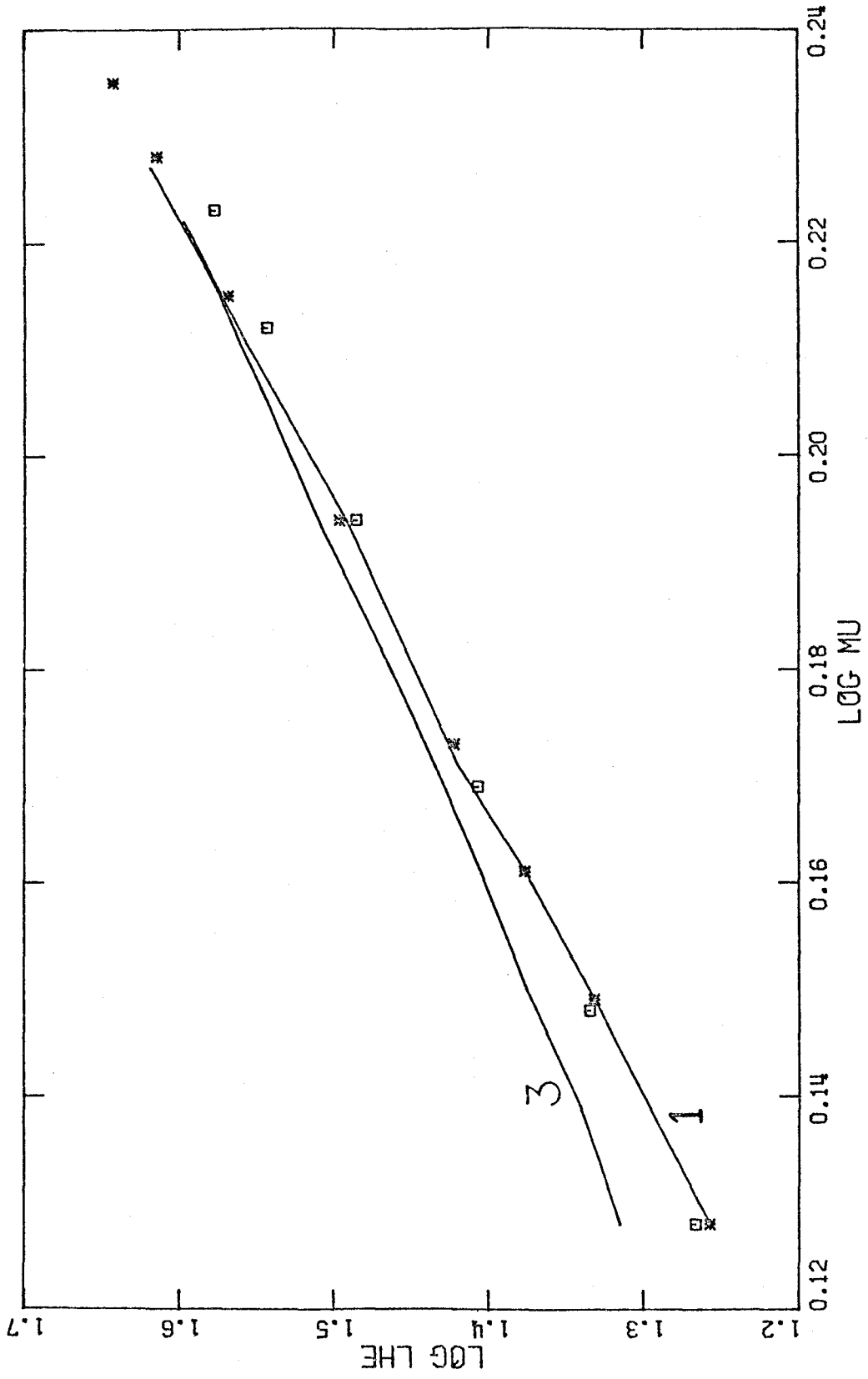
FIGURE 10

Y_c vs. t for HB1 - 4. For plotting purposes, 15 million years has been subtracted from the time variable of HB2, and the same amount added to that of HB4. The effects of rapid mixing are shown for HB1 and HB2; the other curves end at the composition instability.
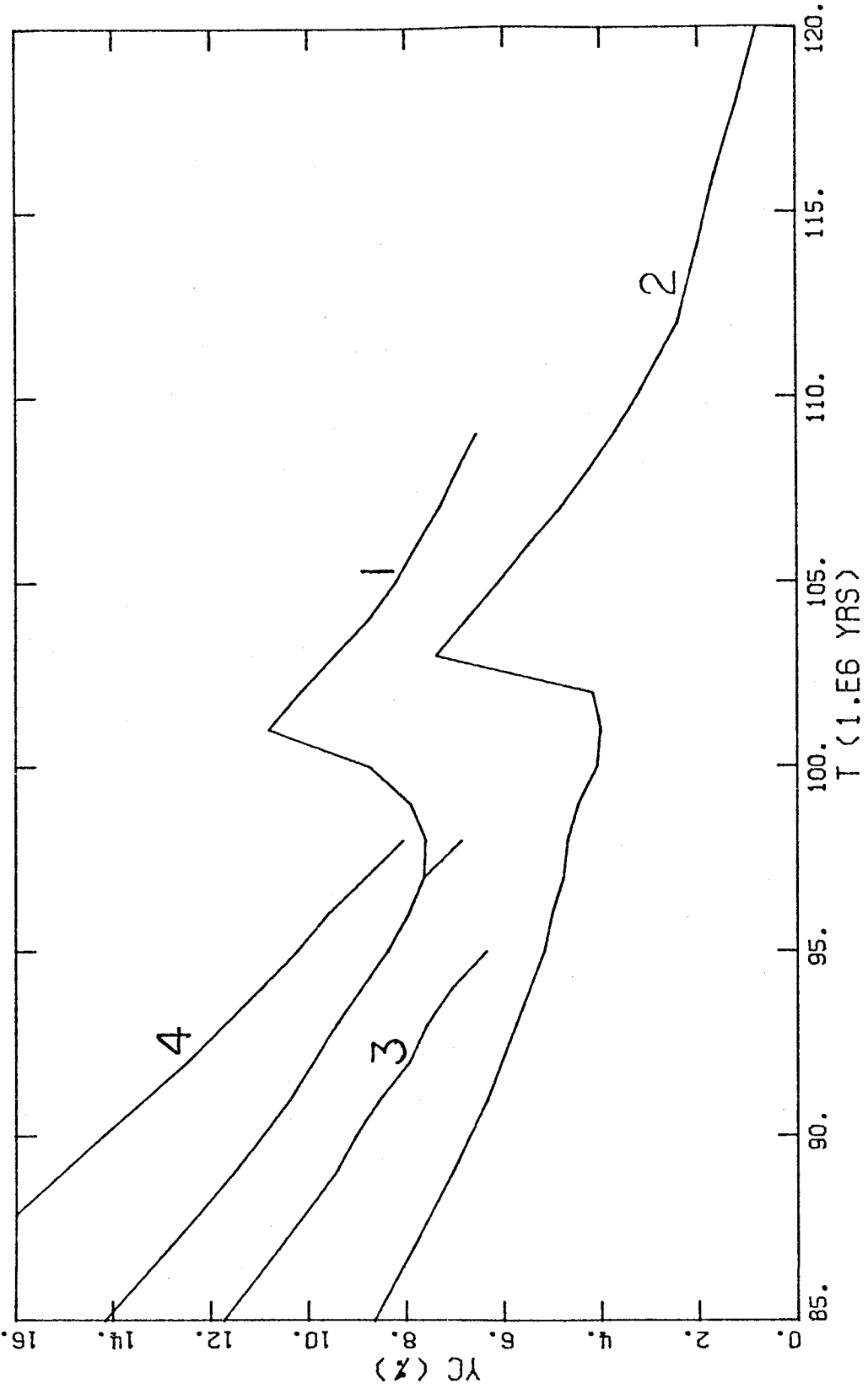
FIGURE 11

Subdwarf B stars in the log L/M - log T_e plane. Asterisks and squares are the observed stars of Greenstein and Sargent (1974), squares representing uncertain measurements. Solid lines are the quasi-evolutionary sequences described in Section 4.3 and Tables 26 and 27. Models with Y_c = .969, .600, .300 and .100 are plotted.
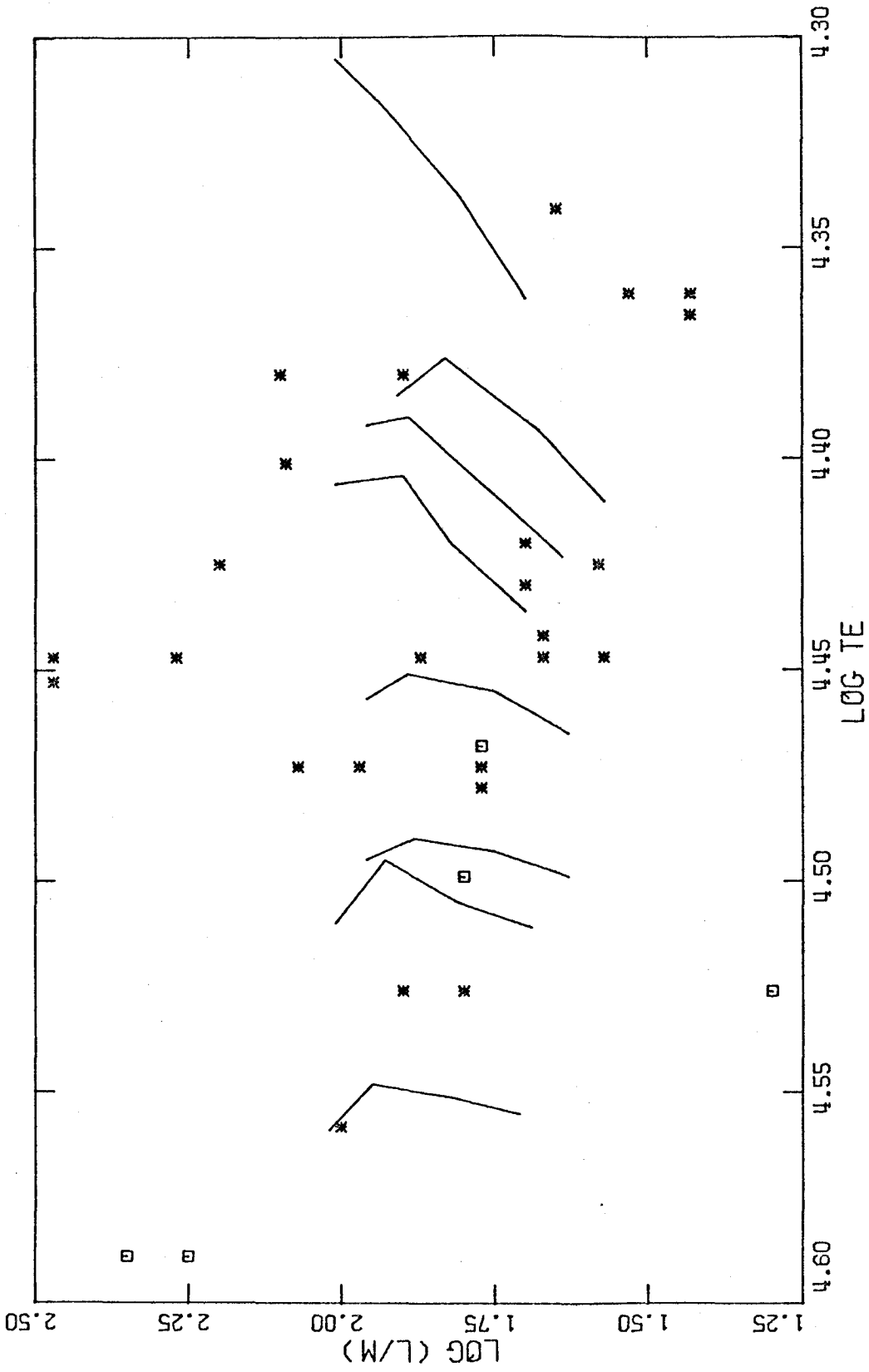
FIGURE 12

Number distributions of sdB stars vs. log L/M.
The observed distribution is N_*; a theoretical distribution
N_p is shown before and after folding with a Gaussian. The
standard deviation σ_*(log L/M) is 0.25, and log L_0/M is
1.48. A logarithmic ordinate is used so that the normali-
zation (arbitrary) may be done by simple vertical shifts.
Theory and observation disagree at high luminosity because
helium-shell burning evolution is not included in N_p. See
Section 4.4 for discussion.

FIGURE 13

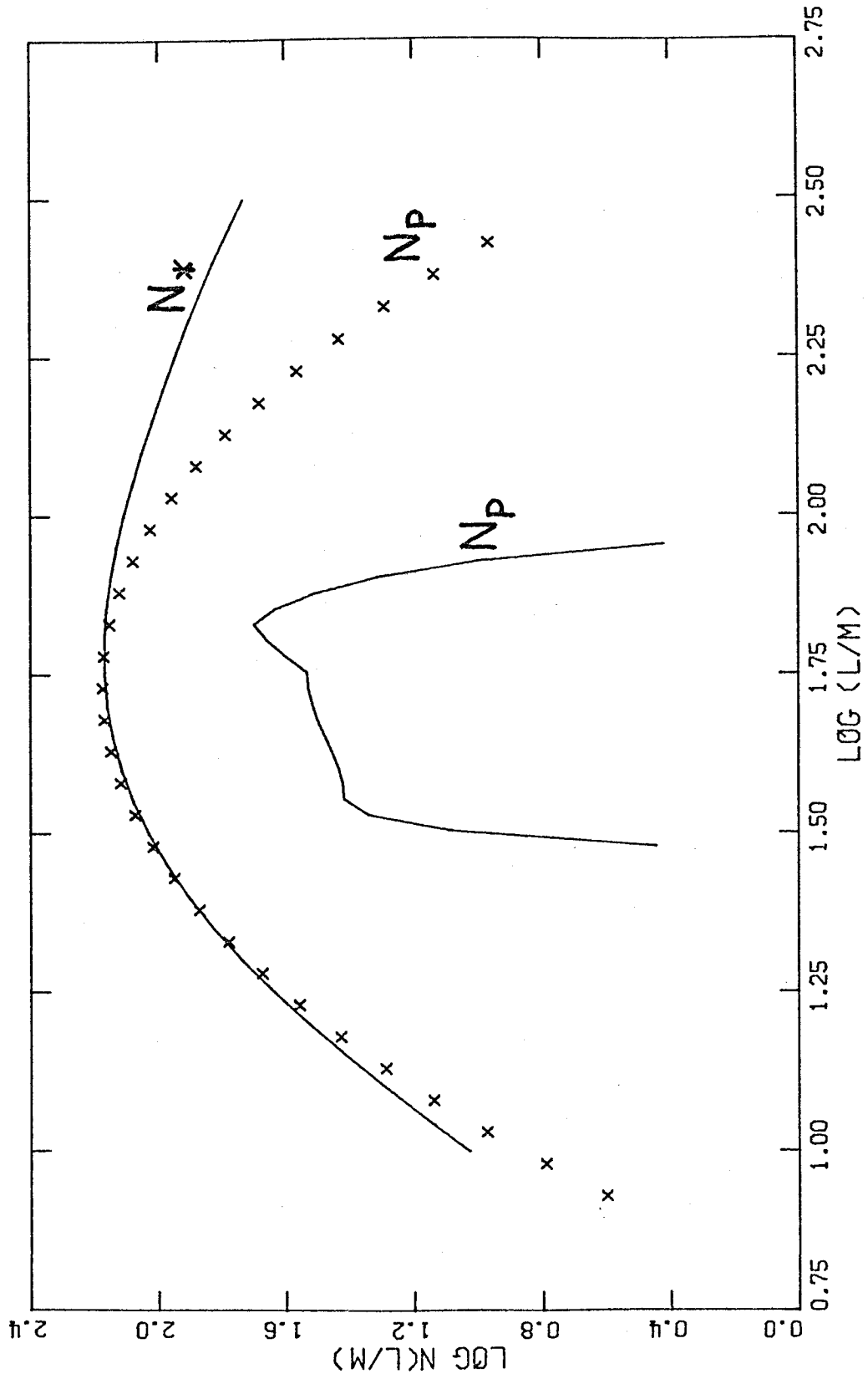Flowchart of the stellar evolution program. The operations are described in detail in Section 3.2 and Appendix A. This chart shows the normal case of two passes through the mixing algorithms; when $Y_c < 0.08$, up to four passes were used.

```
┌──────────────────┐
│ Given a guess for │
│ model at time t   │
└──────────────────┘
        │
        ▼
┌──────────────────┐         ┌──────────────────┐
│ Solve structure  │────────▶│ Compute new model │
│ eqns.,           │         │ atmospheres, if   │
│ holding Xᵢ(M)    │◀────────│ needed           │
│ fixed            │         │                  │
└──────────────────┘         └──────────────────┘
```

Given a guess for model at time t

Solve structure eqns., holding $X_i(M)$ fixed

Compute new model atmospheres, if needed

Test consistency of $X_i(M)$; Vary $X_i(M)$ if necessary

Solve structure eqns., holding $X_i(M)$ fixed

Compute new model atmospheres, if needed

Output model

Test consistency of $X_i(M)$; Vary $X_i(M)$ if necessary

Merge or split mass shells to improve speed, accuracy

Choose Δt; Extrapolate P, T, L, r for guesses at time $t + \Delta t$

Compute $X_i(t+\Delta t)$ using burning rates; Mix abundances only in fully convective regions